Lawrence Berkeley Laboratory
UNIVERSITY OF CALIFORNIA

Materials & Molecular
Research Division

THE PHOTOCHEMISTRY AND KINETICS OF GAS PHASE REACTIONS INVOLVING HO AND Cl RADICALS

Herbert Hoffman Nelson
(Ph.D. thesis)

November 1980

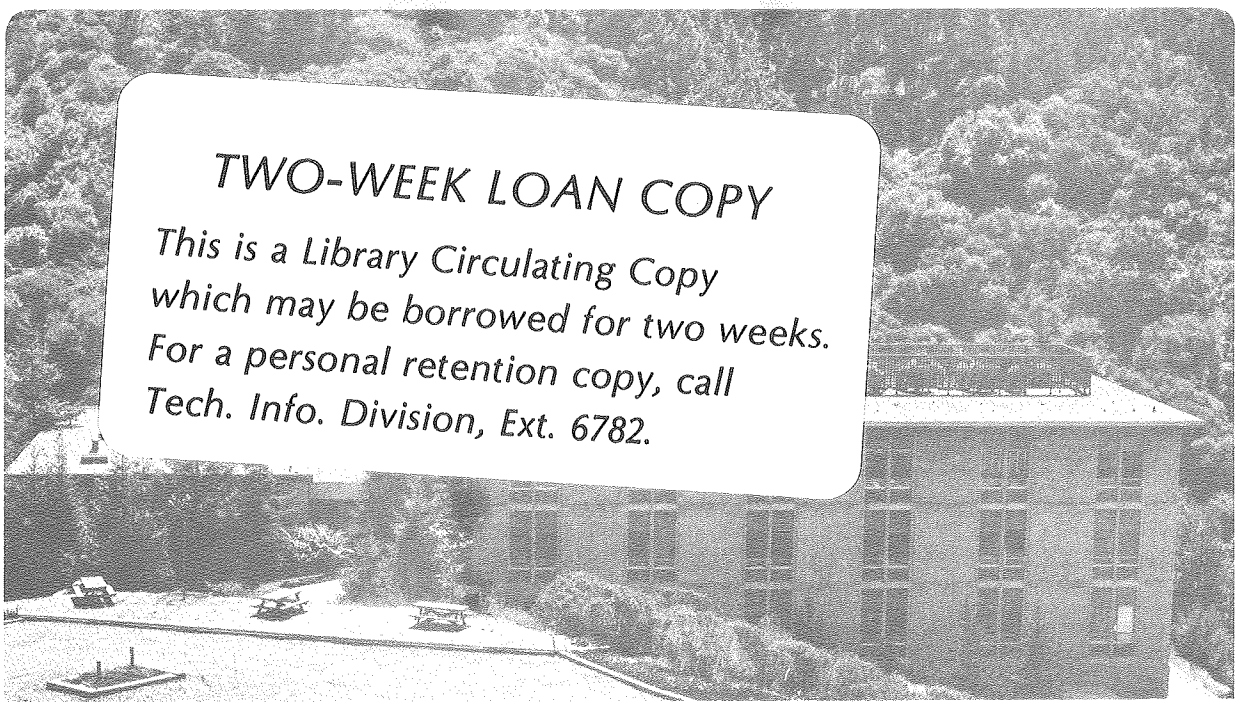

Prepared for the U.S. Department of Energy under Contract W-7405-ENG-48

DISCLAIMER

LBL-11666

THE PHOTOCHEMISTRY AND KINETICS OF GAS PHASE REACTIONS INVOLVING HO AND Cl RADICALS

Herbert Hoffman Nelson

Materials and Molecular Research Division
Lawrence Berkeley Laboratory
and
Department of Chemistry
University of California
Berkeley, California 94720

This work was supported by the U.S. Department of Energy
under Contract No. W-7405-ENG-48.

TABLE OF CONTENTS

Abstract v

I. Introduction. 1

A. Reaction of HO with HNO_3 and H_2O_2 1

B. Reaction of Cl with ClNO and $ClNO_2$. 4

C. Photochemistry of $ClNO_2$ and $ClONO_2$. 6

II. Experimental. 8

A. Methods 8

1. Measurement of Reactants and Products 8
2. Considerations of Interferences 12
3. Interpretation of Data. 14

B. Reactants and Gases 15

1. Nitric Acid and Hydrogen Peroxide 17
2. Nitrosyl Chloride 19
3. Nitryl Chloride 21
4. Chlorine Nitrate. 23

C. Apparatus 25

1. Photolytic Sources. 25
2. Measurement of Precursor Concentration. 29
3. Precursor Mixing and Flow 31
4. Detection of Photolysis Products. 32
5. Laser Energy Measurement. 39
6. Signal Processing 43

D. Experimental Procedures 43

1. Ultraviolet Cross Section Measurements. 43
2. Reaction Kinetics and Photolysis Quantum Yields 45
3. Calibration of Product Detection Systems. 48

III. HO Radical Kinetics 56

A. Kinetic Results 57

1. The Reaction of HO with HNO_3. 57
2. $HO(A^2\Sigma^+)$ Quenching by HNO_3. 64
3. The Reaction of HO with H_2O_2. 68

TABLE OF CONTENTS (cont)

B. Discussion. 74

1. HO + HNO_3 75
2. HO($A^2\Sigma^+$) Quenching. 89
3. HO + H_2O_2 90

IV. Cl Atom Kinetics. 95

A. Kinetic Results 95

1. The Reaction of Cl with $ClNO_2$ 96
2. The Reaction of Cl with ClNO. 97

B. Discussion. 110

1. Cl + ClNO 111
2. Cl + $ClNO_2$. 116

V. The Photochemistry of $ClNO_2$ and $ClONO_2$. 117

A. Experimental Results. 118

1. Cl Atom Quantum Yields. 118
2. O Atom Quantum Yields 120

B. Discussion. 123

1. Cl Atom Quantum Yields. 123
2. O Atom Quantum Yields 128

VI. Conclusion. 132

Acknowledgments. 136
Appendix A 138
Appendix B 140
References 142

THE PHOTOCHEMISTRY AND KINETICS OF GAS PHASE REACTIONS INVOLVING HO AND Cl RADICALS

Herbert Hoffman Nelson

Materials and Molecular Research Division
Lawrence Berkeley Laboratory
and
Department of Chemistry
University of California
Berkeley, California 94720

ABSTRACT

This study examined the kinetics of the reaction of the HO radical with HNO_3 and H_2O_2, the kinetics of Cl atom reactions with ClNO and $ClNO_2$, and the photochemistry of $ClNO_2$ and $ClONO_2$. The ultraviolet absorption cross sections of HNO_3 and $ClNO_2$ were also determined as part of the kinetics work.

The radicals studied were produced by pulsed laser photolysis of the appropriate precursors in a slow flow system and the time evolution of their concentrations was monitored by the technique of atomic or molecular resonance fluorescence. The reaction scheme employed for all the reactions studied is illustrated by the nitric acid case.

$$HNO_3 + h\nu \longrightarrow HO + NO_2$$
$$HO + HNO_3 \longrightarrow H_2O + NO_3$$

The concentration of the photolysis precursor and reaction partner was continuously measured by means of ultraviolet absorption at wavelengths around 200 nm. The HO radicals in both this and the H_2O_2 system were produced by photolysis at 249 nm. Cl atoms were produced by ClNO and

$ClNO_2$ photolysis at 350 nm as well as 500 nm photolysis of ClNO. The photodissociation studies were also carried out at 350 nm.

The rate constant for the reaction of HO with HNO_3 at room temperature was measured to be $(8.2 \pm 1.8) \times 10^{-14}$ cm^3 $molecule^{-1}$ s^{-1}, where the uncertainty reported here and in all cases reflects twice the experimental standard deviation plus an estimate of systematic errors. The nitric acid concentration was determined by absorption at 200 nm where the cross section was measured as 6.5×10^{-18} cm^2. This cross section is in good agreement with the literature[40,59] and the resultant rate constant agrees well with the earlier work of Smith and Zellner[10] and Margitan, Kaufman, and Anderson[11] but is not in agreement with the latest mesurement of Wine et al.[12]

The rate constant for the reaction HO + H_2O_2 was measured as $(1.57 \pm 0.23) \times 10^{-12}$ cm^3 $molecule^{-1}$ s^{-1}. This agrees well with the two latest determinations and serves as a calibration of the experimental apparatus used. The rate constant for collisional quenching of $HO(A^2\Sigma^+)$ by HNO_3 was derived from the relative $HO(A^2\Sigma^+)$ fluorescence quantum yield as a function of HNO_3 concentration. Using a value for the radiative lifetime of the HO upper state of 0.76 μs as recommended by Scofield,[61] the quenching rate constant is calculated to be $(6.8 \pm 1.0) \times 10^{-10}$ cm^3 $molecule^{-1}$ s^{-1}.

The Cl + ClNO reaction rate constant was determined to be $(1.65 \pm 0.32) \times 10^{-11}$ cm^3 $molecule^{-1}$ s^{-1}. This more nearly agrees with the results of Clyne and Cruse[29] than the value recently measured by Grimley and Houston.[30] The rate constant for the reaction of Cl + $ClNO_2$

was found to be $(5.05 \pm 0.75) \times 10^{-12}$ cm^3 $molecule^{-1}$ s^{-1}. This is the first direct measurement of this rate constant.

The photodissociation of $ClNO_2$ was studied in great detail. The absorption cross sections were measured in the ultraviolet and found to be substantially lower than the literature values in the Cl_2 absorption region (300-360 nm). Two product channels were investigated; products representative of the two channels were Cl and O atoms. Absolute calibration for the product detection systems was provided by Cl_2 and NO_2 photolysis respectively. The quantum yields measured for photolysis at 350 nm, calculated using the absorption spectrum measured in this work, are:

$$\phi_{Cl} = 0.93 \pm .1$$

$$\phi_{O} \leq 0.025$$

An upper limit of 0.1 was measured for the O atom channel in $ClONO_2$ photolysis. This matches the limit reported by Chang et al.[37] in another direct measurement.

Harold S Johnston

I. INTRODUCION

During the last decade, the role of the oxides of nitrogen[1] and clorine[2] in determining the stratospheric ozone balance has been the subject of much investigation. This effort has involved laboratory studies of molecules found to be important in the atmosphere, measurements of the concentration profiles of pertinent atmospheric constituents, and computer modeling of atmospheric photochemistry and dynamics. In order to be able to understand the natural stratosphere and predict the results of various natural and man-made perturbations of it, a detailed knowledge of the photochemistry and reaction kinetics of the various atmospheric constituents is required. Some of these important elementary reaction rates and photolysis products have not yet been determined. Others have been studied by several investigators over the years with a variety of experimental techniques but the results are in conflict.

The purpose of this research was to determine the rate constants for several reactions of the HO and Cl radicals and investigate the photochemistry of some molecules that couple the NO_x and ClO_x systems. The kinetic parameters that result will contribute to the understanding of atmospheric photochemistry and theories of reaction rates.

A. Reaction of HO with HNO_3 and H_2O_2

Nitric acid in the stratosphere is primarily formed by the reaction:

$$HO + NO_2 + M \longrightarrow HNO_3 + M \quad . \tag{1}$$

It is thus an important reservoir for both "odd nitrogen" and "odd hydrogen" species (NO_x and HO_x) and, since nitric acid is relatively non-reactive and water soluble, it can be rained out of the troposphere;

representing a sink for HO_x and NO_x. Other loss mechanisms for HNO_3 are photolysis and reaction with HO:

$$HO + HNO_3 \longrightarrow H_2O + NO_3 \quad . \qquad (2)$$

There have been several indirect studies of the kinetics of reaction (2) at high temperatures[3-5] which are reviewed by Hampson.[6] Husain and Norrish[7] used kinetic spectroscopy to monitor the disappearance of HO produced in the flash photolysis of HNO_3 and determined k_2 to be 1.7×10^{-13} cm^3 $molecule^{-1}$ s^{-1} at room temperature. Morley and Smith[8] used a similar system but with resonance absorption detection of HO and measured k_2 to be 1.3×10^{-13}. In both these studies, the nitric acid concentration was determined from pressure measurements in the photolysis cell after expansion of the reactants.

In later work using the flash photolysis/resonance absorption technique,[9,10] Smith and Zellner obtain a lower value for k_2 than the two previous studies. These workers attribute the higher value obtained earlier to the simultaneous removal of HO by reaction (1). Both HNO_3 and NO_2 were measured in the later studies by ultraviolet absorption and the effect of reaction (1) was either neglected or corrected for as appropriate. At about the same time, Margitan, Kaufman, and Anderson[11] published a discharge flow/resonance fluorescence (DF/RF) measurement of k_2 in good agreement with the later values of Smith and Zellner.[9,10]

Very recently, Wine et al.[12] remeasured k_2 by the flash photolysis/resonance fluorescence (FP/RF) technique and reported a value at 295 K (1.32×10^{-13}) which is higher than that previously accepted and a negative temperature dependence. The interpretation of this work

proposed by Wine et. al.[12] raises questions about the long-assumed products of reaction (2), but in an experiment concurrent with this work, Marinelli[13] confirms that the NO_3 channel is the major product channel for reaction (2) by direct observation of the NO_3 produced.

The reaction of hydroxyl radicals with hydrogen peroxide,

$$HO + H_2O_2 \longrightarrow H_2O + HOO \quad , \tag{3}$$

and photolysis are the two main loss processes for H_2O_2 in the stratosphere. In conjunction with the recombination of HOO radicals,

$$HOO + HOO \longrightarrow H_2O_2 + O_2 \quad , \tag{4}$$

reaction (3) provides a parallel path for the reaction of HO with HOO,

$$HO + HOO \longrightarrow H_2O + O_2 \quad , \tag{5}$$

which is an important radical termination step.

In addition, several recent laboratory studies[14,15] have used reaction (3) as a reference for rate constant determinations of other HOO reactions. An accurate value of k_3 is therefore important for calculations of H_2O_2 stratospheric concentrations and absolute rate constants.

There have been five previous determinations of k_3. Greiner[16] used flash photolysis and kinetic spectroscopy to measure a room temperature rate constant of 9.3×10^{-13} cm^3 $molecule^{-1}$ s^{-1}. Hack, Hoyerman, and Wagner[17] employed a discharge flow/ESR system and obtained $k_3 = 8.4 \times 10^{-13}$ at room temperature. In 1979, Harris and Pitts[18] used a flash photolysis/resonance fluorescence apparatus and measured the

room temperature value of k_3 to be 6.8×10^{-13}. On the basis of these three studies, Baulch et al.[19] recommended a value of 8.0×10^{-13}.

Shortly after this, two studies were published which were in sharp disagreement with the recommended rate constant. Keyser[20] worked with a discharge flow/resonance fluorescence system and Sridharan, Reimann, and Kaufman[21] used a discharge flow with laser induced fluorescence detection of HO. Both groups carefully controlled the H and O atom concentrations and the wall reactivity of their flow tubes. Both obtain similar A-factors and activation energies for reaction (3) with a room temperature value of about 1.65×10^{-12}.

B. Reaction of Cl with ClNO and ClN_2

The photochemistry of ClNO has been studied since 1930 when Kistiakowsky[22] showed that the quantum yield for NO production was approximately equal to 2. More recent work[23] shows that the primary process is photolysis to Cl atoms followed by Cl + ClNO:

$$ClNO \xrightarrow{h\nu} Cl(^2P_{3/2,1/2}) + NO(X^2\pi) \qquad (6)$$

$$Cl + ClNO \longrightarrow Cl_2 + NO \qquad (7)$$

The reaction of Cl + ClNO is also important in the recombination of Cl atoms catalyzed by NO.[24] This process proceeds through the mechanism of reaction (8),

$$Cl + NO + M \longrightarrow ClNO + M \quad , \qquad (8)$$

and reaction (7) with the large affinity of Cl for both NO and ClNO explaining the efficiency of the process. Reaction (7) has also been

used as a titration reaction for the determination of Cl atom concentrations in flow experiments.[25-27] An accurate value for k_7 is required in this application to insure that complete reaction occurs in the flow time allotted.

In 1952, Burns and Dainton[28] were able to derive a room temperature value for k_7 of 3.2×10^{-12} cm^3 $molecule^{-1}$ s^{-1}. Their study involved measurements of the retardation of the photochemical production of phosgene (from Cl_2 and CO) by added ClNO. The course of the reaction was followed by the pressure drop as phosgene was formed. Twenty years later, while investigating reaction (7) in connection with Cl atom titration, Clyne and Cruse[29] used a discharge flow/resonance fluorescence system and obtained a room temperature value of 3.0×10^{-11}. Most recently, Grimley and Houston[30] measured $k_7 = 5.4 \times 10^{-12}$ and the rate constant for the analogous Br + BrNO reaction as 5.16×10^{-12}. This work used flash photolysis of XNO to produce X atoms and monitored the production of vibrationally excited NO from reaction (7).

Very little is known about the reactions of nitryl chloride.

$$Cl + NO_2 + M \longrightarrow ClONO + M \qquad (9a)$$

$$Cl + NO_2 + M \longrightarrow ClNO_2 + M \qquad (9b)$$

$ClNO_2$ is presumably formed in reaction (9b), the branching ratio for this reaction is known with little certainty. Niki et al.[31] place an upper limit on $ClNO_2$ production of 20% and a lower limit for process (9a) of 80%. They observed that the isomerization of ClONO to the more stable

$ClNO_2$ was both a heterogeneous and homogeneous process, proceeded in the dark, and had an extra component in the light.

The reaction of Cl with $ClNO_2$,

$$Cl + ClNO_2 \longrightarrow Cl_2 + NO_2 \quad , \tag{10}$$

has been shown to be fast in preliminary work by Clyne referenced in Watson.[32] In a discharge flow experiment at 1 Torr total pressure, Clyne found that $k_{10} >> k_9$ M . Using the recommended value for k_9, this means $k_{10} >> 4 \times 10^{-14}$ cm^3 $molecule^{-1}$ s^{-1}. The only other reports of $ClNO_2$ reactions were early work on the unimolecular decomposition by Johnston and co-workers.[33]

C. Photochemistry of $ClNO_2$ and $ClONO_2$

The absorption spectrum of gaseous nitryl chloride in the ultraviolet has been reported by Illies and Takacs.[34] No work on photolysis products or quantum yields has been reported although the continuous nature of the absorption spectrum suggests a photodissociation quantum yield of 1 in this region.

The calculated wavelength cutoffs for two sets of photolysis products are:

$$ClNO_2 + h\nu \longrightarrow Cl + NO_2 \qquad \lambda < 869 \text{ nm} \tag{11a}$$

$$\longrightarrow ClNO + O \qquad \lambda < 424 \text{ nm} \tag{11b}$$

Both product channels are possible at the photolysis wavelength used in this work.

Chlorine nitrate ($ClONO_2$) plays a major part in atmospheric chemistry because of its role as a reservoir for ClO_x in the lower stratosphere.[35] The reactivity of $ClONO_2$ towards various atmospheric radicals has been shown to be low, therefore photolysis assumes an important place in determining the steady state concentration of $ClONO_2$ in the stratosphere.

There have been two previous studies of the photochemistry of $ClONO_2$. Smith, Chou, and Rowland[36] used a static system with photolysis at 302 nm and inferred the primary step from measured final product identities and ratios. Their work suggests that of the three possibilities,

$$ClONO_2 + h\nu \rightarrow \begin{cases} O(^3P) + ClONO & \lambda < 509 \text{ nm} \quad (12a) \\ Cl + NO_3 & \lambda < 722 \text{ nm} \quad (12b) \\ ClO + NO_2 & \lambda < 1108 \text{ nm} \quad (12c) \end{cases}$$

process (11a) dominates under the conditions used. The maximum wavelength for photodissociation along each of the product channels calculated by Smith et al.[36] is also listed. All three product channels were energetically accessible at the wavelength used. Chang et al.[37] used Very Low Pressure Photolysis in a flow system with mass spectrometric product determination. They used a band of photolysis light centered at 320 nm. As a result of their observation of NO_3, they report $\phi_{12b} = 1.0 \pm 0.2$. They also saw $O(^3P)$ in amounts corresponding to $\phi_{12a} \simeq 0.1$ but they conclude that this results from photolysis of the NO_3 produced in the primary step.

II. EXPERIMENTAL

A. Methods

The choice of experimental techniques used in this study was dictated by several features of the chemical systems chosen for study. The photolysis products in the photochemical systems selected are transient species which undergo secondary reactions with the precursor and other constituents of the system. In order to assure that the true primary process is being measured a pulsed photolysis system with real time, in situ monitoring of products is necessary. In this way, by adjusting the time scale of product measurement, secondary reactions can be ignored while experimental signal-to-noise requirements are satisfied.

Kinetic measurements planned also accommodated themselves well to this system. By manipulating conditions and concentrations, it is possible to arrange that the only significant secondary reactions of the photolysis products are reactions with the precursor. In this way, one series of experiments yields information about photolysis products and quantum yields as well as kinetic data for the reaction of radical products with the photolytic precursor.

1. Measurements of Reactants and Products

Since the kinetics and photochemistry to be studied required several different reactants and at least three product channels, the techniques chosen for their measurement had to meet the dual requirements of sensitivity to the desired radical or molecule while excluding other constituents in the system and the ability to adapt as conditions changed from system to system.

Both the kinetic and quantum yield measurements required a knowledge of the initial reactant concentration. Since the radical generation process was photolysis of this reactant, a flow system was required to avoid depletion of reactant in the photolysis cell. These two factors plus the knowledge that the large rate constants expected for these systems dictated a low concentration of reactant, which implies problems of wall absorption and heterogeneous loss of reactant, lead one to a technique which is capable of continuous measurement; close to if not in the photolysis cell.

In the present work, the method chosen for reactant monitoring was ultraviolet absorption. By limiting the reaction mixture to carrier gas plus the reactant required, whose purity could be checked before and after an experiment, the requirement for specificity could be met. As long as a spectral region could be found in which each reactant had an absorption cross section sufficiently large to allow detection, the generality requirement was also met. Figures 1 and 2 show the ultraviolet absorption cross sections for all 5 reactants encountered in this study. As will be shown later, the region from 195 to 220 nm fulfills all the conditions listed above.

For radical products and intermediates a system capable of real time, in situ measurement was needed. One choice would be the use of secondary reactions to measure concentrations by the production of chemiluminescence or conversion to other, more easily measured products. While this method is highly sensitive and very specific in certain systems, NO/O_3 for example, the radicals encountered in this study are more amenable to detection by the method of resonance fluorescence.

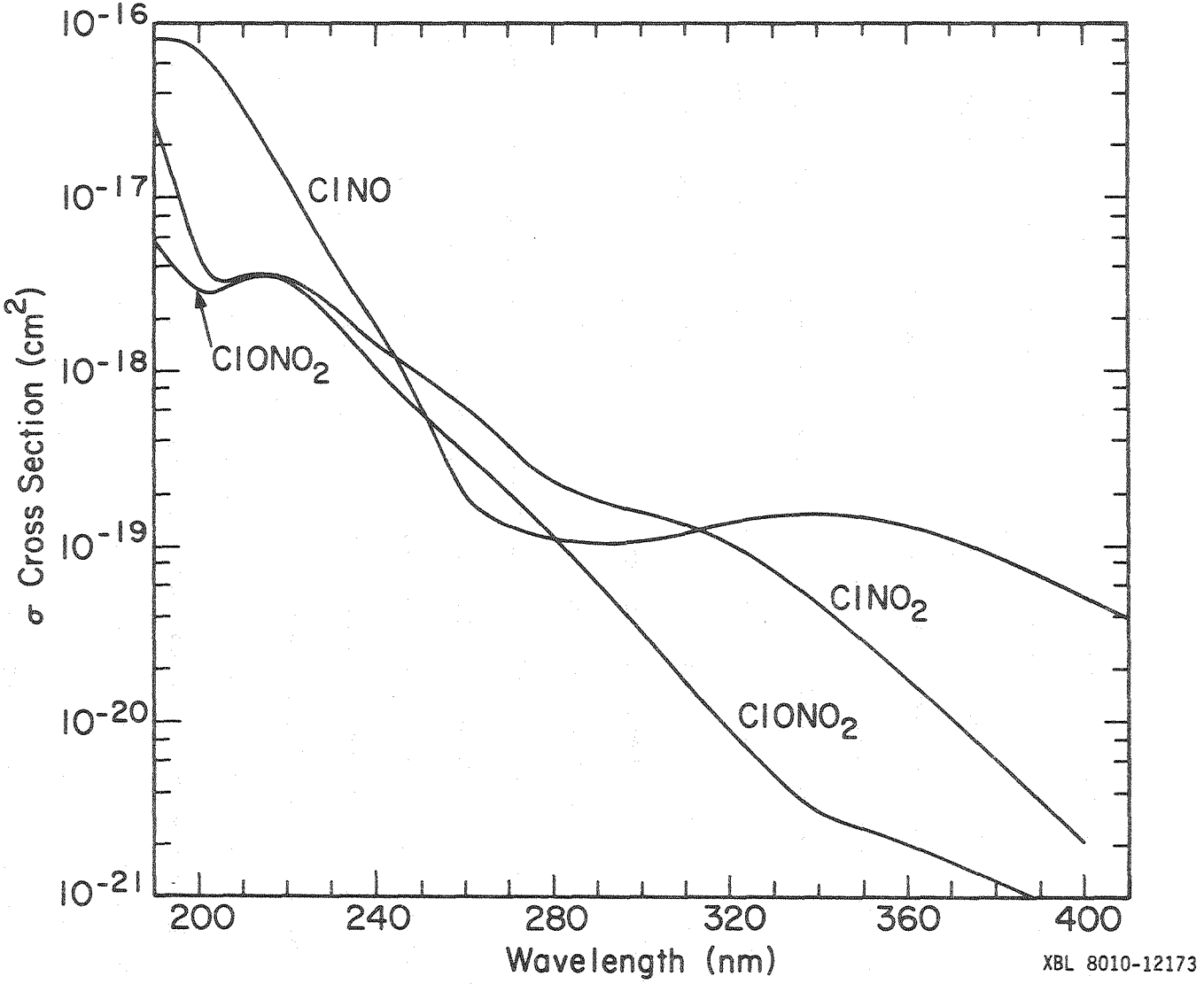

Fig. 1. Ultraviolet absorption spectra of ClNO (ref 38), $ClNO_2$ (ref 34), and $ClONO_2$ (ref 39).

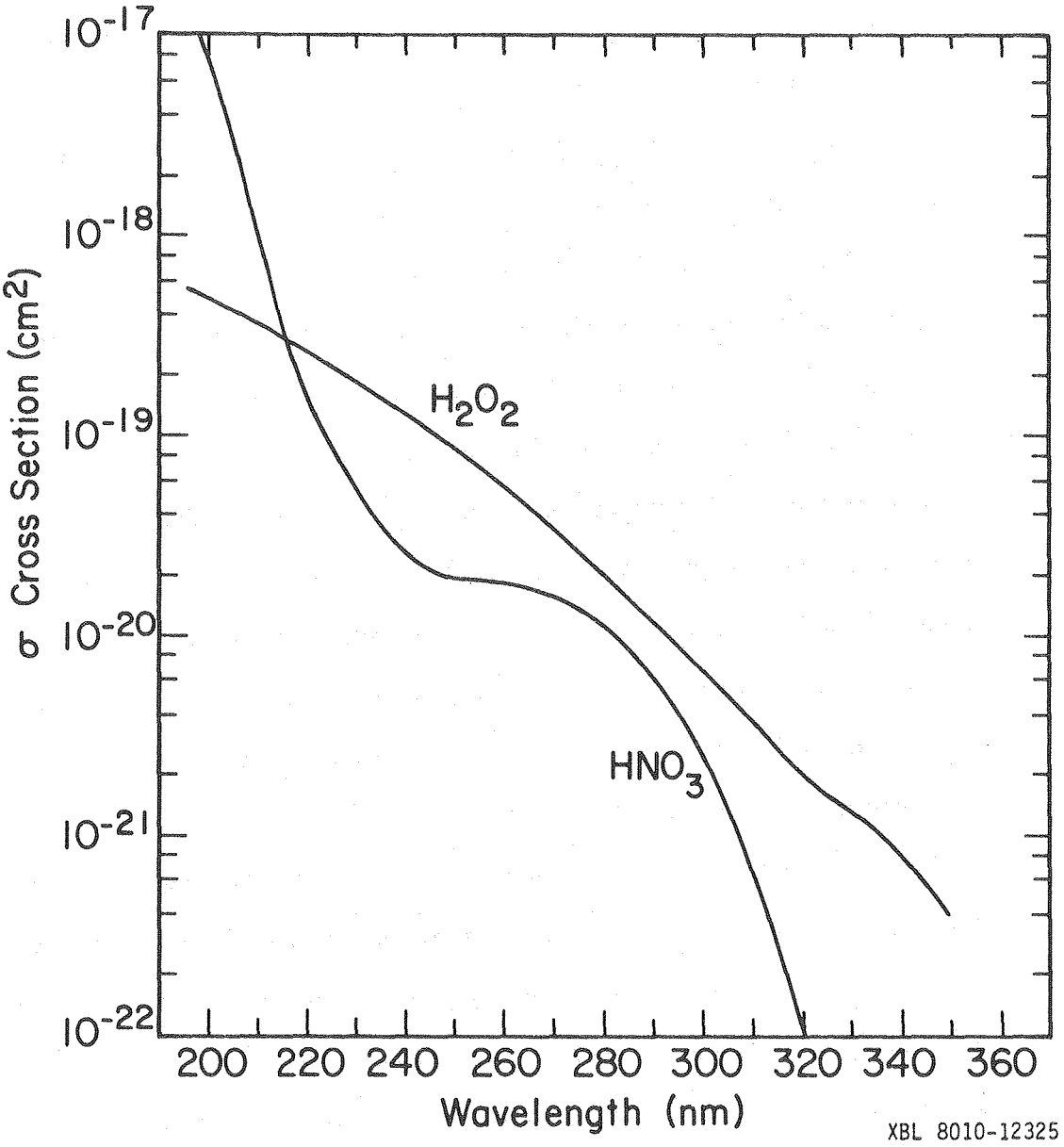

Fig. 2. Ultraviolet absorption spectra of HNO_3 (ref 40) and H_2O_2 (ref 41).

This eliminates the need for other reagents which might not only effect the kinetic results but also the reactant concentration measurements discussed above.

Resonance fluorescence has many desirable features in a study such as this. When the excitation source is a microwave powered lamp, the species to be monitored is often the emitter in the lamp. This provides excellent specificity and sensitivity. The intensities from lamps such as this are relatively high ($\sim 10^{14}$ photons/cm^2/sec) and, especially in the atomic cases, the radiation is concentrated in a few lines. This accounts for the high sensitivity achieved and has the added benefit of keeping background light scattered to the detection system at a minimum. Because of the wide applicability of these sources in laboratory kinetic measurements and atmospheric monitoring systems, much work has been done in this area and a large variety of lamps has been developed.[42]

2. Consideration of Interferences

There are two possible drawbacks to the product measurement scheme outlined above, both of which can be avoided by proper choice of experimental parameters. The high absorption cross sections of the radical species for their resonance radiation, while a factor in the high sensitivity obtained, limit the maximum concentration allowed before light trapping of emitted radiation destroys the method's linearity of response. To be safe, one must keep the atomic species to concentrations below 10^{12} molecules cm^{-3} and the diatomic radicals to $\leq 5 \times 10^{12}$. This is not as serious a limitation in practice as might be thought, as the requirements of low reactant concentration and low fractional conversion to radicals (to avoid seriously depleting the precursor concentration

in the photolysis zone) leave very few opportunities for radical concentrations larger than the above limits.

The sensitivity in a resonance fluorescence measurement is proportional to the fluorescence quantum yield (ϕ_f) for the product of interest. In order to minimize the number of laser shots necessary to obtain data with an acceptable S/N ratio, careful consideration must be given to the choice of M gas employed, especially in the molecular case, and the total pressure. With care, values of $\phi_f > 80\%$ can be realized in these systems.

The second major worry when using the resonance fluorescence technique is the absorption of the VUV or UV resonance radiation by the reactant molecules leading to seriously lowered transmission through the cell or large, local perturbations to the reactant concentration. By flowing reactant through the cell at a reasonable rate (aperture time on the order of 0.1 second) the second problem is avoided. In the worst case encountered, ClNO, the photolysis due to the resonance lamp is ~1% which proved to be quite acceptable. This reactant photolysis does maintain the radical steady state concentrations, and thus the background light scatter, at levels approaching those produced by the laser flash (especially in the Cl experiments), but since this is a DC phenomenon and the radical lifetimes after the flash are on the order of milliseconds the experimental signal-to-noise is not affected unacceptably.

The low precursor concentrations used also negate the first concern. Even for precursor cross sections at the wavelengths of the resonance lamp of 10^{-17} cm^2 attenuations of <5% are calculated in all cases.

3. Interpretation of Data

As is usual in systems such as this, the experimental constraints encountered and ease of data reduction lead one to arrange concentrations so as to study each reaction under pseudo-first order conditions. In the experiments to be reported here, the ratio of precursor to radical was always >100 and often as high as 10^4. No deviations are therefore expected from pseudo-first order behavior.

During a typical kinetics or quantum yield experiment, 2^9 to 2^{14} laser shots were accumulated in a multichannel scaler. The experimental curve consisted of three parts. First came approximately 2 ms of pre-trigger baseline; 100-400 channels depending on the channel width used. This information allowed background signal levels to be established long after the previous decay was completed. After this came the instantaneous (on the time scale of data collection) appearance of the radical population produced by the laser photolysis. This signal then decayed exponentially as the radicals reacted with precursor and diffused out of the detection viewing region. Finally, in all but the slowest decays, the signal returns to the pretrigger baseline and a check can be made that no baseline drift occurred.

After subtraction of the baseline, the data, which are in the form of counts per interval vs time, are linearized and fit to the form

$$\ln (\text{signal}) = -k't + b$$

by the method of linear least squares. This procedure requires care that correct weighting is maintained after linearization.[43] The full details of the derivation of the equations and linearization procedure

are contained in Appendix A. The quantity b, which is the signal at time t = 0, is further normalized by the accumulated laser energy density, the reactant concentration, and the number of laser shots. This is now equal to a relative quantum yield. Conversion to an absolute quantum yield occurs upon comparison to the photolysis of a reference compound (NO_2 or Cl_2) for which absolute quantum yields are well established.

The other parameter which results from the fit of the data is k'. In an experiment such as this the measured k' (or $1/\tau_{observed}$) consists of 2 terms, the rate constant for the reaction of interest times the concentration

$$k' = k[\text{Reactant}] + k_d$$

of the stable reactant and k_d which is a sum of radical diffusion out of the beam, reaction with the carrier gas or its impurities, or any other removal process not proportional to reactant concentration. By using the same pressure of carrier gas and experimental configuration for each measurement in a series, k_d remains constant from run to run. At this point, the standard plot of k' vs reactant concentration yields k for the reaction as its slope and k_d as the zero intercept.

B. Reactants and Gases

The carrier gases used in this study and the extra pure helium used in the O atom lamp were supplied by Lawrence Berkeley Laboratory and were used without futher purification. Typical impurity levels as quoted by the supplier are listed in Table 1.

Table 1. Typical impurity levels for gases used.[a]

	High Dry Nitrogen[b]	Extra Pure Helium[b]	"Prepurified" Argon[b]	High Purity Helium[c]
N_2	99.999%	1 ppm	5 ppm	14 ppm
He	---	99.998%	---	99.995%
Ar	5 ppm	0.1 ppm	99.999%	1 ppm
O_2	1.5 ppm	0.2 ppm	2 ppm	1 ppm
H_2O	1.5 ppm	0.3 ppm	---	12 ppm
CO_2		0.1 ppm	0.5 ppm	1 ppm
Ne		---	---	14 ppm
THC[d]		---	0.5 ppm	1 ppm
H_2		---	1 ppm	1 ppm

[a]As quoted by Supplier
[b]LBL issue
[c]Matheson Gas Company, used in halogen/helium mixtures
[d]Total hydrocarbons as CH_4

The rare gases for use in the excimer laser were supplied by Airco Inc. and were Airco grade 4.5 (99.995%) which met or exceeded the purity requirements stated by the laser manufacturer.

Two halogen/helium mixtures were used in this study both supplied by the Matheson Company. A 10% fluorine in helium mixture was used in the laser gas mixture as recommeded by Lumonics and thus needs no further discussion. The Cl atom lamp was run on a 0.1% Cl_2 in helium mixture. Even though the total O_2 impurity quoted for this mixture (see Table 1) is greater than that in the extra pure He used in the O atom lamp, very little O atom radiation was observed from the Cl atom lamp. This will be discussed further in a later section.

All reactant purifications were carried out in a glass vacuum manifold outfitted with either Kontes high vacuum Teflon stopcocks or Westef high vacuum, glass bore stopcocks with Viton O-rings on both. The vacuum line was evacuated with a liquid nitrogen trapped, air cooled oil diffusion pump and/or a Welch Duo-Seal roughing pump. All connections to bulbs and gas cylinders were made with stainless steel Cajon Ultra-Torr fittings equipped with Viton O-rings. Gas pressures were measured by either a Barocel Model 511 AH-11 or a Baratron Model 220-2A6 capacitance manometer; the range of both instruments was 0-100 Torr.

The details of the preparation and purification of each reactant used is described in the following sections.

1. Nitric Acid and Hydrogen Peroxide

Nitric acid was prepared by the classic method as described by Johnston, Chang, and Whitten.[44] Anhydrous HNO_3 is distilled from a mixture of sodium or potassium nitrate in 96% sulfuric acid. Typically

100 ml potassium nitrate was dissolved in 100 ml 96% sulfuric acid in a 250 ml flask. The flask and its contents were cooled and the dissolved air pumped away. The temperature of the flask was raised to ~300 K and the nitric acid was collected in a bulb immersed in a CCl_4/liquid nitrogen slush at 250 K with the first and last portion of the distillate being discarded. It is very important to keep the NO_3^-/H_2SO_4 mixture below 313 K to minimize decomposition of the HNO_3 and to keep the receiving bulb above 243 K to avoid trapping water with the product nitric acid.

The nitric acid prepared in this manner invariably had a 0.1-0.2% NO_2 impurity as determined by near UV absorption measurements. The product collected was a white solid at dry ice temperature and was stored at this temperature (196 K) for several weeks with no evidence of further decomposition.

Most of the experiments to be described in this work were performed with HNO_3 made from KNO_3/H_2SO_4 solutions. Only at the very end of the study did I learn that the conventional wisdom called for the use of $NaNO_3$ instead of KNO_3.[45] Several preparations were carried out using each of the nitrate salts. No difference in product yield or purity was observed. Presumably, the choice of $NaNO_3$ was based on an impurity present in the potassium nitrate available at the time. There was no difference in the impurity levels stated by the manufacturers of the nitrate salts used in this work.

Some thought was given to the effect of various possible impurities in the nitrates used. Cox[46] has prepared nitrous acid by dissolving sodium nitrite in sulfuric acid. This would be the fate of any nitrite

impurity in the present work. Nitrous acid, however, is not stable in storage as is nitric acid and decomposes to H_2O, NO, and NO_2. As was noted, no increase in the measured NO_2 concentration was observed upon storage.

Any chloride impurity would lead to HCl production. This was discounted as an interference for two reasons. First, the HCl boiling point is so low that any HCl formed would be pumped away when the reaction mixture was degassed. Even if some HCl was trapped in the nitric acid, no interference is expected. The HCl absorption cross section at 200 nm[47] is at least 10 times smaller than that of HNO_3 ($< 5 \times 10^{-19}$ vs 6.5×10^{-18}) so a trace amount would not interfere with the absorption measurement of nitric acid concentration. The rate constant for the reaction of HO + HCl is 6.6×10^{-13} cm^3 $molecule^{-1}$ s^{-1} at room temperature,[19] sufficiently slow that trace HCl impurities would not effect the measurement of the HO + HNO_3 rate constant.

Hydrogen peroxide was purchased as a 90 or 98 percent solution from FMC Corporation. Before use, the peroxide was transferred to a pyrex saturator and pumped on to degas the solution and remove some of the water. The peroxide solution contains a trace amount of stabilizer, which is a non-volatile inorganic sodium salt. Molina[48] has shown that the amount of stabilizer in the gas phase in an experimental set-up such as this is negligible.

2. Nitrosyl Chloride

ClNO of 97% minimum purity was obtained from Matheson Gas Company. The most likely impurities resulting from the manufacturing process used by Matheson are NO_2 and Cl_2 with NO as a product of thermal decomposition.

Following the purification scheme of Illies and Takacs,[34] samples of the product supplied by Matheson were degassed repeatedly at 77 K and then distilled twice from 196 K to 77 K with the first and last quarters of the distillate discarded. This procedure was designed to remove NO_2 which has a vapor pressure of only 0.05 Torr at 196 K. It has been claimed that this procedure also removes residual Cl_2 or NO (vapor pressure 50 and 4000 Torr at 196 K) but ClNO is a solid at this temperature and no reduction of the Cl_2 impurity was obtained.

Nitrosyl chloride with minimum chlorine impurity was prepared as follows. Approximately 150 Torr of ClNO that had been degassed and separated from the NO_2 impurity was condensed into a 5 liter bulb equipped with a glass finger. The bulb was then filled to one atmosphere with twice distilled NO and left in the room lights for 3-4 days. This converted a portion of the Cl_2 impurity into ClNO. A dry ice slush at 196 K was placed under the finger and the ClNO present was trapped. The residual Cl_2 and NO were then pumped off. The Cl_2 impurity, as measured by deviation of the absorbance at 200 nm of a sample from that calculated using the absorption cross sections reported in the literature, was successively lowered after each of these freeze, pump, thaw cycles. Nitrosyl chloride of sufficient purity to confirm the previously measured cross sections results from this procedure. The purified ClNO could be stored at 196 K for days with no evidence of thermal decomposition. Nitrosyl chloride is very susceptible to photochemical degradation due to its absorption throughout the visible. All purifications and transfers were carried out in the dark.

3. Nitryl Chloride

$ClNO_2$ was prepared using the method of Volpe and Johnston.[33b] Anhydrous hydrogen chloride (Matheson Gas Company, 99%) was further dried by passage through a trap maintained at 196 K. From there the HCl was bubbled through a fritted glass tube into a solution containing 25 ml 90% nitric acid, 60 ml 95% sulfuric acid, and 70 ml 30% fuming sulfuric acid. The product nitryl chloride was trapped at 196 K in a bulb with a calcium chloride drying tube attached to the outlet to prevent atmospheric water from entering the system.

Volpe[49] suggests that the formation of nitryl chloride and various impurities takes place according to the following reactions:

$$HNO_3 + 2H_2SO_4 \longrightarrow NO_2^+ + H_3O^+ + 2HSO_4^- \qquad (13a)$$

$$HCl + NO_2^+ + HSO_4^- \longrightarrow ClNO_2 + H_2SO_4 \qquad (13b)$$

$$2HCl + NO_2^+ + HSO_4^- \longrightarrow Cl_2 + NOHSO_4 + H_2O \qquad (13c)$$

$$HCl + NOHSO_4 \longrightarrow ClNO + H_2SO_4 \qquad (13d)$$

As can be seen, the initial step involves formation of the nitryl ion in solution. Subsequent reaction of HCl with the nitryl ion leads to formation of the desired $ClNO_2$ and some Cl_2 impurity. In the preparations carried out during the course of this study, Cl_2 was always present as an impurity of 10–20%. The removal of the Cl_2 will be discussed below. The real danger arises from the other product of reaction 13c, nitrosyl sulfuric acid. Volpe[49] reports that whenever the reaction was allowed to proceed past the halfway point, sufficient nitrosyl sulfuric

acid builds up that reaction (13d) becomes important, producing ClNO. Nitrosyl chloride is an impurity that causes serious interferences with the kinetics and quantum yield measurements in the nitryl chloride system but is very difficult, if not impossible in practice, to remove. Therefore extreme care was taken to stop the preparations long before ClNO production should begin. Typical preparations were stopped after about 30% conversion of the initial HNO_3. No evidence of ClNO was found in an examination of the visible absorption spectrum of 750 Torr of the $ClNO_2$ product. This places an upper limit of 0.01% on the nitrosyl chloride impurity.

The molecular chlorine impurity assumes great importance when the photolysis studies are carried out at 350 nm. This is close to the peak of Cl_2 absorption cross section and the ratio $\sigma_{Cl_2}/\sigma_{ClNO_2}$ is 10.6. Extra care then becomes important in assuring that minimum Cl_2 remains. Chlorine was removed from the nitrosyl chloride by partial evaporation at 175 K. At this temperature the vapor pressure of Cl_2 is 14 Torr while that of $ClNO_2$ is ~3.5 Torr. Volpe[49] reports, and this work confirms, that purification of $ClNO_2$ by partial evaporation at 196 K is not possible. Obviously a constant boiling mixture of Cl_2 and $ClNO_2$ is obtained which prevents removal of the unwanted Cl_2. At 175 K (methanol/LN_2 slush) almost all of the color in the initial product can be removed. The nitryl chloride remaining was a very pale yellow, possibly colorless liquid and a white solid.

The other impurity of consequence, NO_2, was removed by distilling the remaining $ClNO_2$ from 196 to 77 K. As in the previous purifications,

NO_2 remains in the initial flask at these temperatures and final product with NO_2 less than 0.15% is collected.

A modification of this prep has been reported by Illies and Takacs.[34] These workers maintained the acid mixtures in an ice bath to suppress the formation of molecular chlorine in the prep. The residual Cl_2 was removed by treatment with activated charcoal. Attempts to duplicate these results in this study were not successful. Approximately 15% Cl_2 impurity was formed in the $ClNO_2$ made using ice temperature reactants; about the same as a room temperature prep. After treatment with activated charcoal, the telltale yellow color of Cl_2 was still present in the liquid sample.

4. Chlorine Nitrate*

$ClONO_2$ was prepared by the method of Schmeisser[50] which entails the reaction of Cl_2O with N_2O_5 both of which are almost quantitatively converted to $ClONO_2$.

The Cl_2O required was prepared according to the method of Cady,[51] the stoichiometry of which is illustrated in reaction (14).

$$2Cl_2 + (n+1)\ HgO \longrightarrow Cl_2O + HgCl_2 \cdot nHgO \qquad (14)$$

A stream of nitrogen and Cl_2 was dried by passage through 96% H_2SO_4. The two gases are then directed through a 1 meter tube containing a mixture of dried HgO and crushed glass (added to ensure porosity of the solid). The effluent gases were collected at 196 K in a trap with a calcium chloride drying tube on the outlet. The product that resulted

---

*Thanks to W. J. Marinelli for the experimental work.

was Cl_2O with approximately 20% Cl_2 impurity and was used in the $ClONO_2$ prep without further purification.

Dinitrogen pentoxide was prepared using the method of Schott and Davidson[52] in an apparatus described and constructed by Connell.[53] Highly purified and dried oxygen was split into two streams. One was directed through an Ozone Research and Equipment Company Model 03B1-0 ozonator. The other stream was bubbled through a flask containing liquid NO_2/N_2O_4 then through a regulating needle valve and to a mixing "tee". The two flows are adjusted so that the visible NO_2 is completely absent several centimeters downstream from the mixing point and excess O_3 is detected at the output. As a further test of reaction, the exothermicity noticeably warms the tubing used in the vicinity of the reaction zone. After flowing the N_2O_5/O_3 mixture for a time to sweep all the water possible from the apparatus, the product N_2O_5 is collected as white, needle-shaped crystals at 196 K. N_2O_5 produced in this manner invariably contains 10% HNO_3 impurity.[53] This presumably forms in the heterogeneous reaction of N_2O_5 with water on the walls of the collection flask and production manifold. No attempt was made to remove the HNO_3 as subsequent handling and transfer of the N_2O_5 would only result in further HNO_3 production. Before use, the O_2 carrier gas is pumped from the storage flask.

To complete the preparation of $ClONO_2$, quantities of Cl_2O and then N_2O_5 are condensed into a flask serving as the reaction vessel. The flask is connected to the atmosphere through a drying tube, placed in a slush at 195 K, and allowed to slowly warm to 273 K. At this point the flask is gently agitated to cover any remaining N_2O_5 with the liquid

Cl_2O and the reaction is complete. The $ClONO_2$ is distilled from the reaction vessel leaving behind any unreacted N_2O_5 and HNO_3 impurity. The principal impurities remaining are Cl_2 from the original Cl_2O prep and unreacted Cl_2O. These are both removed by partial evaporation of the product mixture at 157 K. Both impurities are removed below the detection limit (by UV absorption measurements) by this procedure, although the trace Cl_2O which obviously remains made some of the planned experiments impossible. This problem will be discussed in a later chapter. As was the usual procedure, the chlorine nitrate was stored in the dark at 195 K several days before use without any evidence of decomposition.

C. Apparatus

A schematic diagram of the apparatus used is shown in Fig. 3. The following sections describe the individual components in more detail.

1. Photolytic Source

Two photolysis sources were used in this work. Early survey experiments on nitrosyl chloride and calibration of detection systems were carried out with a slightly modified commercial flash lamp pumped dye laser which typically produced 30 mJ of 500 nm light in a 400 ns pulse. The base laser was a Phased-Radiation (Phase-R) Model 2100-C equipped with a 15 mm ID coaxial flash lamp. It was operated in the triax configuration which entails insertion of a second annular tube of 8 mm ID to provide a channel of flowing water between the lamp and the central dye. This configuration reduced the energy output somewhat but allowed an increase in the repetition rate to 0.5 Hz by providing a shock wave and heat absorbing layer which reduced schlieren effects and thermal

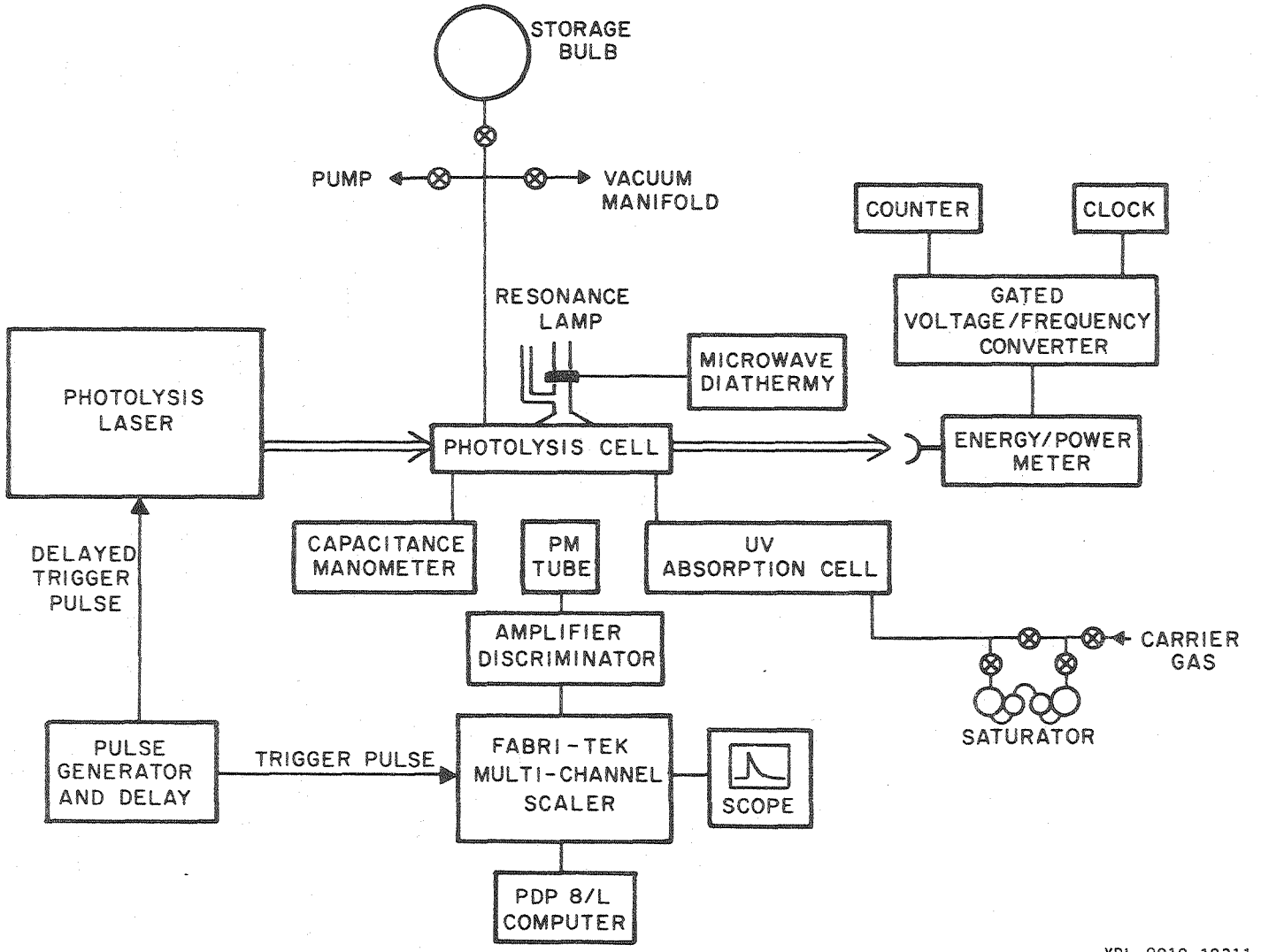

Fig. 3. Schematic diagram of the experimental apparatus.

lensing. The use of a triax is also reported to increase the ultraviolet doubling efficiency due to the more Gaussian beam profile obtained, but this effect was not observed in this work.

Close temperature matching of the dye and cooling water was discovered by Magnotta[54] to be essential for maximum laser output and repetition rate. Thermal control consisted of circulating both dye and cooling water through parallel systems which included a stainless steel reservoir with circulating pump, a coil of 50 feet of thin-wall stainless steel tubing immersed in a 50 gallon tank of agitated water, the laser head, another coil in the same room temperature bath, and return lines to the reservoir. Differential temperatures were continuously monitored with in-line thermistors and the temperature differential was kept below 0.01 K.

The laser beam was dispersed by a 1200 line/mm high energy grating from PTR optics operated in the Littrow configuration. The laser bandwidth was ~5Å with the cavity length most frequently employed. All experiments reported here were performed using Coumarin 504 (Exciton Chemical Corp.) in methanol at 500 nm. Wavelength and bandwidth measurements were performed as follows. A pellicle in the beam path split off part of the laser pulse and directed it through a 1 meter monochromator onto the face of a P.A.R. 1205 D Vidicon tube from which an optical multichannel analyzer (OMA) displayed a spectrum on a CRT screen with a resolution of 0.4Å per channel. Gate pulses from the OMA fired the laser and initiated the vidicon scan after a 20 μs delay to avoid RFI pickup from the laser. Wavelength calibration of the monochromator/OMA

system was accomplished using the output of a Neon calibration lamp and the known Ne lines.

The entire laser assembly was enclosed in a grounded, metal clad room to shield the detection and signal averaging equipment from RFI resulting from the laser spark gap.

The photolysis source for all other experiments was a Lumonics Model 860-1 Excimer laser on loan from the San Francisco Laser Center. It was operated on the KrF transition at 249 nm or the XeF transition at 350 nm as appropriate. The excimer laser was typically operated with a gas mixture that contained about 60% of the rare gas concentration recommended by the manufacturer. Laser power was somewhat higher and the life of a gas fill was as long using this modification which minimized usage of the expensive rare gases Kr and especially Xe.

The output energy of the excimer operating on KrF is 250 mJ per pulse maximum and about 150 mJ per pulse at the minimum discharge voltage. The experiments reported here required far less energy (5-30 mJ) and so some method of beam attenuation was required. The characteristics of the excimer output suggested an easy solution to this problem. The beam divergence is relatively high (11.2 x 18.8 mrad) and the output beam is large even at the output optic so sufficient attenuation could be achieved by placing the excimer ~1.5 meters from the photolysis cell and using a series of apertures to reject the unwanted light. A 2 cm diameter circular aperture was placed 15 cm in front of the photolysis cell and served to block most of the unneeded laser pulse. Another aperture was placed immediately in front of the cell window and served to define the beam that transitted the photolysis cell and impinged

on the power meter located immediately after the cell. Both apertures were constructed of 1.5 mm Al sheet with the appropriate hole punched and then blackened with graphite to minimize back reflection.

2. Measurement of Precursor Concentration

The ultraviolet absorption system used for measurement of precursor concentrations is shown in Fig. 4. The radiation from a Beckman Deuterium lamp which passed through a 3.2 mm aperture in the housing was chopped at 400 Hz by an American Time products tuning fork chopper. The beam was then reflected and directed through a 97.5 cm optical path, 2.3 cm ID absorption cell and impinged upon the entrance slit of a McPherson Model 218, 0.3 meter monochromator. The monochromator was equipped with a 2400 line/mm grating blazed at 150 nm and 100 μm slits which resulted in a bandpass of 3 Å (FWHM). After exiting the monochromator the light struck the cathode of an RCA IP-28 photomultiplier tube operating at -900 V. The resulting signal from the PMT was amplified and sent to a lock-in amplifier whose output was displayed on a digital voltmeter.

After warm-up times of several hours to overnight, the optical baseline was stable for hours. Drifts of a few parts in 200 were noted from the beginning of the day to the end. On the time scale of one kinetic experiment, no drift occurred after sufficient warm-up time.

The monochromator wavelength drive was calibrated by measuring the position of 12 Hg lines from 222 to 313 nm.[23] The relative positions agreed to 0.5 Å. Response of the system in the visible was tested in two ways. First a series of neutral density filters was introduced into the beam and the decrease in signal checked. Having satisfied this test, the monochromator was set at 350 nm and several calibrated

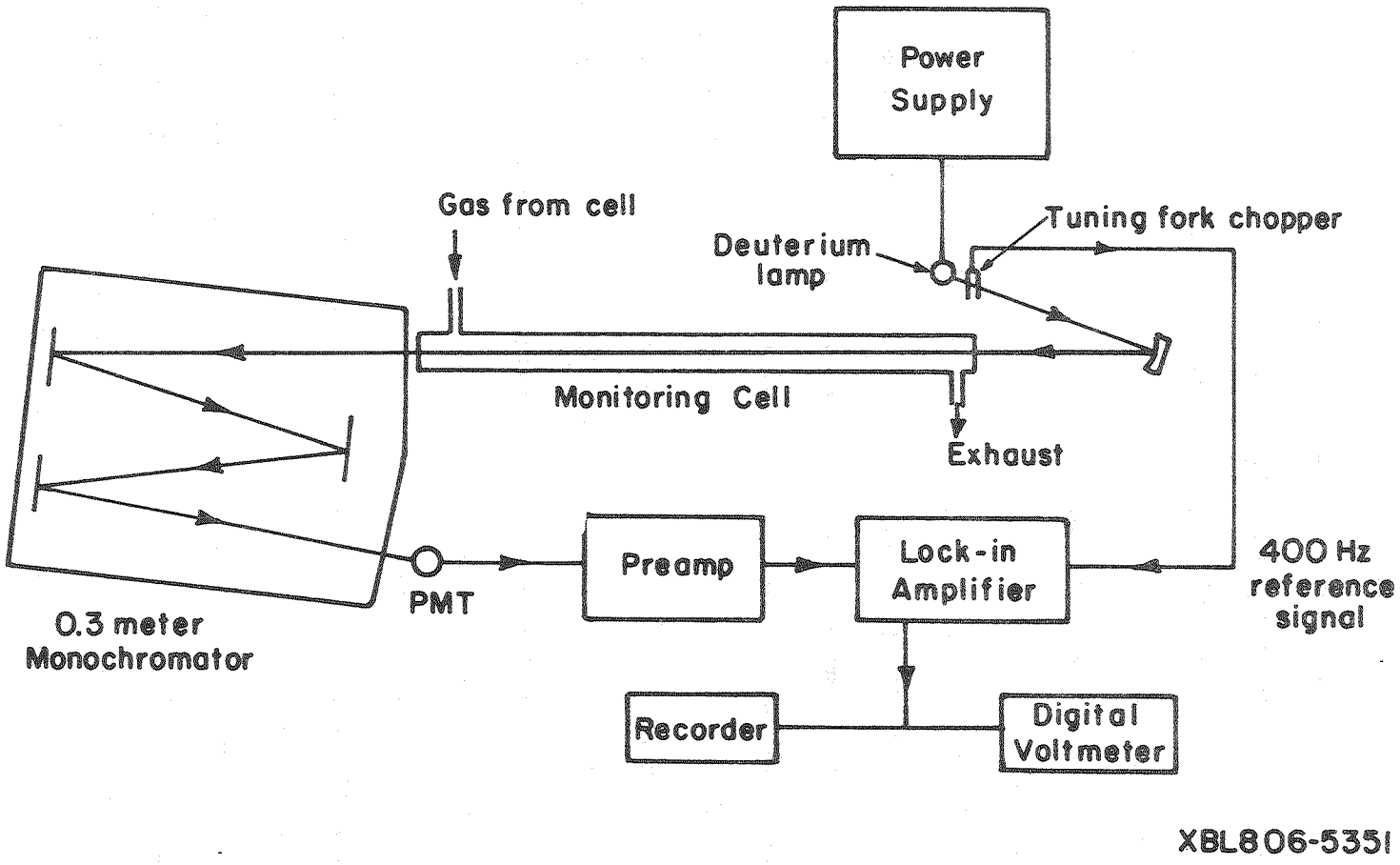

Fig. 4. Ultraviolet absorption system used for measurement of precursors.

NO_2/N_2 mixtures were flowed through the cell at measured total pressures. Calculated NO_2 concentrations were in excellent agreement with those quoted by the supplier.

3. Precursor Mixing and Flow

The photolytic precursors were contained in a pyrex saturator maintained at a constant temperature by immersion in a dewar containing an appropriate solvent/liquid nitrogen slush. After passage through a flow meter, the carrier gas was split into two streams; the flow rate to both streams was controlled by stainless steel needle valves. One stream of carrier flowed over the precursor resulting in partial saturation. After exiting the saturator, the two streams were recombined and directed through the UV absorption cell where the concentration of reactant was continuously monitored. The gas stream then entered the photolysis cell where the pressure was measured by a Baratron MKS Model AHS-100 capacitance manometer and was pumped through a glass vacuum manifold and liquid nitrogen trap by a rotary mechanical pump.

The concentration of product and total pressure stabilized within 5 minutes in this system. Over the course of an experiment, reactant concentration typically drifted less than 3% except at the lowest concentrations where a drift of 5% was not uncommon. The saturator containing the precursors was equipped with a manifold that allowed the gas stream to pass over the liquid reactant or bypass it entirely. I_o was easily measured before and after each run by use of this option.

A few of the ClNO photolysis experiments were performed with a ClNO/Ar mixture from a storage bulb rather than the saturator. Small

quantities of this mixture were metered into the main flow before the UV absorption cell; all other procedures were identical with those above.

4. Detection of Photolysis Products

The product detection systems and the standard photolysis cell are pictured in Figs. 5 and 6. The microwave driven resonance lamp, which was designed along the lines suggested by Watson,[55] consisted of a #9 O-ring joint with a gas inlet located as close to the window as possible in order to minimize self-reversal of the emitted radiation. The resonance lamp window was attached with a thin coat of Torr-Seal vacuum epoxy around the perimeter of the window to minimize contact with lamp gases and VUV radiation. Lamp fuel gas passed through a stainless steel needle valve, which served to drop the pressure to the desired operating range, and then into the lamp. Exhaust gas from the lamp was pumped by a rotary mechanical pump through a liquid nitrogen trap. Residence time using this configuration was approximately 2 seconds. Black anodized aluminum collimators were inserted at the resonance lamp input and fluorescence collection output of the cell to minimize scattered light and light piping through the walls of the cell.

The photolysis cell, designed by Magnotta,[54] consisted of a 3.8 cm diameter, 10 cm long laser path and two large, perpendicular Wood's horns facing the lamp and photomultiplier tube which was connected through a #13 O-ring joint serving as the optical exit port. The entire cell and optical exit tube were externally blackened, and the cell volume minimized to decrease reactant decomposition during flow through the cell.

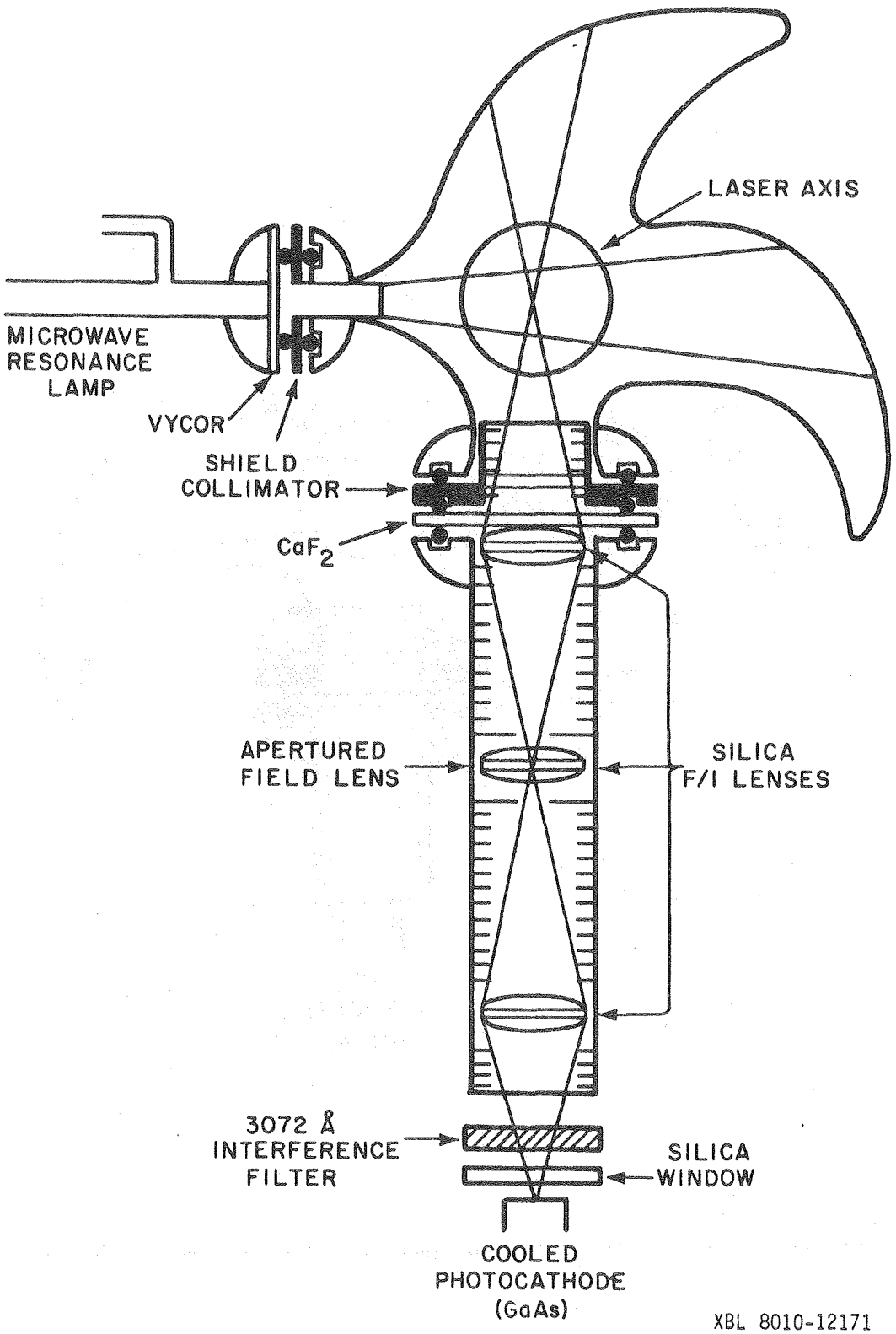

Fig. 5. HO detection system and photolysis cell used in this work.

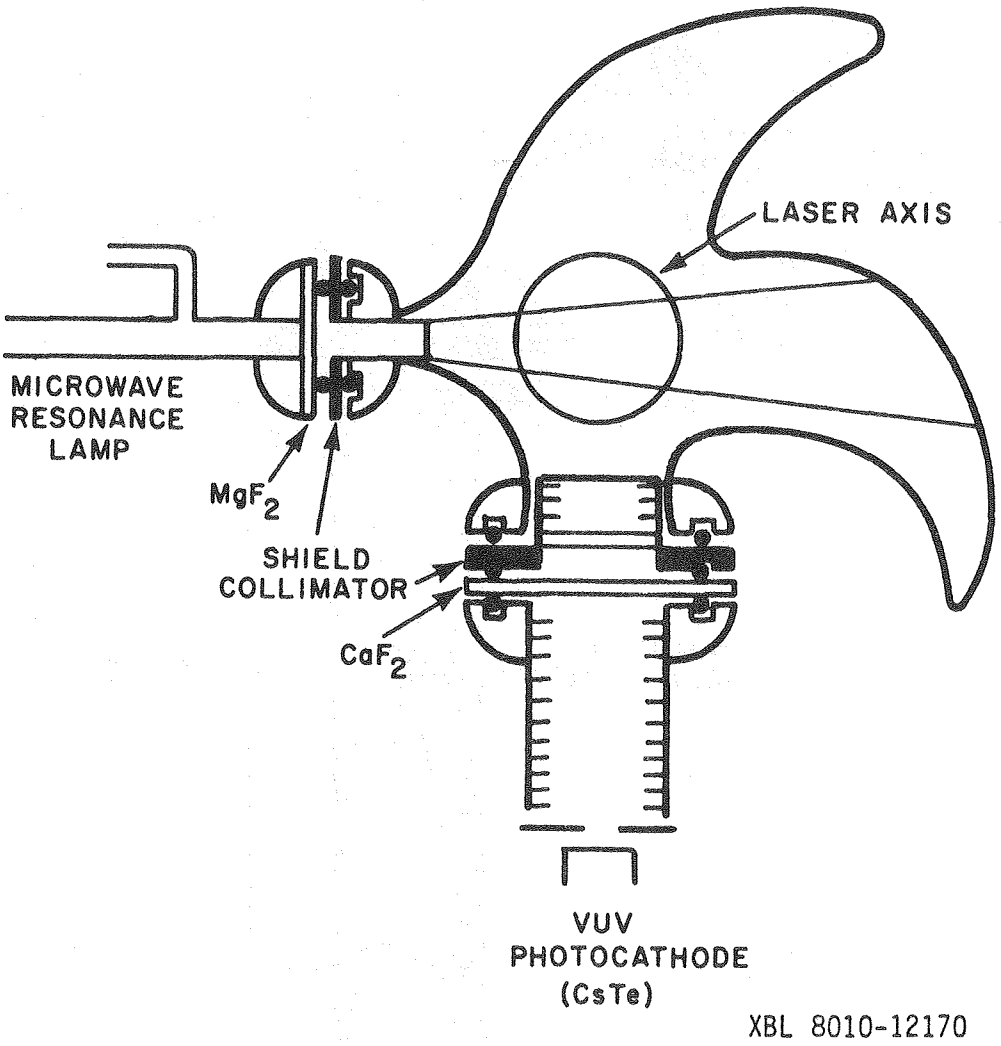

Fig. 6. Atomic detection system and photolysis cell used in this work.

The microwave source was a current stabilized Burdick Model MW/200 Medical Diathermy, which operated at 2.54 GHz, coupled to the cell by a 1 m waveguide and Evenson cavity. The cavity was air cooled to minimize heat build-up and the resulting fluctuations in resonance radiation output.

For HO radical detection, the lamp gas was a 3% H_2O in Ar mixture at 600 m Torr total pressure. This was prepared by bubbling Ar through a water saturator, into a ballast volume, and through the needle valve into the lamp. Because of the trace impurities of N_2 and O_2 in the Ar carrier gas used (see Table 1), several VUV O and N atom resonance lines and UV NO lines were present in the lamp output as well as the Lyman -α line at 121.5 nm and the desired HO bands. Because these extra lines would needlessly contribute to background levels and DC reactant photolysis, this resonance lamp was sealed with a 3 mm thick Vycor window which had a transmission cutoff of 200 nm. The output spectrum of the resonance lamp in the vicinity of the 308 nm (0-0) band of the $A^2\Sigma^+ - X^2\pi_i$ transition is shown in Fig. 7 along with the transmission spectrum of an interference filter with nominal center wavelength of 307.2 nm. There was also some output from the 1-0 band around 281 nm but this amounted to less than 10% of the total intensity.

The fluorescence excited by the resonance lamp, exited the cell through a CaF_2 window and was focused with three (f/1) Suprasil-1 lenses contained in a baffled optical tube onto the cooled GaAs cathode of an RCA 31034 photomultiplier tube through the 307 nm interference filter, which blocked both laser light and NO emission not absorbed by the Vycor lamp window. The photomultiplier tube was operated in the negative

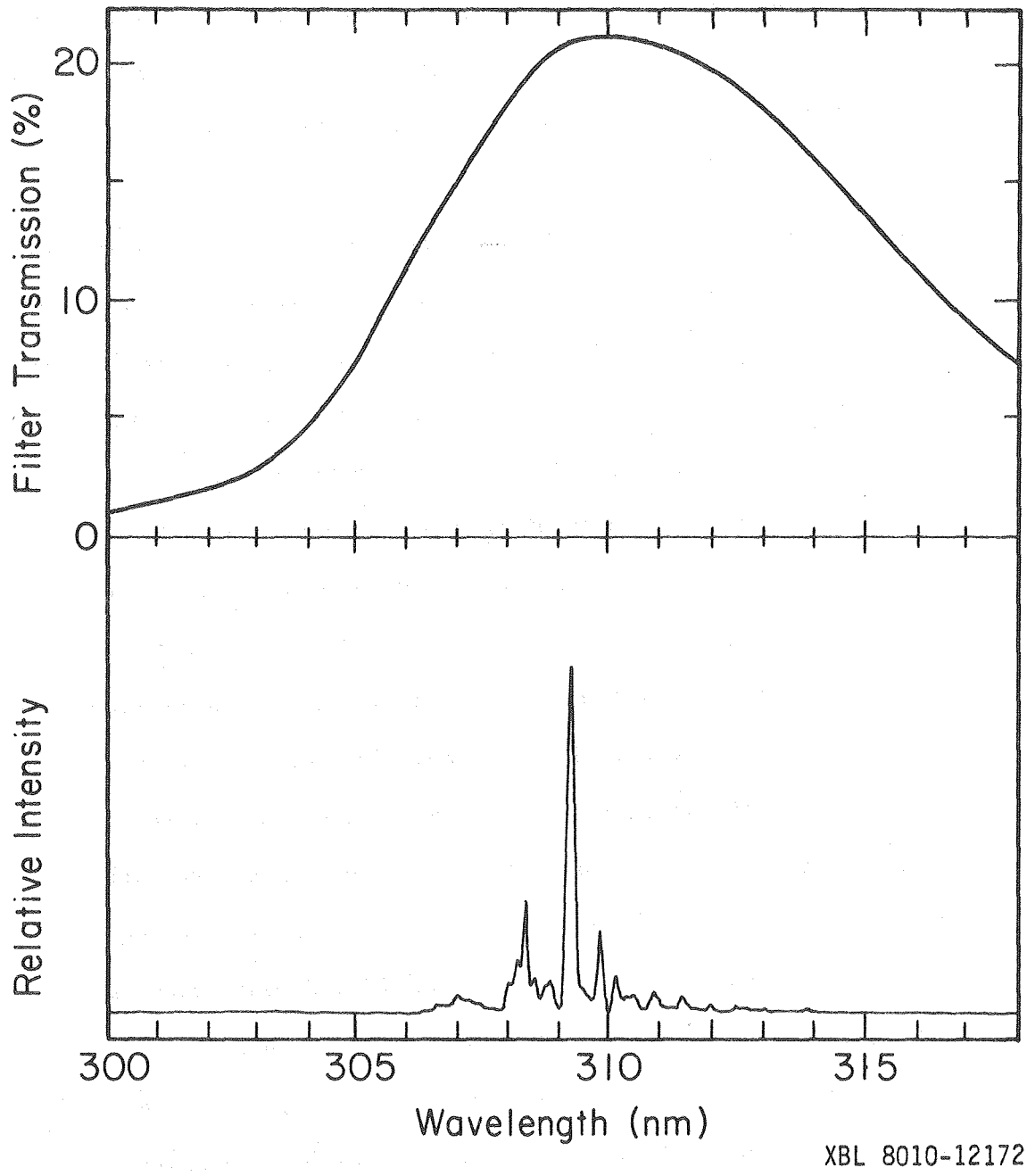

Fig. 7. Lower panel: emission spectrum of the HO resonance lamp.
Upper panel: transmission spectrum of the interference filter used for HO detection.

high voltage cathode configuration for photon counting and was contained in a magnetically and RF shielded housing. Cold N_2 blow-off from a container of liquid N_2 was blown through the housing to cool the tube while warm, dry N_2 was blown over the housing window to prevent condensation build-up.

For the O and Cl atom studies, the detection system was changed somewhat: the resonance lamp window was changed to MgF_2, the lenses were removed and the optical tube shortened, and the photomultiplier tube was changed to one with a CsTe cathode for use in the vacuum ultraviolet. The only filter in this case was the CaF_2 exit window which did not pass Lyman -α radiation.

The Cl lamp was run on a 0.1% Cl_2 in He mixture[29] at 1 Torr total pressure. The spectrum of the Cl atom lamp is shown in Fig. 8 from which it can be seen that the most intense lines are members of the $^4P - {}^2P$ multiplet at 138.0 ($^4P_{3/2} - {}^2P_{3/2}$) and 139.0 nm ($^4P_{5/2} - {}^2P_{3/2}$). Also to be noted is the small contribution to the total fluorescence intensity from the O atom triplet around 130 nm despite the previously discussed O_2 impurity in the lamp mixture. A nitrogen line at 141.2 nm was of much greater intensity but was of little consequence since no N atom production is expected in the experiments planned in this work.

The O atom lamp was run on extra pure helium, which has enough O_2 impurity to produce O resonance radiation. A higher total intensity could be produced by using more concentrated O_2/He mixtures but the detection sensitivity was lower indicating significant reversal of the O atom lines.[54] The spectrum of the O atom lamp, which consists of

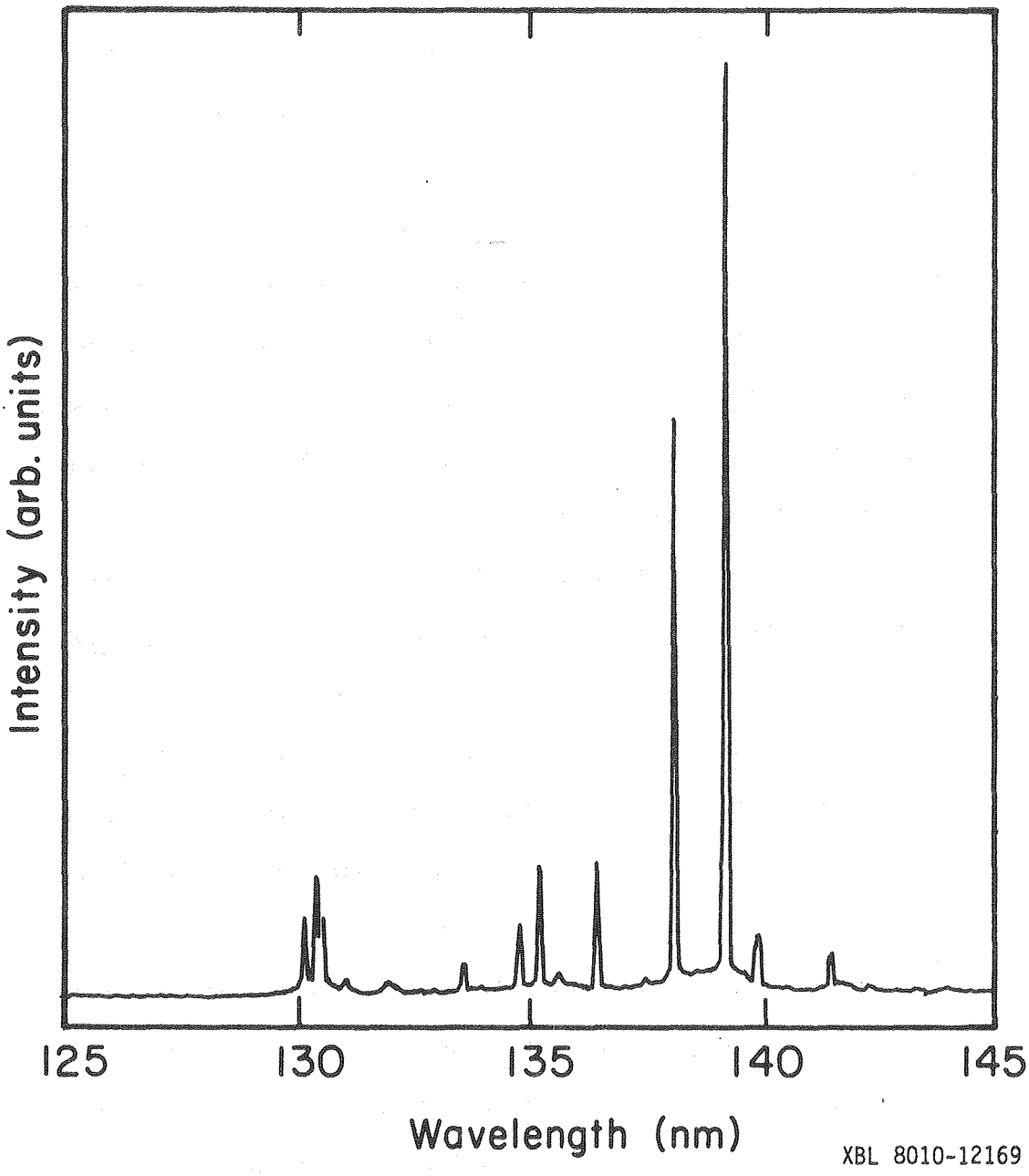

Fig. 8. Emission spectrum of the Cl atom resonance lamp.

a $^3S_1 - {}^3P_{2,1,0}$ triplet at 130.2, 130.5, and 130.6 nm, is shown in Fig. 9. Note that at the resolution used, the lines at 130.5 and 130.6 nm are incompletely resolved.

5. Laser Energy Measurements

When using the Phase-R as the photolysis source, pulse energy measurements were obtained with a Gentec system. This consists of a "spectrally flat," pulse intensity integrating pyroelectric joule meter (Model ED200) and a peak reading sample and hold with digital display (Model PRJ-D). This unit was calibrated by Magnotta[54] and checked after this work by Marinelli.[13]

Experiments with the excimer as photolysis source were run at a repetition rate of 30 Hz, which is above the response limit of the Gentec system. For these runs, average laser power was measured with a Scientech Model 36-0001, surface absorbing power meter with a response time constant of 10 seconds. Since all experiments were run with flowing gas mixtures, it was possible to start the laser pulsing about 1 minute before initiation of product detection and power measurement to insure that correct readings were obtained. Over the course of a 2-9 minute measurement, laser drift was $< 5\%$. The signal from the power meter head, which is a voltage proportional to the power, was amplified 10x and fed to a gated voltage to frequency converter, the output of which was counted continuously throughout an experiment. A separate clock controlled the V/F gate and timed the counting period. This system provided a convenient, relatively precise method of measuring the average pulse energy for use in quantum yield experiments.

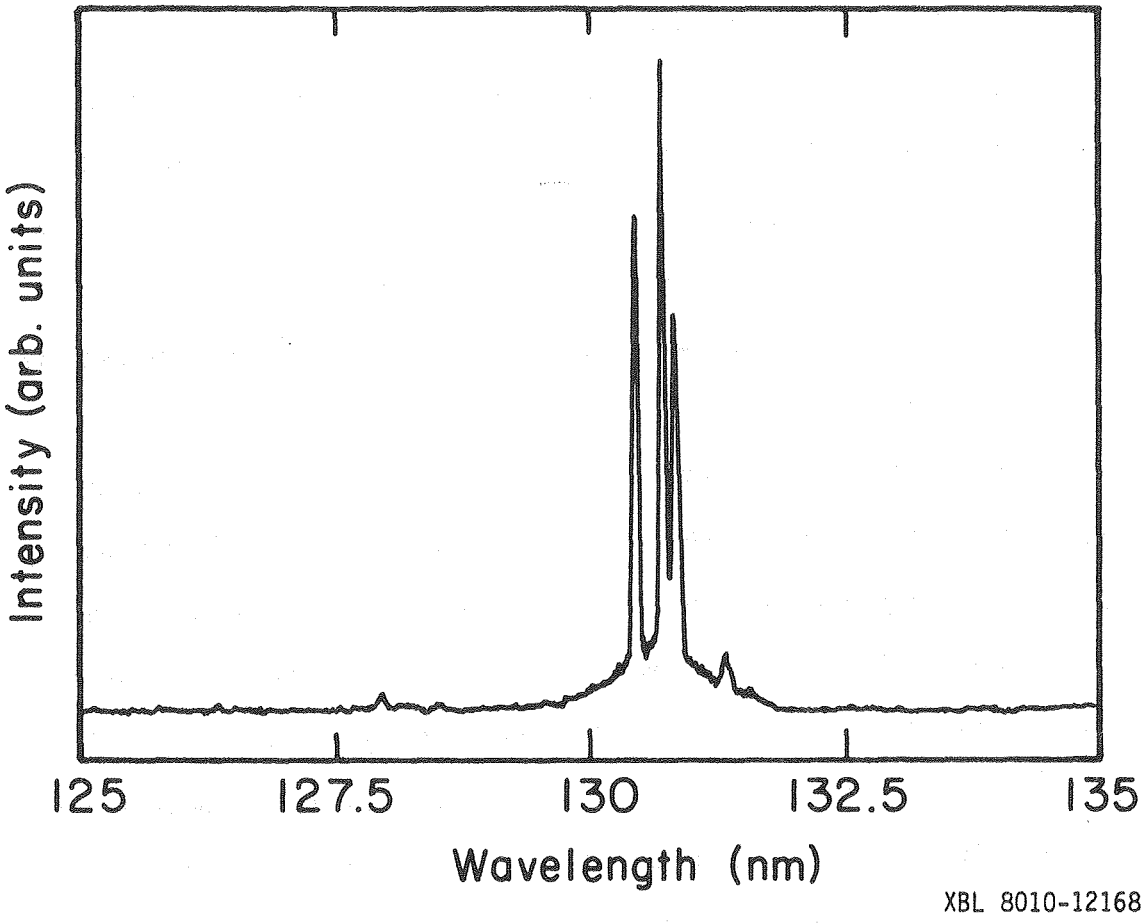

Fig. 9. Emission spectrum of the O atom resonance lamp.

Calibration of the head was performed by electrical substitution heating. Voltage from a Heathkit Model IP-1711 power supply was applied to the internal heater of the power meter. The heater resistance was specified by the manufacturer and confirmed by current measurements. The system output frequencies as a function of power dissipated in the head are listed in Table 2 and shown plotted in Fig. 10. The system response is seen to be linear over the region in which experiments were performed.

Table 2. Power meter calibration.

V/F Output (Hz)	Power (Watts)
92	.096
203	.216
363	.384
458	.486
566	.599
812	.863
1109	1.175
1453	1.535

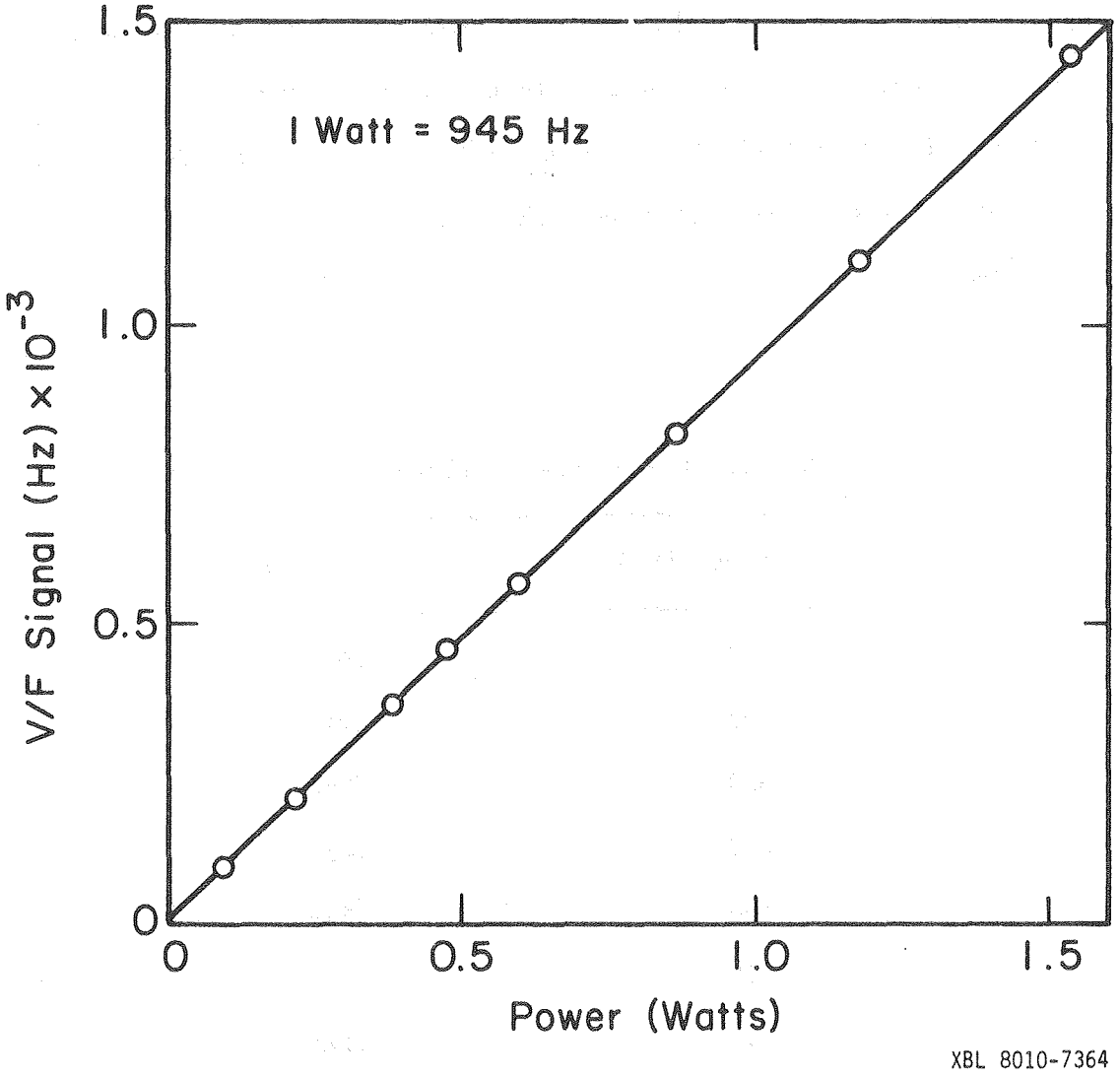

Fig. 10. Experimental V/F output frequency vs electric power dissipated in the power meter.

6. Signal Processing

All fluorescence signals were handled by the photon counting technique. The output of the monitoring photomultiplier tube was fed into a P.A.R. Model 1121, high gain amplifier/discriminator operated in the single threshold mode. The 1121 was interfaced to an S.S.R. Model 1105 photon counter which was modified with an ECL/TTL converter and a high speed line driver. The output signal was then sent to a Nicolet Instruments (Fabritek) Model 1074 Instrument Computer which was operated in the multichannel scaler mode. The Fabritek memory was filled in 1024 channel segments at scan times of 5 to 20 μs/channel.

The Fabritek sweep was initiated by the sync pulse from a Datapulse Model 102 pulse/delay generator. The laser was triggered, after a pre-trigger time of 2 - 5 ms, by another pulse from the delay generator. At the conclusion of the experiment the contents of the Fabritek memory were transferred to paper tape for long term storage. Data manipulation and rate constant calculations were performed in a PDP 8/L minicomputer which is interfaced to the Fabritek.

D. Experimental Procedures

1. Ultraviolet Cross Section Measurements

The nitric acid absorption cross section at 200 nm was measured in the absorption cell used for all reactant concentration measurements and shown in Fig. 4. As in the kinetic experiments, nitric acid was picked up from a saturator maintained at 250 K by one part of a stream of He. After saturation, various amounts of the HNO_3/He were mixed into the main flow of pure He and directed to the absorption cell. The nitric acid concentration was kept in the same range as when

experiments were performed; this led to an optical density in the range 0.5 to 1.5, the absorbance best suited to cross section determinations. In order to complete a measurement in a reasonable length of time, the total flow rate was much higher than during the kinetic experiments (3 l min^{-1} vs 0.3); the measured cross section should be independent of flow rate. After flowing through the absorption cell, the HNO_3/He mixture was sent either around or through a titration cell for determination of the average HNO_3 concentration. The titration cell contained a NaOH solution, typically 10^{-4} moles in 200 ml H_2O, and two drops of bromthymol blue whose indicator range is pH 6 to 8. During a typical titration the flow was sent through the titration cell and the timer was started. The absorbance of the gas stream was continuously monitored (absorbance drifts of 10% were tolerated) during the course of the titration. After the endpoint was reached, the average absorption, total gas flow, and total moles of HNO_3 from the titration were used to calculate an absorption cross section.

Careful measurement of the HNO_3 absorption cross section from 215 to 180 nm and routine spectroscopic measurements of nitric acid and all other gases used were carried out on a Varian Instruments Cary 118C spectrometer. These measurements were made to establish the composition of reaction mixtures at each stage of reactant preparation, determine impurity levels in the final products, or confirm literature values of cross sections for UV monitoring.

A 10 cm long, 2.5 cm diameter cell was used for the absorbance measurements. The Cary, which is a double prism instrument, was

operated with a 0.1 mm slit in most cases which resulted in a bandpass of 1.2 Å (FWHM) at 200 nm and 11Å at 350 nm.

Static determinations of the HNO_3 cross sections were performed in the following manner. The absorption cell was connected to a vacuum line and evacuated for measurement of I_o. After this, nitric acid vapor was expanded into the cell and allowed to remain several minutes before pumping out. This wall pacification procedure was repeated twice more. The desired pressure of nitric acid was then admitted to the cell and the absorption spectrum recorded. Some of the measurements were made on HNO_3/N_2 mixtures. In this case, I_o was measured with the N_2 present and, after adding HNO_3 to the cell, it was brought to the total pressure chosen with N_2.

2. Reaction Kinetics and Photolysis Quantum Yields

As mentioned previously, the reactants were maintained in a constant temperature slush bath during each experiment. The temperature required was a function of the reactant vapor pressure, concentration required, and flow rate. The actual choices are listed in Table 3. Because of the large range of nitric acid investigated, several slush baths were used.

Table 3. Saturator temperatures for each experiment.

Reactant	Slush bath	T (K)
HNO_3	o-xylene/liquid nitrogen	244
	acetonitrile/liquid nitrogen	232
	m-xylene/liquid nitrogen	224
H_2O_2	ice	273
ClNO, $ClNO_2$, $ClONO_2$	ethanol/liquid nitrogen	157

Each individual measurement of a psuedo-first order rate constant, k', was performed in the same general way. After general system warm-up, the precursor detection system was tuned to the appropriate wavelength and I_o was measured with all the carrier gas flowing around the saturator. Part of the flow was diverted through the saturator and I was monitored until the flow of reactant stabilized. At this point, laser firing was started and the power meter began to register. After several response time constants of the power meter, I was checked to see that no drift had occurred and the multichannel scaler sweep and energy integration timer were started simultaneously. After the desired number of laser shots, the sweep and integration were halted, final I of the UV monitor was recorded, and all flow diverted around the saturator so as to check final I_o. Typical drift of precursor concentration during a run was 1-2% with any run in which drift was greater than 7% rejected.

The multichannel scaler memory contents were displayed on an oscilloscope and subjected to the data analysis scheme discussed in section A.3. The total counts from the energy integration were normalized by

the calibration factor derived in section C.5., the total integration time as recorded by the system timer, and the laser repetition rate as measured by a Heathkit Model IM-4110 frequency counter which was calibrated against a Hewlett-Packard Model 5246L counter. This manipulation resulted in the average energy per shot.

The laser energy had to be measured for the reduction of the quantum yield data but was also recorded during the purely kinetic runs. This allowed the calculation of the average initial radical concentration for each run which was useful for several reasons. All experiments were carried out with the radical concentration at the upper end of the linear range, therefore knowledge of the radical concentration was important as a check that linearity was maintained. Knowing the radical concentration also allowed the calculation of a detection sensitivity for each run. This was used in the nitric acid study to derive the efficiency of quenching the HO $^{2}\Sigma^{+}$ state and in all experiments as a means of detecting long term variations of the resonance lamp output or photomuliplier tube response.

Within each kinetic system, the above measurement of k' was repeated as a function of precursor concentration. The concentration ranges used were chosen to make the experimental decay time constants range from 0.5 to 20 milliseconds. The lower limit corresponds to the fastest decay that could be reliably measured in the present study and the upper limit was imposed by diffusion out of the detection zone. In order to test this last assertion and insure that third order reactions were not responsible for the observed decays, several of the systems were also studied as a function of total pressure.

3. Calibration of Product Detection Systems

Examination of the output of atomic resonance lamps using the resolution shown in Figs. 8 and 9 is only useful for determination of impurity lines or other interferences. Okabe[56] has discussed the various emission profiles that are encountered from atomic resonance lamps of several classes. The high intensity lamps used in this work belong to Okabe's Class D: Resonance Lamps with Two Layers. In order to understand the emission of a lamp of this kind, it is necessary to consider both the emitting layer of excited atoms in the plasma and an absorbing layer along the window. This leads to an emitted line which is Doppler broadened at the high temperature of the discharge and exhibits self reversal due to absorption by the cooler, more dense absorbing layer. The utility of the lamp for excitation of room temperature radicals in the photolysis cell varies according to the degree of self-reversal the lamp exhibits. For this reason, an actual check of the detection sensitivity is the only meaningful way to assure oneself that the chosen lamp is fulfilling its purpose.

Two checks of the performance of the Cl atom lamp used in this study were performed. The sensitivity was measured and a check was made to insure that the fluorescence signal scaled linearly with the Cl atom concentration over the range of concentrations encountered in the photochemical and kinetic studies. The source of Cl atoms in these experiments was the photolysis of Cl_2

$$Cl_2 + h\nu \xrightarrow{\lambda = 350} Cl + Cl \qquad (15)$$

by the 350 nm XeF band of the excimer laser. A 0.06% Cl_2 in Ar mixture was prepared and the Cl_2 concentration verified by UV absorption. Various dilutions of this mixture in pure Ar were flowed through the photolysis cell at 10 Torr total pressure and photolyzed by the laser. The resonance fluorescence signal was monitored as a function of time after the flash using 20 μs channels and the signal was accumulated for 4096 laser shots. Average laser energy was measured simultaneously by the method described in section C.5.

The experimental decay curves were fit to an exponential and the amplitude and decay time constant extracted. The decay time constant in each case was 10 ms, which is a measure of Cl atom diffusion under these conditions. The amplitudes were converted to count rate and are listed in Table 4 along with the corresponding Cl atom concentration which was calculated from the measured laser energy, Cl_2 concentration, and Cl_2 absorption cross section.[57] These data are plotted in Fig. 11.

As can be seen, the Cl atom detection system response is linear for Cl concentrations below 1.5×10^{11} molecules cm^{-3}. The slope of the line fit to the data in Fig. 11 yields the reciprocal sensitivity which is 4.9×10^{6} molecules cm^{-3} Hz^{-1}. This sensitivity is in the range normally encountered for systems such as this.[55] The calculated intercept is 164 Hz which is 0 within the experimental error.

Table 4. Cl detection sensitivity

Fluorescence count rate (Hz) x 10^{-3}	[Cl] Concentration (molecules cm^{-3}) x 10^{-10}
4.77	2.27
7.10	3.35
11.68	5.77
17.20	8.04
22.9	11.0
24.5	11.8
29.8	14.5

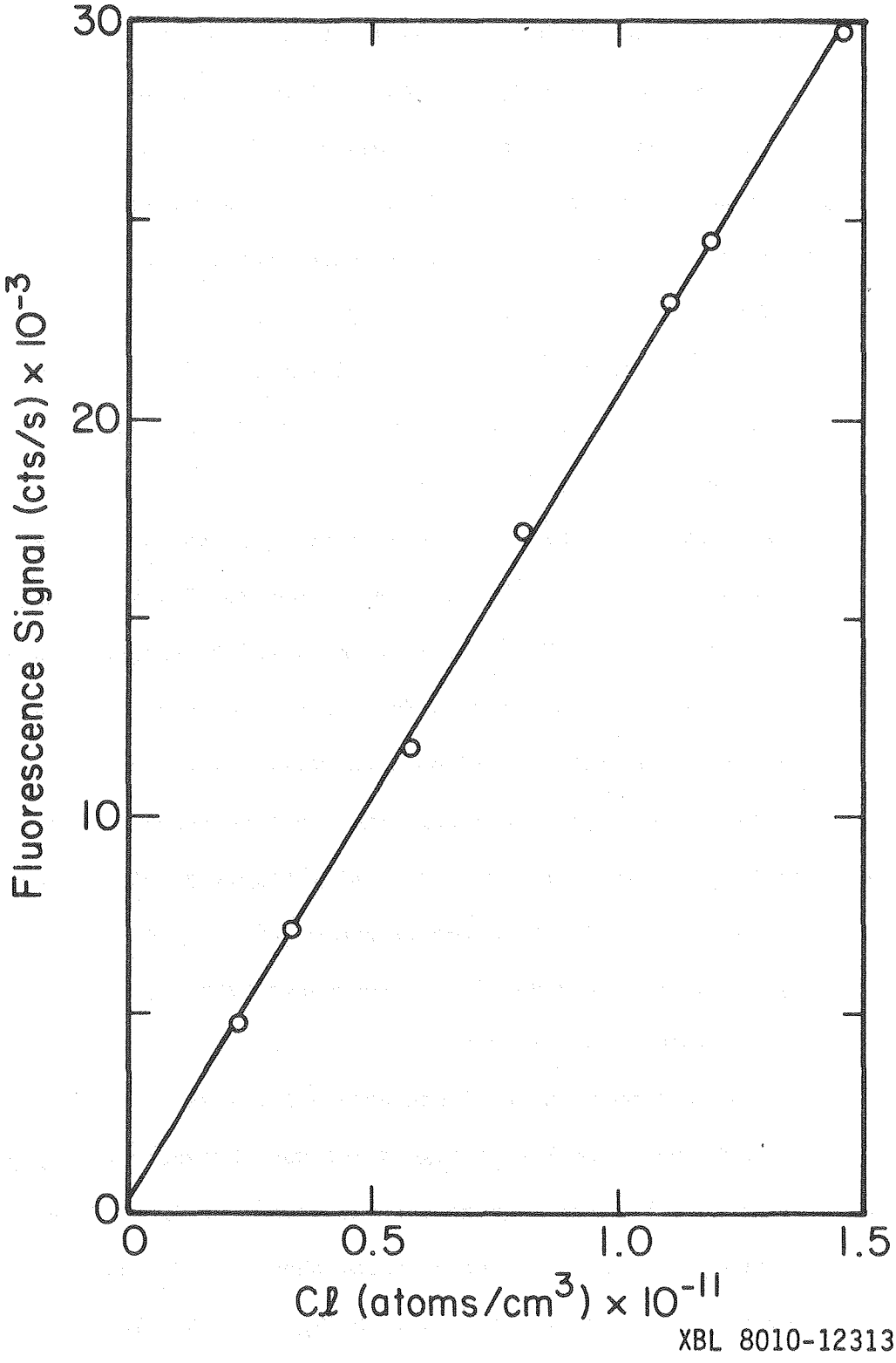

Fig. 11. Cl atom fluorescence signal vs concentration.

Although this calibration seems like a straightforward process, there were two complicating factors which merit discussion. A relatively large number of laser shots was needed to obtain acceptable signal-to-noise in the Cl atom decays. Clyne and Cruse[29] have noted emission from molecular chlorine resonance series excited by the Cl atom lamp. These bands were first measured from 140-180 nm and assigned by Rao and Venkateswarlu.[58] Dispersion of the emission in the work of Clyne and Cruse[29] showed that it extends to 135 nm; all wavelengths at which the monitoring PMT is sensitive.

The accuracy of the calculated Cl atom concentrations is uncertain on two counts. Concentration determinations for Cl_2 were based on dilution ratios of the Cl_2/Ar mixture measured by pressure in a flowing system. The fraction photolyzed was calculated using Cl_2 absorption cross sections tabulated at 10 nm intervals. Since this is a region of relatively steep slope in the Cl_2 cross section curve, the cross section used is only an approximation. But, as the purpose of this calibration was to prove linearity of system response and give an indication of the degree of self-reversal in the resonance lamp, the quality of the results obtained is sufficient.

An O atom lamp with the identical fuel gas as that used in the present work and a similar configuration was characterized by Magnotta[54] so only one calibration measurement was made. An O_3 in N_2 mixture was flowed through the UV absorption system where the O_3 concentration was measured by its absorption at 253.7 nm ($\sigma_{O_3} = 1.15 \times 10^{-17}$ cm^2) and then into the photolysis cell. The Phase-R operating at 600 nm was used as the photolytic source.

$$O_3 + h\nu \xrightarrow{\lambda > 310 \text{ nm}} O_2 + O(^3P) \qquad (16)$$

The average O atom concentration was calculated from the known O_3 visible cross section,[59] the measured O_3 concentration, and the measured average laser energy. The calculated sensitivity was 8.05×10^5 molecules cm^{-3} Hz^{-1}.

Comparison of this number with the measured Cl atom sensitivity illustrates the effect of self-reversal in the Cl lamp. The Cl atom absorption cross section for the resonance radiation is approximately 2 times that of O atoms.[56] Since the signal observed in a resonance fluorescence experiment is of the form:

Signal = Radical Concentration x Source Intensity x Absorption x Fluorescence Efficiency x Detector Efficiency ,

the larger absorption should lead to larger signals and thus lower sensitivities. The O atom lamp is run with helium with a typical O_2 impurity of 0.2 ppm. The tank used was selected by Magnotta[54] for its superior lamp output. The maximum impurity, however, is only 0.5 ppm. Thus, although the total intensity of the O atom lamp is lower than the Cl lamp (run on 0.1% Cl_2 in He) the Cl emission line obviously suffers greater self-reversal due to the greater Cl density between the plasma and the exit window.

There are two components of the HO detection system to be checked. In this system the resonance fluorescence is focused onto the PMT cathode to overcome some of the reduction of sensitivity due to the lowered

molecular absorption coefficients. Sensitivity is thus a function of both lamp output and accuracy of focusing the fluorescence signal.

Two parameters of the HO resonance lamp, the emission intensity in the 308 nm band and the HO detection sensitivity, were therefore measured before its use. For the total intensity measurement, the 308 nm band was isolated by the interference filter to be used in the experiment and passed through a cell containing approximately 4 Torr NO_2 and 400 Torr N_2. By measuring the NO_2 concentration as a function of time exposed to the resonance lamp, a photolysis rate constant can be determined. An emission intensity of 1.4×10^{15} photons cm^{-2} s^{-1} is calculated using the NO_2 absorption cross section determined by Graham.[59]

Only a qualitative test of the HO detection sensitivity was possible at the time due to use of the Phase-R as a photolysis source, but this confirmed that the detection system was aligned properly. A mixture of O_3, H_2O, and Ar was flowed through the cell. The relative concentrations of each component were determined by pressure measurements. The frequency doubled output of the Phase-R at 290 nm was used for O_3 photolysis. At this wavelength, the quantum yield for production of $O(^1D)$ is close to 1.

$$O_3 + h\nu \xrightarrow{\lambda < 310} O_2 + O(^1D) \qquad (17)$$

$$O(^1D) + H_2O \longrightarrow HO + HO \qquad (18)$$

The $O(^1D)$ produced reacted primarily with H_2O, which was present in a 10:1 ratio to O_3, to produce 2HO radicals. The sensitivity measured in this experiment was 3×10^7 molecules cm^{-3} Hz^{-1} with an experimental

uncertainty of at least a factor of 2 due to the many approximations made. This sensitivity combined with typical noise levels leads to a limit of detectivity with S/N=1 of 5×10^9 after 4096 shots. This is somewhat worse than that reported by Wine, Kreutter, and Ravishankara[60] but is adequate for the work planned.

III. HO RADICAL KINETICS

Each of the HO reactions reported in this work were studied by measurement of the relative HO concentration as a function of time after the initiating laser pulse. The HO decay time was used to derive rate contants for the reaction of HO with HNO_3 and H_2O_2. Quenching of the $HO(A^2\Sigma^+)$ state by HNO_3 was derived from the relative amplitudes of the HO signals. HO radicals were produced by laser photolysis of the precursors with the 249 nm KrF transition of the excimer.

All experiments were performed using Ar as the carrier gas. This choice was made for reasons of detection sensitivity. Twelve experimental measurements of the $HO(A^2\Sigma^+)$ state lifetimes have been reviewed by Schofield.[61] He suggests a value of 0.76 μs for the lifetime of v'=0. All possible molecular carrier gases have a large value for the collisional quenching rate constant of this $^2\Sigma^+$ state. The most favorable of these is N_2 for which Schofield[61] recommends $k_{19}(N_2) = 2.2 \times 10^{-11}$ cm^3 molecule^{-1} s^{-1}.

$$HO(A^2\Sigma^+) + M \longrightarrow HO(X^2\pi) + M \qquad (19)$$

However at a total pressure of 10 Torr at which it is more convenient to work, the HO fluorescence quantum yield with N_2 as the carrier would be only 0.16. The Ar quenching efficiency however is at least 500 times lower[61] than that for N_2 and the fluorescence quantum yield will be essentially 1. Another consideration, although minor, is Ar quenching of vibrationally excited $HO(A^2\Sigma^+)$. As mentioned previously, about 10% of the HO resonance lamp emission is in the 1-0 band of this transition.

The interference filter in front of the monitoring PMT does not pass this resonance fluorescence. Ar quenches the upper state vibration with a rate constant of $\simeq 3 \times 10^{-12}$.[61] This results in about 40% of the HO excited to v'=1 being quenched to v'=0 before they fluoresce.

A. Kinetic Results

1. The Reaction of HO with HNO_3

Nitric acid was monitored by its absorption at 200 nm. This was not the ideal wavelength for this purpose since the cross section is very steep at this wavelength and the possibility of error is therfore large. Because of the low HNO_3 concentration used in this work, the absorption at longer wavelengths, where the cross section curve is flatter, is below the detection limit for the UV monitoring cell. At the short wavelength peak of the absorption curve, atmospheric absorption of the deuterium lamp output results in insufficient light for accurate detection.

There were three previous measurements of the HNO_3 absorption cross section at 200 nm reported in the literature which differed by 20%. Because of this, the cross section was measured during the course of these experiments by the flowing titration method. The 200 nm cross section was measured as 6.5×10^{-18} cm^2 and this value was used in the calculation of all rate constants. There is good agreement on the HNO_3 cross section at 249 nm. Using a value of $\sigma = 1.9 \times 10^{-20}$ cm^2 in conjunction with laser intensities of less than 3×10^{16} photons cm^{-2} $shot^{-1}$ results in photolysis of less than 0.06% of the HNO_3 precursor per shot.

The nitric acid used in these experiments contained approximately 0.15% NO_2. This impurity was measured throughout the course of the

kinetic measurements by periodically expanding the nitric acid from the saturator to a pressure of approximately 5 Torr in the UV absorption cell and measuring the NO_2 concentration by its absorption at 350 nm. The detection system response in this wavelength region was checked during the course of the experiments by measurements on a calibrated NO_2/N_2 mixture. The measured HO radical decays were corrected for the effects of the reaction HO + NO_2 + M (Reaction 1).

The HO decay curve collected in a typical kinetic experiment is shown in Fig. 12. In this case, the signal after 16,384 laser shots was accumulated using 20 μs channel widths. Notice the one channel spike due to laser electrical noise at the beginning of the decay. These data are shown plotted in Fig. 13 as ln(signal-background) vs channel number. Four hundred points, representing HO decay over two orders of magnitude, were fit in order to obtain a pseudo-first order rate constant and signal amplitude. This figure illustrates the number of points fit and the divergence of the experimental data for a typical experiment. The HNO_3 data are somewhat better than that collected for the other HO systems because of the larger number of laser shots per point (16,384 vs 4096) in the nitric acid work.

Although the reaction kinetics were measured at three pressures, primary emphasis was placed on experiments at 10 Torr total pressure for experimental reasons. The results of 19 pseudo-first order rate constant determinations at 10 Torr are listed in Table 5 and shown plotted vs nitric acid in Fig. 14. The line shown in the figure was drawn to fit the results at the lowest 16 concentrations. Three later experiments

at much higher nitric acid concentrations were performed in order to overlap with data collected in another experiment by Marinelli.[13]

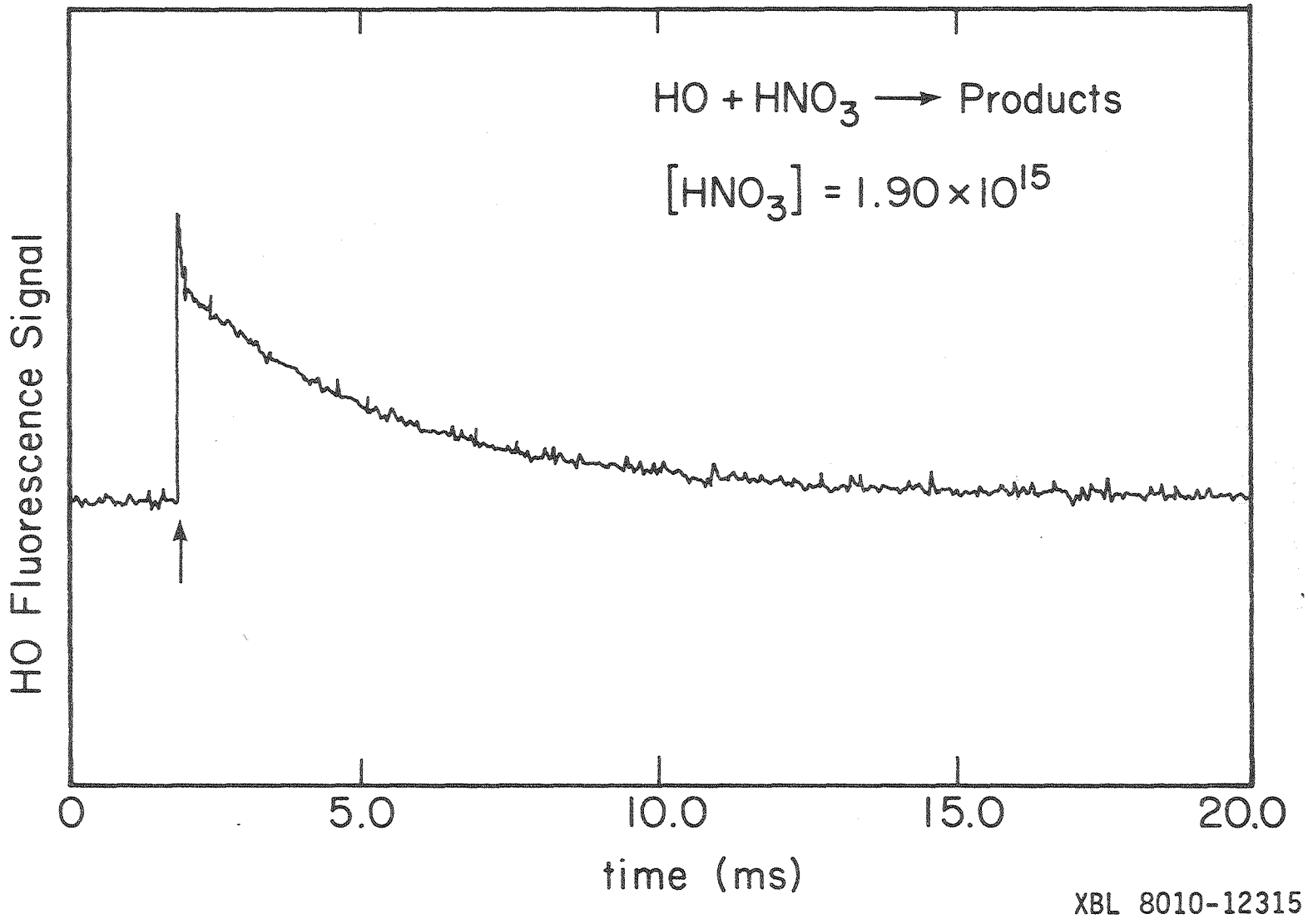

Fig. 12. Typical HO fluorescence signal vs time in the HO + HNO_3 system.

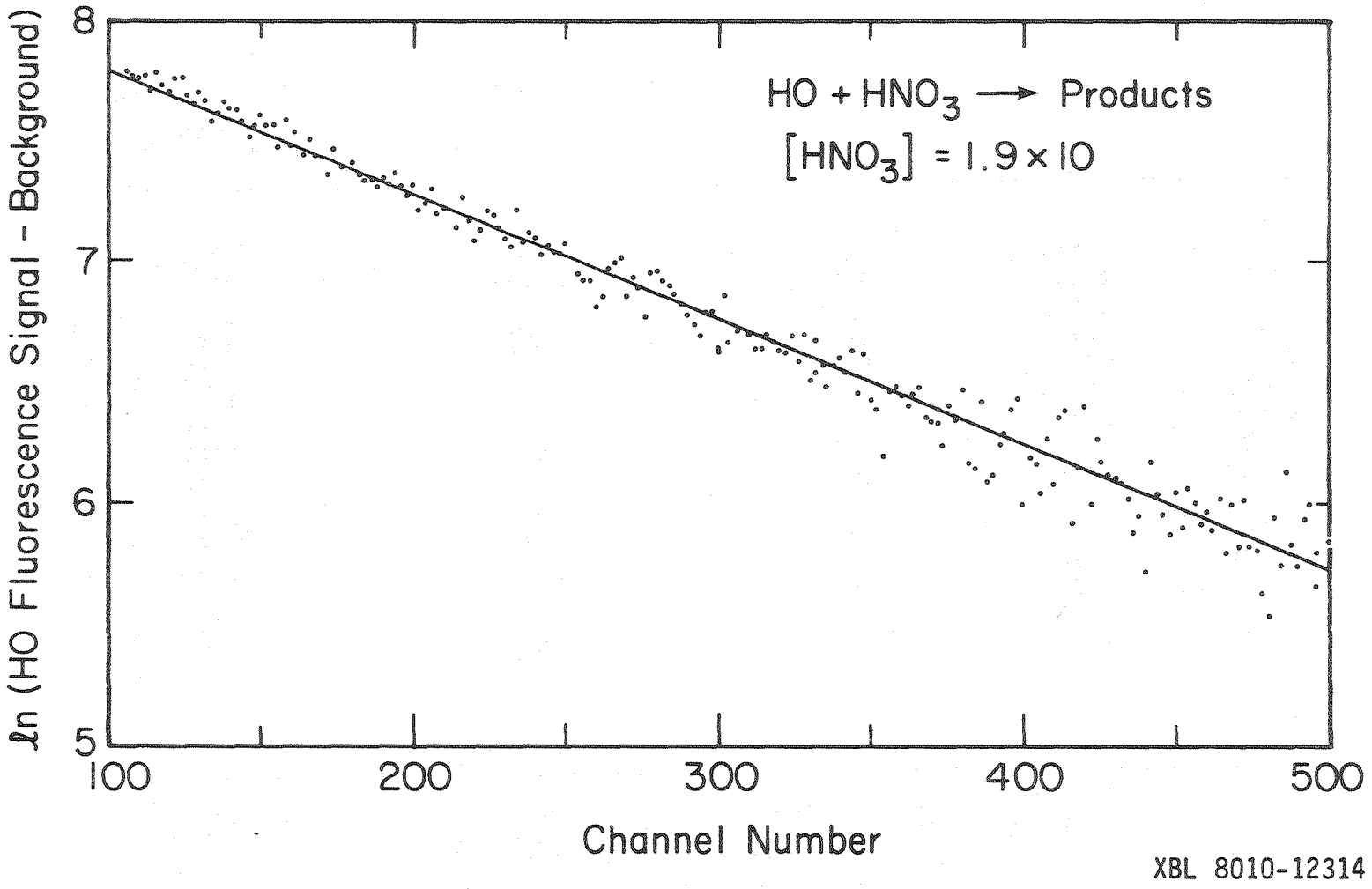

Fig. 13. ln(signal-background) vs channel number for the HO + HNO_3 run of Fig. 12.

Table 5. Kinetic data at 10 torr in the HO + HNO_3 system.

$[HNO_3] \times 10^{-14}$ (molecules cm^{-3})	$I_{laser} \times 10^{-16}$ (photons cm^2 $shot^{-1}$)	$[HO]_{calc} \times 10^{-11}$ (molecules cm^{-3})[a]	$k'_{measured}$ (s^{-1})	$k'_{corrected}$ (s^{-1})[b]
1.32	--	--	123.2	123.1
2.20	.92	.40	120.9	120.8
2.31	2.25	1.02	122.5	122.4
3.94	1.70	1.32	138.5	138.3
6.67	--	--	155.8	155.4
7.05	2.63	3.65	162.1	161.7
8.08	.71	1.13	164.6	164.1
9.08	2.16	3.86	174.6	174.0
11.3	1.42	3.16	194.4	193.7
11.5	.83	1.88	194.3	193.6
13.3	.76	2.00	206.1	205.3
15.6	--	--	227.5	226.5
17.5	.30	1.04	239.4	238.3
19.0	.95	3.55	258.2	257.0
23.1	.82	3.75	298.9	297.4
27.6	.27	1.47	329.3	327.6
32.1	1.01	6.40	328.7	326.7
54.5	.66	7.08	514.8	511.4
87.7	.55	9.55	814.9	809.4

[a] $[HO]_{calc} = \sigma I[HNO_3]$ where $\sigma = 1.93 \times 10^{-20}$ cm^2

[b] Corrected using $k(HO + NO_2) = 4.2 \times 10^{-13}$ and $[NO_2] = .15\%$

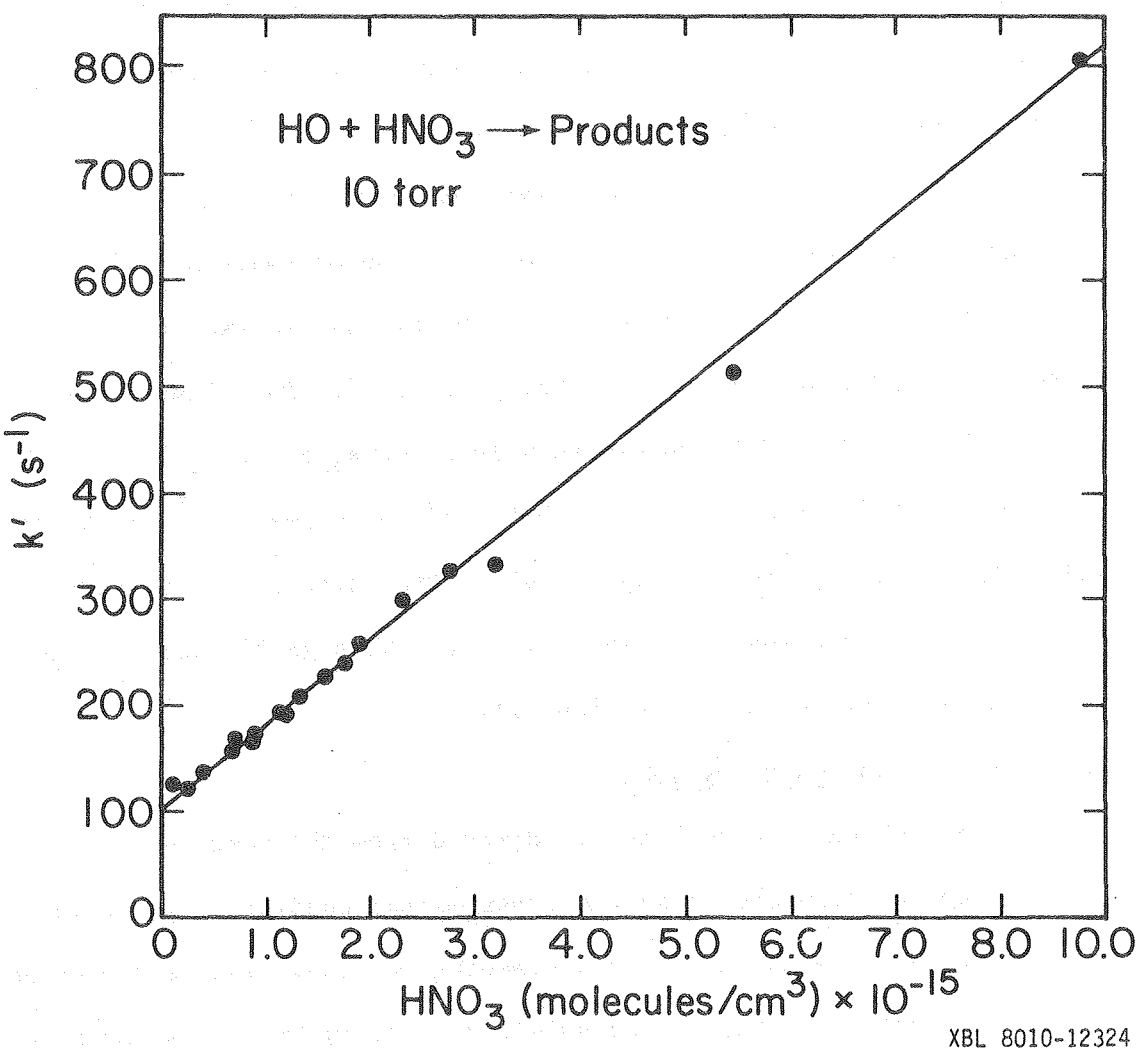

Fig. 14. Data for the HO + HNO_3 reaction at 10 Torr total pressure.

The initial HO concentration in these runs was much higher than the other runs and so the possibility of error is larger. These three points however agree well with the line determined earlier. Inclusion of these points in the data set to be fit, reduces the intercept somewhat but doesn't affect the calculated rate constant.

The data collected at total pressures of 25 and 50 Torr along with the appropriate correction for the contribution of reaction (1) are listed in Table 6. All data collected in this system except the three highest points at 10 Torr are plotted in Fig. 15. The linear least squares fit to these data result in values for k_2 of $8.0 \pm 0.3 \times 10^{-14}$, $9.2 \pm 0.6 \times 10^{-14}$, and $7.5 \pm .9 \times 10^{-14}$ cm^3 $molecules^{-1}$ s^{-1} at 10, 25 and 50 Torr total pressure respectively. The calculated intercepts for the three lines are 104, 113, and 259 s^{-1}. The significance of these values will be discussed in section B.1.

2. $HO(A^2\Sigma^+)$ Quenching by HNO_3

The quenching rate constant is derived from the data collected in the kinetic measurements so the experimental conditions for this section are exactly those of the preceeding section. The rate constant for collisional quenching of the $HO(A^2\Sigma^+)$ state by HNO_3 is so much larger than that for Ar that for the nitric acid concentration range used the $HO(A^2\Sigma^+)$ fluorescence quantum yield depends only on nitric acid quenching. From a measure of the relative fluorescence quantum yield and the known fluorescence lifetime,[61] the nitric acid quenching rate constant can be calculated.

Table 6. Kinetic data at higher pressures in the HO + HNO_3 system.

$[HNO_3] \times 10^{-14}$ (molecules cm^{-3})	$I_{laser} \times 10^{-16}$ (photons cm^2 $shot^{-1}$)	$[HO]_{calc} \times 10^{-11}$ (molecules cm^{-3})[a]	$k'_{measured}$ (s^{-1})	$k'_{corrected}$ (s^{-1})[b]
Total Pressure = 25 torr		$k(HO + NO_2) = 9.1 \times 10^{-13}$ cm^3 $molecule^{-1}$ s^{-1}		
3.52	.78	.54	145.0	144.5
5.37	.73	.78	164.2	163.5
7.10	.48	.67	171.6	170.6
8.69	1.10	1.88	193.9	192.7
9.26	.69	1.26	196.9	195.6
13.7	1.03	2.75	243.0	241.1
15.2	.93	2.19	251.2	249.1
20.1	1.13	4.47	317.0	314.3
25.0	.52	2.55	358.6	355.2
38.5			460.5	455.3
Total Pressure = 50 torr		$k(HO + NO_2) = 1.50 \times 10^{-12}$ cm^3 $molecule^{-1}$ s^{-1}		
2.02	2.55	1.01	271.9	271.4
4.81	2.63	2.50	299.6	298.5
6.29	2.68	3.32	309.9	308.5
9.43	1.10	2.04	320.1	318.0
13.1	.94	2.43	368.2	365.3
23.4	.46	2.13	437.4	432.1

[a] $[HO]_{calc} = \sigma I [HNO_3]$ where $\sigma = 1.93 \times 10^{-20}$ cm^2

[b] Corrected using $[NO_2] = .15\%$

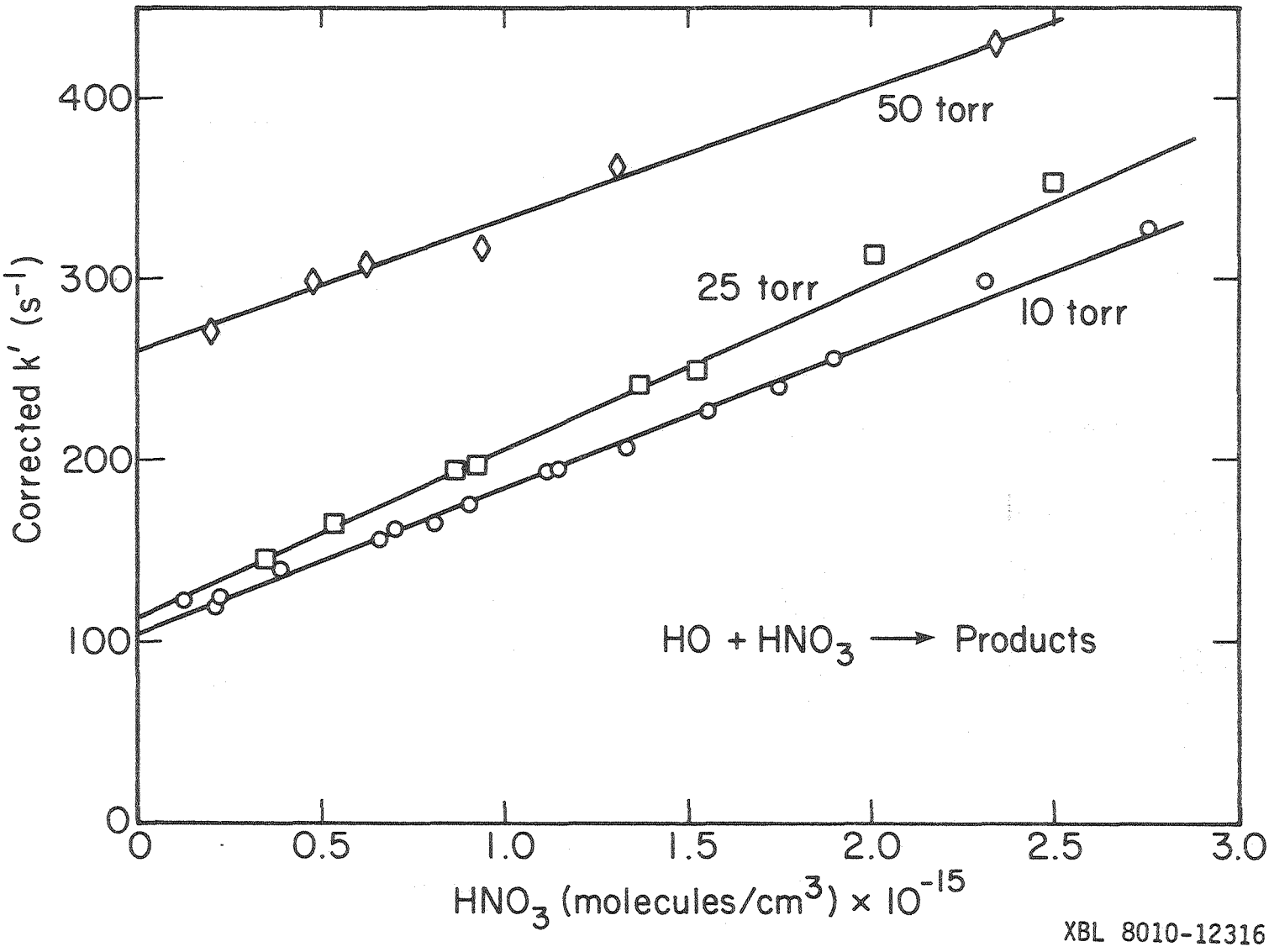

Fig. 15. All data collected for the HO + HNO_3 reaction.

The intial concentration of HO radicals formed by the laser pulse is calculated

$$[HO]_{t=0} = \sigma_{HNO_3} I[HNO_3] \tag{20}$$

using Eq. (20) where I is the laser intensity. The signal resulting from this HO is the zero time intercept of the measured decay curve and is calculated using

$$\text{Signal} = C \cdot \phi_f \cdot [HO]_0 \tag{21}$$

the steady state approximation for $HO(A^2\Sigma^+)$ by Eq. (21), where ϕ_f is the HO fluorescence quantum yield and C is an apparatus constant. This constant is itself made up of two parts. The population of $HO(A^2\Sigma^+)$ is a function of the resonance lamp intensity and the HO absorption coefficient. The other component of C is the proportionality constant between fluorescence rate and signal which is a product of cell collection efficiency and the monitoring PMT quantum efficiency. Substituting the full expression for fluorescence quantum yield leads to Eq. (22). This can be

$$\text{Signal} = C \cdot (1 + k_Q[HNO_3]/k_f)^{-1} \cdot [HO]_0 \tag{22}$$

rearranged to give Eq. (23)

$$[HO]_0/\text{Signal} = 1/C + k_Q[HNO_3]/k_fC \tag{23}$$

from which it is seen that a plot of $[HO]_0$/Signal vs nitric acid concentration results in a line width intercept = 1/C and slope equal to k_Q/k_fC. For the fitted line, slope/intercept yields k_Q/k_f.

The assumed apparatus constant C includes the production of $HO(A^2\Sigma^+)$ by the resonance lamp, the intensity of which can change from day to day because of variations in microwave power, total pressure in the lamp, or percentage H_2O in the fuel gas. Meaningful calculations can therefore only be made using data from within a single set of experiments. The data from two such series are listed in Tables 7 and 8 and both sets are plotted together in Fig. 16. The results calculated from the two sets of data are in reasonable agreement and lead to a calculated ratio $k_Q/k_f = 5.22 \times 10^{-16}$. Using the fluorescence lifetime suggested by Schofield,[61] the quenching rate constant derived is 6.9×10^{-10} cm^3 $molecules^{-1}$ s^{-1}.

3. Reaction of HO with H_2O_2

The hydrogen peroxide concentration in the UV absorption cell was measured at 200 nm. The absorption cross section used was 4.67×10^{-19} cm^2, which is the value reported by Molina and Molina.[40] Even at this wavelength the absorbance of the samples was less than 10% which restricted the range of peroxide concentration that could be used. The typical experiment involved photolysis of 0.1% of the initial reactant per pulse leaving $[H_2O_2]/[HO]$ ratios of at least 500.

The pseudo-first order rate constants measured at 10 Torr total pressure are listed in Table 9 and shown plotted in Fig. 17. The rate constant which results from a linear least squares fit to these data is $1.57 \pm .1 \times 10^{-12}$ cm^3 $molecules^{-1}$ s^{-1} and the intercept is 150 ± 10. Since this result confirms the rate constant measured in two flow tube experiments at ~ 1 Torr total pressure, no further investigations at other total pressures were performed.

Table 7. $HO(A^2\Sigma^+)$ quenching by HNO_3. Series 1.

$[HNO_3]$[a] $\times 10^{-14}$	I_{laser}[b] $\times 10^{-15}$	$[HO]_{calc}$[a] $\times 10^{-11}$	Intercept[c]	$\frac{[HO]_{calc}}{Intercept}$[d] $\times 10^{-6}$	Total pressure[e]
2.31	22.5	1.02	5253	6.36	10
3.52	7.83	.543	643	6.91	25
5.37	7.34	.776	957	6.65	25
7.05	26.3	3.65	3659	8.17	10
9.26	6.89	1.26	1143	9.00	25
13.3	7.62	2.00	1685	9.72	10
15.2	9.31	2.19	2256	10.1	25
19.0	9.48	3.55	2493	11.6	10
20.1	11.3	4.47	3171	11.6	25

[a] molecules/cm^3

[b] photons/cm^2 shot

[c] counts/20 μs channel

[d] molecules cm^{-3}/Hz

[e] Torr

Table 8. $HO(A^2\Sigma^+)$ quenching by HNO_3. Series 2.

$[HNO_3]$[a] $\times 10^{-14}$	I_{laser}[b] $\times 10^{-15}$	$[HO]_{calc}$[a] $\times 10^{-11}$	Intercept[c]	$\frac{[HO]_{calc}}{Intercept}$[d] $\times 10^{-6}$	Total pressure[e]
2.02	25.5	1.01	767	1.08	50
4.81	26.3	2.50	1469	1.39	50
6.29	26.8	3.32	1800	1.51	50
8.69	11.0	1.88	928	1.66	25
9.08	21.6	3.86	1660	1.90	10
9.43	11.0	2.04	953	1.76	50
13.1	9.4	2.43	1038	1.91	50
13.7	10.3	2.75	1043	2.16	25
23.4	4.62	2.13	776	2.25	50
25.0	5.17	2.55	762	2.74	25

[a] molecules/cm^3

[b] photons/cm^2 shot

[c] counts/20 μs channel

[d] molecules cm^{-3}/Hz

[e] Torr

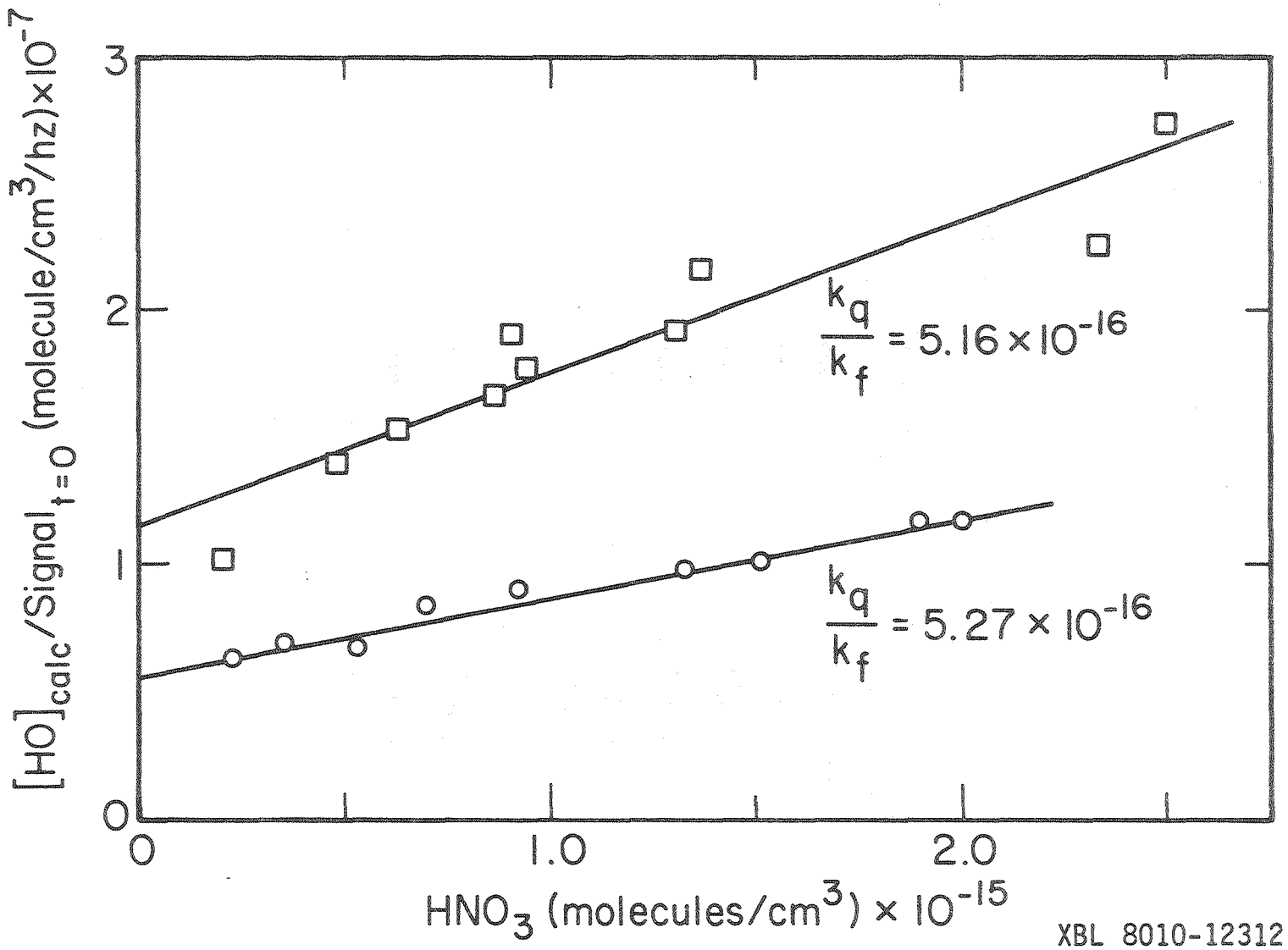

Fig. 16. Data for the collisional quenching of $HO(A^2\Sigma^+)$ by HNO_3.

Table 9. Kinetic results in the HO + H_2O_2 system

H_2O_2 (molecules cm^{-3})	measured k' (s^{-1})
3.13×10^{14}	566
5.11×10^{14}	871
5.12×10^{14}	905
6.95×10^{14}	1081
7.73×10^{14}	1294
9.91×10^{14}	1607
1.08×10^{15}	1770
1.49×10^{15}	2420
2.07×10^{15}	3049

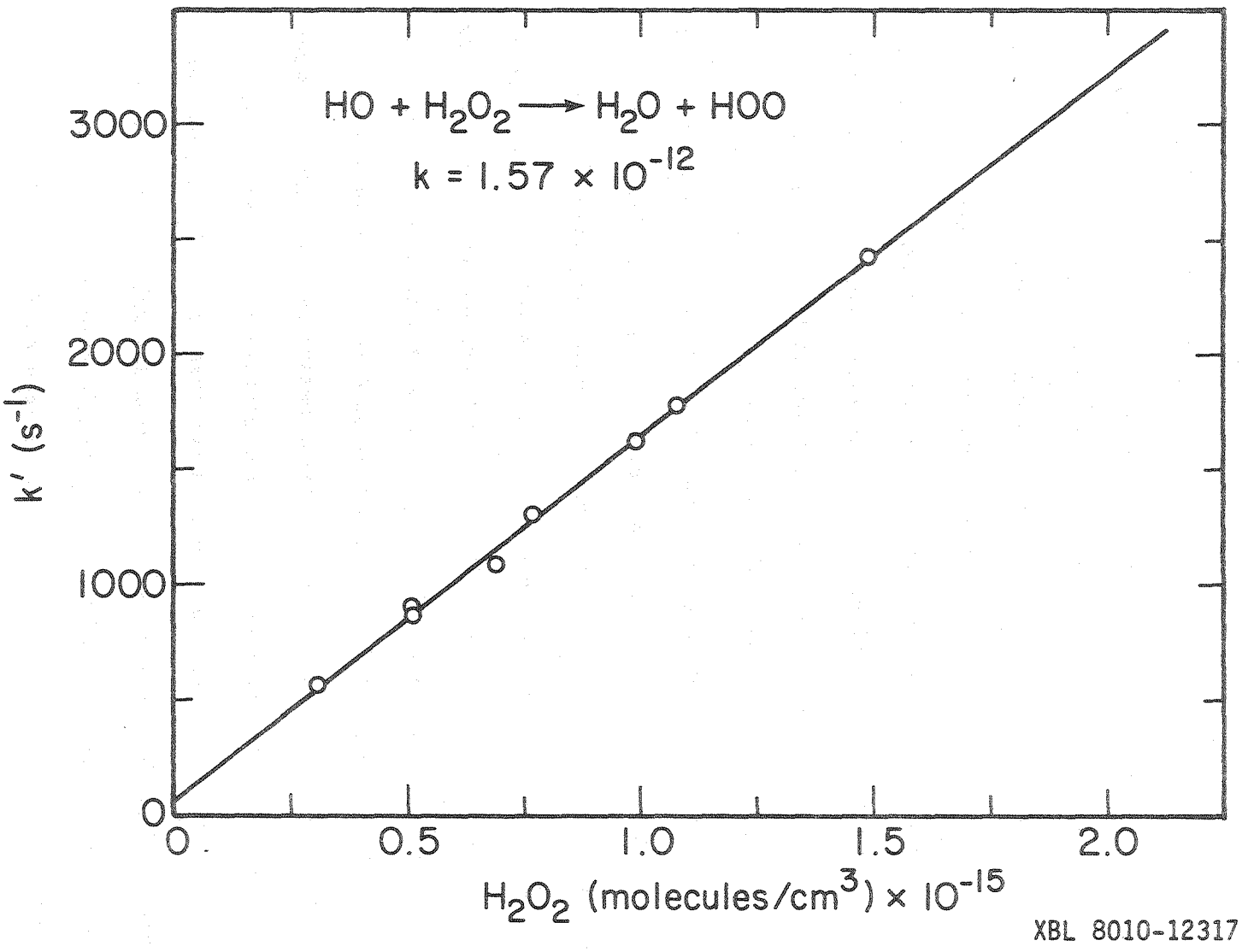

Fig. 17. Data collected for the HO + H_2O_2 reaction.

B. Discussion

A great deal of work was done early in the course of this work to insure that the precursor concentration measured in the UV absorption cell was equal to that in the photolysis cell. This is a necessary condition for accurate measurement of reaction rate constants. Indeed, after an initial series of ClNO photolysis experiments to be discussed in the next chapter and a few survey experiments in the HNO_3 system a concentration mismatch was discovered. In the experimental configuration used for these early experiments, a rather large pressure drop was discovered between the photolysis and monitoring cells. This led to an apparent rate constant much larger than that finally calculated.

After reversing the original order of the photolysis and monitoring cells, further measurements were made to determine if a pressure differential still existed. This effort took two forms, the first of which was a direct measurement of the total pressure in both the UV absorption cell and the photolysis cell. The first indications were that there was still a pressure drop from cell to cell but more careful measurements at several points along the flow system indicated that any pressure drop was at most 10%. The culprit in the first measurement was the placement of the Barocel which was used to read the photolysis cell pressure. In fact, it was positioned in such a manner than the cell pressure was 27% higher than the reading while normal flow was maintained. Therefore all total pressures listed in the kinetic results section should be taken as nominal values; the true values can be obtained by multiplying by 1.27.

The second, somewhat less accurate, test of the flow system involved UV absorption measurements in the photolysis cell concurrent with these normally employed in the UV cell. The light source for this experiment was a GTE DE50A deuterium lamp that was operated DC. After passage through the photolysis cell the light was dispersed by a Bausch and Lomb 0.2 m monochromator equipped with 1.5 mm slits; the resulting bandpass was ~12 nm. The selected light was detected by a PMT with CsTe photocathode whose output was measured with a picoammeter. The accuracy of this measurement was limited by the shorter path length of the photolysis cell (10 vs 97.5 cm) and the larger bandwidth and greater degree of scattered light in the monochromator used. Within the experimental uncertainty, however, this experiment confirmed the conclusion that little or no pressure drop occurs in the system in use for these kinetic and photochemical measurements.

1. $\underline{HO + HNO_3}$

As stated in the results section, the HNO_3 absorption cross section was measured in the flow system by titration during the course of the experiments. The value obtained based on 4 titrations was $6.5 \pm 0.8 \times 10^{-18}$ cm^2, where the uncertainty is one standard deviation. At the conclusion of the photolysis experiments, nine more repetitions of the titration experiment were performed and the value based on all 13 runs is $7.1 \pm 0.8 \times 10^{-18}$ cm^2. These two results are well within the experimental uncertainty of each other so the value obtained during the experiments is the one used for data analysis.

As a result of later reflection, several possibilities for error in the above measurements of the nitric acid cross section were investi-

gated. The titrations described were carried out at one atomosphere total pressure for reasons of experimental ease while the actual kinetic experiments were conducted at reduced pressure. The nitric acid spectrum in this region is a continuum, however, so no variation with total pressure should be observed. Confirming this, Graham[59] measured the cross section at both low pressure (<10 Torr) and atmospheric pressure and observed no difference. The titrations were also carried out with much higher gas flow rates than the kinetic measurements raising the possibility that differing wall adsorption of HNO_3, which is known to be quite "sticky" on Pyrex, led to a systematic error. This was investigated by going to the other end of the flow range, a static cell. The 10 cm quartz cell and Cary system described in Chapter II was used for these measurements. An attempt was made to avoid wall adsorption problems by twice expanding nitric acid vapor into the evacuated cell before filling it for the absorption measurements. Cross sections measured at low nitric acid concentrations were still systematically lower than those from high concentrations indicating that approximately 1.6×10^{14} molecules cm^{-2} were being adsorbed onto the walls of the cell. At 200 nm the cross section measured in the static cell was $6.0 \pm .2 \times 10^{-18}$ cm^2. This is within the experimental error of the earlier flowing determinations and the deviation is in the direction that would be expected if wall adsorption was not totally accounted for. The cross sections were measured for the range 180-210 nm in order to span the junction region where VUV measurements and UV measurements meet but don't overlap enough for accurate comparison. They are listed in Table 10 along with the flow system value.

Table 10. Nitric acid cross sections measured in this work.

(nm)	$\sigma_{\text{static system}}$ $(cm^2)^a$	$\sigma_{\text{flow system}}$ $(cm^2)^b$
210	9.9×10^{-19}	---
208	1.57×10^{-18}	---
206	2.34×10^{-18}	---
204	3.22×10^{-18}	---
202	4.42×10^{-18}	---
200	6.0×10^{-18}	6.5×10^{-18}
198	7.62×10^{-18}	---
196	9.48×10^{-18}	---
194	1.09×10^{-17}	---
192	1.27×10^{-17}	---
190	1.46×10^{-17}	---
188	1.55×10^{-17}	---
186	1.62×10^{-17}	---
184	1.62×10^{-17}	---
182	1.61×10^{-17}	---
180	1.58×10^{-17}	---

[a] $[HNO_3]$ measured by pressure

[b] $[HNO_3]$ measured by acid-base titration

These data are plotted in Fig. 18 along with all values for the absorption cross section reported in the literature. Substantial agreement among the several measurements, especially after considering the experimental difficulties associated with nitric acid concentration determination, is exhibited in this figure with the exception of the results of Okabe[62] which appear to be 20% lower than the others. Okabe[62] determined the concentration of nitric acid in his system by total pressure measurements after expansion of the vapor. The experience gained in this work leads one to conclude that wall adsorption problems could easily account for this discrepancy. The cross sections used in this work are certainly in agreement with the previous determinations. A quantitative comparison of all measurements at both 200 nm and the 249 nm photolysis wavelength is shown in Table 11.

A small correction was applied to each of the measured decays to correct for the contribution of reaction (1),

$$HO + NO_2 + M \longrightarrow HNO_3 + M \qquad (1)$$

the recombination of HO and NO_2, to the total HO removal rate. Throughout the experiments the NO_2 concentration was measured as 0.15% of the total. This leads to a correction of 3% in the worst case. The CODATA Task Group on Chemical Kinetics[19] has recently issued a series of recommendations on kinetic data for atmospheric chemistry. They have reviewed the literature through 1978 on reaction (1) and issued a recommendation for the rate constant. They represent the rate constant in the fall-off between the low pressure third-order limit and the high pressure second-order limit by means of a reduced fall-off curve where

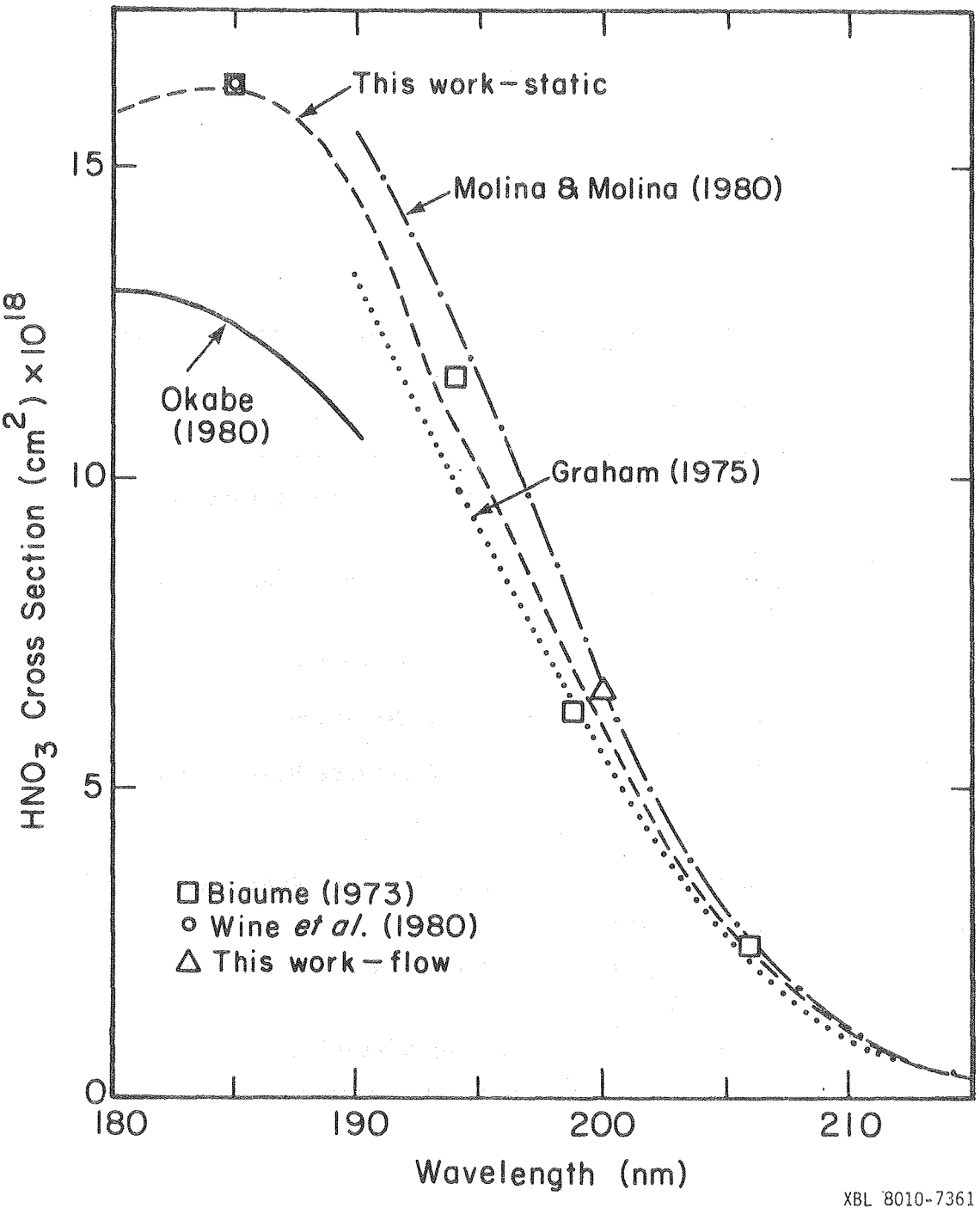

Fig. 18. Summary of the measured HNO_3 absorption cross sections in the region 180 to 210 nm.

Table 11. Summary of HNO_3 absorption cross sections near 200 and 249 nm.

λ(nm)	σ(cm^2)	Method	Reference
198.9	6.19×10^{-18}	Static/Pressure Measurement	63
199	6.3×10^{-18}	Static/Pressure Measurement	59
200	5.5×10^{-18}		
200	6.61×10^{-18}	Flowing/Titration	40
200	6.5×10^{-18}	Flowing/Titration	this work
200	6.0×10^{-18}	Static/Pressure Measurement	this work
248.5	1.98×10^{-20}	Static/Pressure Measurement	63
249	1.97×10^{-20}	Static/Pressure Measurement	59
250	1.95×10^{-20}		
250	1.91×10^{-20}	Flowing/Titration	40

k/k_∞ is plotted against $[M]/[M]_c$. More details of the derivation and application of this curve which is due to Troe[64] will be found in Appendix B. The second order rate constant at a specified concentration of third body M is evaluated by use of Eq. (24)

$$k = k_o\ (1 + [M]/[M]_c)^{-1}\ F([M]/[M]_c) \qquad (24)$$

in which $[M]_c$ is the concentration of M where the extrapolated value of $k_o[M]$ would be equal to k_∞ and F is a broadening factor which can be calculated or as in this case, derived from a fit to the available experimental data. At 300 K, the CODATA panel recommends $k_o(N_2) = 2.6 \times 10^{-30}$ cm^6 $molecule^{-2}$ s^{-1}, a value of $[N_2]_c = 6.2 \times 10^{18}$ molecules cm^{-3}, and $F_c = 0.75$ (see Appendix B). The work reported here was carried out with Ar as the M gas, so corrections must be made to the rate constant calculated to reflect the relative efficiencies of Ar and N_2 as third bodies in reaction (1). The recommended value for the ratio $\beta(N_2)/\beta(Ar)$ is 2.6 but this appears to be based solely on the result of an absolute measurement of k_o in Ar by Glanzer and Troe.[65] Several other measurements of the relative efficiencies have been reported[66-69] however and the average of all the values is 2.1. Using this ratio plus the recommendations for nitrogen as input, the rate constants for reaction (1) at nominal pressures of 10, 25, and 50 Torr are 4.2×10^{-13}, 9.1×10^{-13}, and 1.5×10^{-12} cm^3 $molecules^{-1}$ s^{-1}. These rate constants and the measured NO_2 level of 0.15% were used to calculate the corrected pseudo-first order rate constants listed in Tables 5 and 6.

An explanation is required for the seemingly contradictory values obtained as intercepts in the plots of pseudo-first order rate constant

vs nitric acid concentration. The "zeroeth order" interpretation of the intercept is that it is a measure of k_d, the rate constant for diffusion of the HO produced in the laser photolysis out of the resonance fluorescence detection zone. This rate constant should be the product of a collection volume term which is dependent on cell geometry and a diffusion rate constant which should vary inversely with pressure. In this approximation, the intercept will be lower at each succeedingly higher M gas pressure. Another contribution can be made to the measured intercept by reaction of the HO with impurities in the M gas used. This adds another term independent of $[HNO_3]$ to the k' expression. The intercept measured is then the sum of a term which varies inversely with pressure and one that increases linearly with pressure; behavior not unlike that seen in this work.

An experiment was performed to confirm the intercepts obtained from the fits to the HNO_3 data and confirm the explanation developed above. HO radicals were produced by the photolysis of O_3 in the ultraviolet in the presence of excess H_2O at various total pressures of Ar. This is exactly the system used to calibrate the HO detection system and the details are discussed in Chapter II. On the time scale of 10-20 ms the only HO removal processes in this system are diffusion and reaction with Ar impurities. The HO removal rate constants measured are listed in Table 12. The agreement between the two methods is excellent except at 50 Torr. Interpretation of these data requires the solution of three simultaneous equations of the form of Eq. (25).

$$\text{Intercept} = k_d/M + k_r \cdot M \qquad (25)$$

The data collected in the O_3/H_2O system seem to be internally consistent and lead to values of k_d = 1000 Torr s^{-1} and k_r = 8 x 10^{-17} cm^3 $molecules^{-1}$ s^{-1} based on the Ar concentration. This diffusion rate constant agrees well with a simple calculation based on hard sphere collisions and an estimate of the product detection volume. Table 1 in the preceeding chapter lists the impurities for the Ar used in this work. The reactions of HO with various hydrocarbons are relatively slow,[19] therefore the impurity levels listed are not sufficient to explain the observed reaction rates. The flow procedures used obviously introduced additional impurities into the Ar carrier used which are responsible for the observed HO removal. The high value of the intercept in the 50 Torr HNO_3 case does not seem to be consistent with the rest of the data. The rate constant from these data were also somewhat lower than at the other two pressures but reference to Fig. 15 shows that the 50 Torr data is clearly inconsistent with an intercept of 170 s^{-1}. No explanation of this anomoly is obvious at this time.

Table 12. HO removal rate constant in the zero pressure limit.

Nominal pressure	k(HNO_3 system) (s^{-1})	k(O_3/H_2O system) (s^{-1})
10 Torr	104	108
25 Torr	113	117
50 Torr	259	174

A summary of the work reported on the reaction of HO with HNO_3 around room temperature is given in Table 13. The earlier work at much higher temperatures was reviewed by Hampson[6] and will not be discussed here. Two points can be made about the flash photolysis/kinetic spectroscopy experiment of Husain and Norrish.[7] Their primary concern was measurement of the NO_3 produced following flash photolysis of nitric acid and NO_2. In the experiments in which they looked at the appearance of the NO_3 spectrum, they report HO radical lifetimes that are much too long to support the rate constant derived in the later kinetic measurements. Nitric oxide was also observed in these experiments presumably from photolysis of the products NO_2 and NO_3. Excess NO_2 over that produced in the initial photolytic step was also observed due to the fast reaction between NO and NO_3. The kinetic measurements were performed at 500 Torr N_2 rather than the 50 Torr in the spectroscopy experiments. Using a rate constant for HO + NO_2 calculated from the CODATA recommendations, it would only require an NO_2 concentration equal to 1% of the measured HNO_3 to account for the different between the work of Husain and Norrish[7] and that measured in this study.

The first work on this reaction in the laboratories of Ian Smith was that reported by Morley and Smith.[8] This was primarily a study of the reaction of HO radicals with NO_2 and NO but a few measurements were also made on the reactions of HO and O with nitric acid. These involved photolysis of HNO_3 or HNO_3/NO_2 mixtures for the HO and O reactions respectively. No mention is made of the HNO_3 purity although from their later work it seems likely that NO_2 was not negligible. Only a few measurements were made so the error limits on the rate constant derived

Table 13. Summary of reported rate constants for HO + HNO_3.

Temp. range (K)	k_{298}[a]	A factor[a,b]	E/R(K)[b]	Method	Reference
298	1.7×10^{-13}	--	--	Flash Photolysis/Kinetic Spectroscopy	7
298	1.3×10^{-13}	--	--	Flash Photolysis/Resonance Absorption	8
230-490	9.0×10^{-14}	9.0×10^{-14}	~0	Flash Photolysis/Resonance Absorption	9
228-472	8.0×10^{-14}	8.0×10^{-14}	~0	Flash Photolysis/Resonance Absorption	10
270-470	8.9×10^{-14}	8.9×10^{-14}	~0	Discharge Flow/Resonance Fluorescence	11
224-366	1.3×10^{-13}	1.52×10^{-14}	-649	Flash Photolysis/Resonance Fluorescence	12
298	8.2×10^{-14}	--	--	Flash Photolysis/Resonance Fluorescence	this work

[a] cm^3 $molecules^{-1}$ s^{-1}

[b] $k(T) = A \exp(-E/R \cdot T)$

are rather wide. The rate constant reported, which includes no correction for the effects of reaction (1), is $1.3 \pm .5 \times 10^{-13}$ cm^3 $molecules^{-1}$ s^{-1}. The reaction was studied in more detail in later work which includes a note by Zellner and Smith[9] and a full report by Smith and Zellner.[10] In the earliest of these two flash photolysis/resonance absorption studies, NO_2 impurity was monitored by absorption measurements at 310 nm and found to be 1.4%. Corrections were applied to the measured rate constant based on the Morley and Smith[8] work and experiments on NO_2 doped HNO_3 samples performed by Zellner and Smith.[9] In the later work[10] the nitric acid used was much more carefully purified so no correction was necessary for NO_2 even at the lowest temperatures studied.

In both of the later flash photolysis studies from Smith's laboratory the HNO_3 concentration in the reaction mixture was determined from pressure measurements. The mixtures were held in a storage bulb for up to a day before being admitted to the photolysis cell. The rather large HNO_3 wall adsorption discussed in the section on cross section measurements could be the source of a serious error in both of these studies. Wall adsorption leads to less HNO_3 available for reaction and consequently slow HO decays. Depending on the surface to volume ratio of the storage flask and photolysis cell and the care exercised in conditioning the walls before preparing a reaction mixture or admitting it to the cell a large under estimate of the actual reaction rate constant is possible due to this wall adsorption.

The flow tube results of Margitan, Kaufman, and Anderson[11] agree well over the temperature range studied with the latest work by Smith

and Zellner.[9,10] The results at the lowest temperatures studied in this work (272 K) were much higher than at the other three temperatures but were discarded by the authors because of excessive contribution to the measured decay from wall removal of HO and an insufficient number of measurements. Even this value of $k_2 = 1.2 \times 10^{-13}$ cm^3 molecule^{-1} s^{-1} is not as large as the higher values measured in the early flash photolysis work and the study of Wine et al.[12] Nitric acid concentrations in this work were calculated from measured flow rates of nitric acid vapor from a storage bulb. This is the most likely source of error in these measurements. An error would result if significant decomposition of the nitric acid occurred in the storage bulb or, as would be most likely, while passing through the 6 mm stainless steel tubing used as the sliding injector. The authors report several tests to insure that this problem does not arise and the precautions described seem satisfactory.

The flash photolysis/resonance fluorescence work of Wine et al.[12] was carried out in an experimental apparatus almost identical to the one used in the experiments reported in this chapter. They determined nitric acid concentrations by VUV absorption measurements using the 185 nm Hg line. As is seen from Fig. 18, the cross section measured and used by Wine et al.[12] is in excellent agreement with the work of Biaume[63] and this study. Experiments were performed in which the absorption cell was placed both before and after the photolysis cell and the measured value of k_2 was unaltered. One possible problem in their work concerns the photolysis source used in most of their measurements. A flash lamp was used and the quartz window of the cell transmitted

light down to 165 nm. It is possible that other products or excited states result from nitric acid photolysis at these short wavelengths. They did, however, perform two series of experiments using the 249 nm output of a KrF laser and no significant differences were seen. Other HO reactions have been studied by these authors in this same apparatus with generally good agreement with literature values.[69] Wine et al.[12] appear to have performed these experiments quite carefully and anticipated all criticisms by thorough calibrations. The explanation for the differences between their work and that of Margitan, Kaufman, and Anderson,[11] Smith and Zellner,[10] and that reported here is not readily apparent although much thought has been given to this question.

The experimental determination of k_2 reported in the present work was also performed with great care. The pseudo-first order rate constant was measured over a 66-fold range of nitric acid concentration and about 24-fold range of initial HO concentration. Because of experimental difficulties, no measurement of the linear range of HO detection was made in this work. The largest initial HO concentration encountered however was 9.5×10^{11} molecules cm^{-3} with most experiments below 3×10^{11} and some down to 5×10^{10}. No deviation from linearity for an HO decay of two orders of magnitude was noticed (compare Fig. 13) and no systematic variation of rate constant calculated with initial HO concentration is observed. The HNO_3/HO ratio varied from 4000-7000 so there was never any doubt that a pseudo-first order analysis was appropriate.

The largest term in an estimation of the experimental uncertainty for this reaction arises from the variation of k_2 measured at each of the three pressures. Another significant term is due to the lack of

precision in the flowing determination of the absorption cross section. After consideration of these uncertainties and including an estimate of other possible systematic errors, a rate constant for the reaction of HO + HNO_3 at room temperature of $k_2 = 8.2 \pm 1.8\ 10^{-14}$ cm^3 $molecule^{-1}$ s^{-1} is reported.

2. $HO(A^2\Sigma^+)$ Quenching by HNO_3

The measured values for the collisional quenching rate constant for HNO_3 depend on many of the same experimental parameters discussed above. Therefore, the possible errors in measured nitric acid concentrations due to incorrect values of the absorption cross section or pressure differentials in the flow system are the same as discussed in the preceeding section and contribute equally to the resultant uncertainty. The quenching rate constant is derived only from the amplitudes of the experimental decay curve however so no contribution from diffusion or reaction rate constant errors is encountered. The internal consistency of the data is quite good. In both sets of data used to derive the quenching rate constant, runs at several total pressures are encountered and no systematic deviations are observed. The agreement between the two sets of data is also quite good (~2%).

Schofield[61] has recommended the following values of $HO(A^2\Sigma^+)$ quenching rate constants with applicable molecules: 5.0×10^{-10} cm^3 $molecules^{-1}$ s^{-1} (H_2O), 7×10^{-10} (CH_3OH), 1.3×10^{-10} (CO_2), and 2.8×10^{-10} (NO_2). The value for HNO_3 derived in this study, $6.8 \pm 1.0 \times 10^{-10}$ agrees quite well with the rate constant for other efficient quenchers of $HO(A^2\Sigma^+)$.

3. $\underline{HO + H_2O_2}$

There have been three recent measurements of the H_2O_2 absorption cross sections which are in very close agreement.[40,41,48] The value measured by Molina and Molina[40] at 200 nm was used in this work even though it was slightly lower (~4%) than the other measurements at this wavelength because it is the only one for which the spectral band width was reported.

The earlier direct measurements of the rate constant for reaction of HO with H_2O_2 are summarized in Table 14. There are two separate experimental regimes in the work reported by Greiner.[16] At the highest temperature he used, the reaction was studied at three H_2O_2 concentrations all of which yield straight line ln[HO] vs time plots. The rate constant calculated at this temperature is also in agreement with the Arrhenius expression obtained in the two latest flow tube studies.[20,21] At the lower temperatures curved plots were obtained (see Fig. 2, ref. 16). Greiner interpreted the first part of these plots as due to a reaction second-order in HO, probably reaction (26).

$$HO + HO + H_2O_2 \longrightarrow 2H_2O_2 \qquad (26)$$

The rate constant for this reaction would have to be 2×10^{-27} cm^6 molecules^{-1} s^{-1} to explain Greiner's data. Sridharan, Reimann, and Kaufman[21] have reanalyzed the data of Greiner[16] by assuming that the initial slope is the true measure of reaction (3) and the curvature results from back reactions caused by buildup of other atom/radical species. This is plausible because the initial HO concentration in Greiner's work was as high as 8×10^{14} molecules cm^{-3}. They have

Table 14. Summary of reported rate constants for HO + H_2O_2.

Temp. range (K)	k_{298}[a]	k(T)[a]	Method	Reference
300-458	9.3×10^{-13}	$4.08 \times 10^{-13} T^{1/2} \exp(-604/T)$	Flash Photolysis/Kinetic Spectroscopy	16
298-670	8.4×10^{-13}	$7.97 \times 10^{-12} \exp(-670/T)$	Discharge Flow/ESR	17
298	6.8×10^{-13}	----	Flash Photolysis/Resonance Fluorescence	18
245-423	1.64×10^{-12}	$2.51 \times 10^{-12} \exp(-126/T)$	Discharge Flow/Resonance Fluorescence	20
250-459	1.69×10^{-12}	$2.96 \times 10^{-12} \exp(-164/T)$	Discharge Flow/LIF[b]	21
298	1.57×10^{-12}	----	Flash Photolysis/Resonance Fluorescence	this work

[a] units = cm^3 $molecule^{-1}$ s^{-1}

[b] LIF = Laser Induced Fluorescence

successfully modeled the decay curves shown by Greiner[16] with a computer simulation involving 14 reactions and a value for k_3 in agreement with the two latest flow tube studies.

Two points can be made about the work of Hack, Hoyerman, and Wagner.[17] Their detection technique for HO radicals (ESR) was relatively insensitive so large HO concentrations were required; about 3×10^{13} molecules cm^{-3} in this study. HO radicals were produced by the reaction of H atoms with NO_2 which although it is a standard method, also produces NO in the same concentrations as HO. Hack et al. dismiss any problem associated with the back reaction of HOO produced in the primary reaction with this ambient NO based on their companion measurement of k_{27}.

$$HOO + NO \longrightarrow HO + NO_2 \qquad (27)$$

Later work[70] however shows that the rate constant for reaction (27) is 30 times larger than the value measured by Hack et al.[17] This led them to underestimate the contribution of back reaction (27) to the measured HO concentrations. The flow rates in the Hack et al. study were also very large and the experimental signal-to-noise was low in order to remain in the region where the authors supposed that data reduction would be simplified. This adds an extra measure of uncertainty to the results obtained.

The flash photolysis study of Harris and Pitts[18] employed a flash lamp as the photolytic source and H_2O and H_2O_2 as the precursors to HO production. H atoms are also a product of the water photolysis and at the lowest wavelengths used, the H + HOO channel has been observed in H_2O_2 photolysis.[71] Both H and HO must have been present at large

concentrations since at the highest peroxide pressures used, the authors noted the onset of mixed order kinetics. A possible back reaction in this system is H + HOO which has a recommended rate constant of 3.2 x 10^{-11} cm^3 $molecule^{-1}$ s^{-1}. Sridharan et al.[21] find that they can model the decays obtained in these experiments using a [HO]/[H] ratio of 3 and a total radical concentration on the order of 10^{12} molecules cm^{-3}

The two latest flow tube determinations by Keyser[20] and Sridharan, Reimann and Kaufman[21] are almost identical in experimental configuration and result obtained. The concentrations of other, interfering radicals such as O, H and NO were carefully controlled in both studies. A variety of flow tube surface treatments and methods of HO production were attempted and no difference noted. This lends further confirmation to the idea that heterogeneous removal of HO or reaction with some unknown impurity in the flow tube gas mixture was responsible for the larger values of k_3 obtained in these two experiments.

The flash photolysis study reported in this chapter avoided some of the problems noted in the three earliest determinations of this rate constant. The resonance fluorescence technique was used for detection of HO radicals; the inherent sensitivity of this method allowed measurements to be carried out with initial HO concentrations $<3 \times 10^{11}$ molecules cm^{-3}, two or three orders of magnitude lower than the radical concentrations encountered in some of the earlier work. These lower radical concentrations reduce greatly the possibility of parallel or succesive radical-radical reactions which complicate the kinetic analysis. HO radicals were generated solely from the 249 nm photolysis of H_2O_2 where other channels appear to play a small role at most.[56] H_2O which is

an impurity in the peroxide used does not photolyze at this wavelength. The reaction mixture was very clean, only H_2O_2, H_2O, and Ar, so the possibility of competing radical-molecule reactions is also quite small.

In view of the above and the close correspondence between the result of this study and the two latest flow tube determinations of k_3 two conclusions can be reached. First and most obvious, the previously recommended value for the rate constant of HO + H_2O_2[19] appears to be low by a factor of two. Second, the experimental method used for the study of HO reactions appears to be free from any serious flaws and therefore the rate constants measured can be accepted with a fair degree of certainty.

The value for k_3 determined in this work is $1.57 \pm 0.23 \times 10^{-12}$ cm^3 $molecule^{-1}$ s^{-1} where the uncertainty is a sum of the experimental standard deviation and an estimate of possible systematic errors in the work.

IV. Cl ATOM KINETICS

A. Kinetic Results

The Cl atom reactions reported in this chapter were studied by methods identical to those discussed previously. Chlorine atoms were produced by photolysis of the precursor at 350 nm with the excimer laser operating on the XeCl transition or at 500 nm with the dye laser and Coumarin 504. The absorption cross sections for both of the reactants and the possible impurities in each are such that photolysis at 249 nm would have been more favorable than at 350 nm. The photomultiplier tube used had a high sensitivity at 249 nm however and the large signal due to scattered laser light made kinetic measurements impractical. Even at 350 nm there was a short (~100 μs) time after the laser flash when cell fluorescence excited by the laser interfered with the data analysis. Even in the case with the fastest decay, the Cl signal was followed at least 1 ms or 10 times the interference length.

The choice of carrier gas in the Cl atom system is not as critical as it was in the HO system. Since the absorption cross sections of the atoms are much larger than HO and the resonance lamp intensity is concentrated in a few lines, the overall detection sensitivity is much higher and a fluorescence quantum yield much less than 1 can be tolerated. Bemand and Clyne[72] have measured quenching rate constants for the analogous Br transitions and find that the quenching half pressure for the Br (5s) $^4P_{5/2}$ state is about 7.5 Torr of N_2 with the Ar value ~50x higher. The radiation lifetime of the Cl (4s) $^4P_{3/2}$ is about 10 times greater[73] than the Br state for which the quenching measurements were made and so the fluorescence quantum yield for this state should be

0.9 at 10 Torr N_2 and 0.8 at 25 Torr. The other major line from the Cl atom lamp originates from Cl $^4P_{5/2}$ which has a longer radiative lifetime[73] than the Br $^4P_{5/2}$ state by a factor of 5 and is therefore considerably quenched by the M gas used, especially N_2. The gain in signal that would have been realized through the use of Ar was foregone because: a) signal-to-noise ratios in the experiment were high using N_2, and b) the small factor by which the signal was expected to increase (~2) was offset by the possible problems that would be encountered due to a higher level of impurities in the Ar available for use.

1. The Reaction of Cl with $ClNO_2$

The nitryl chloride was contained in a saturator at 157 K and flowed through the cell at concentrations of 0.5 to 8 x 10^{14} molecules cm^{-3}. $ClNO_2$ concentrations were monitored in the UV absorption cell at 210 nm. This corresponds to a flat part of the absorption spectrum reported by Illies and Takacs[34] and therefore diminishes some of the possibilities for error due to wavelength calibration mistakes or bandpass differences from the reported cross sections.

Nitryl chloride photolysis at 350 nm was the source of Cl atoms for the kinetic measurements. The absorption cross section for $ClNO_2$ at 350 nm was reported by Illies and Takacs[34] as 3.06 x 10^{-20} cm^2. Photolysis intensities less than 1.5 x 10^{16} photons cm^{-2} $shot^{-1}$ resulted in photolysis of less than 0.05% of the $ClNO_2$ per shot. The residence time of the precursor in the photolysis zone was <0.1s (~3 shots) so the concentration perturbation due to photolysis or reaction was negligible.

Chlorine resonance fluorescence signals were collected with channel times of 5, 10 or 20 microseconds and the data were reduced in the

standard manner. A plot of ln (fluorescence intensity - backgound) vs time is shown in Fig. 19 for a typical experiment in this series. The channel width in this instance was 20 μs. Note the contribution in the first five channels after the laser pulse of the cell fluorescence mentioned above. The limits of the straight line fit in this particular instance are denoted by arrows in the figure. These limits represent decay of an order of magnitude in Cl atom concentration and are representative of the number of channel fit for all runs in this system.

Psuedo-first order rate constants were measured for total pressures of 10 and 25 Torr and using both Ar and N_2 as the buffer gas. The results of these experiments are listed in Table 15 and shown plotted in Fig. 20. A least squares fit to the data at both pressures results in the line shown in Fig. 20. The rate constant derived is k_{10} = $5.05 \pm 0.24 \times 10^{-12}$ cm^3 $molecule^{-1}$ s^{-1}. The intercept of the fitted line is 226 ± 100 which within the experimental uncertainty equals the previously measured rate for Cl diffusion out of the viewing region. The uncertainty shown for both quantities is twice the computed standard deviation.

2. The Reaction of Cl with ClNO

Measurements of the reaction of Cl with nitrosyl chloride (reaction (7)) were carried out with two different experimental configurations. Initial experiments employed dye laser photolysis of ClNO at 500 nm as the Cl atom source. The absorption cross section of nitrosyl chloride at 500 nm is 1.39×10^{-20} cm^2 and the Phase-R output was typically 30 mJ per pulse or 7.5×10^{16} photons cm^{-2} $pulse^{-1}$. This translates into photolysis of 0.1% of the reactant ClNO per pulse. The ratio ClNO/Cl

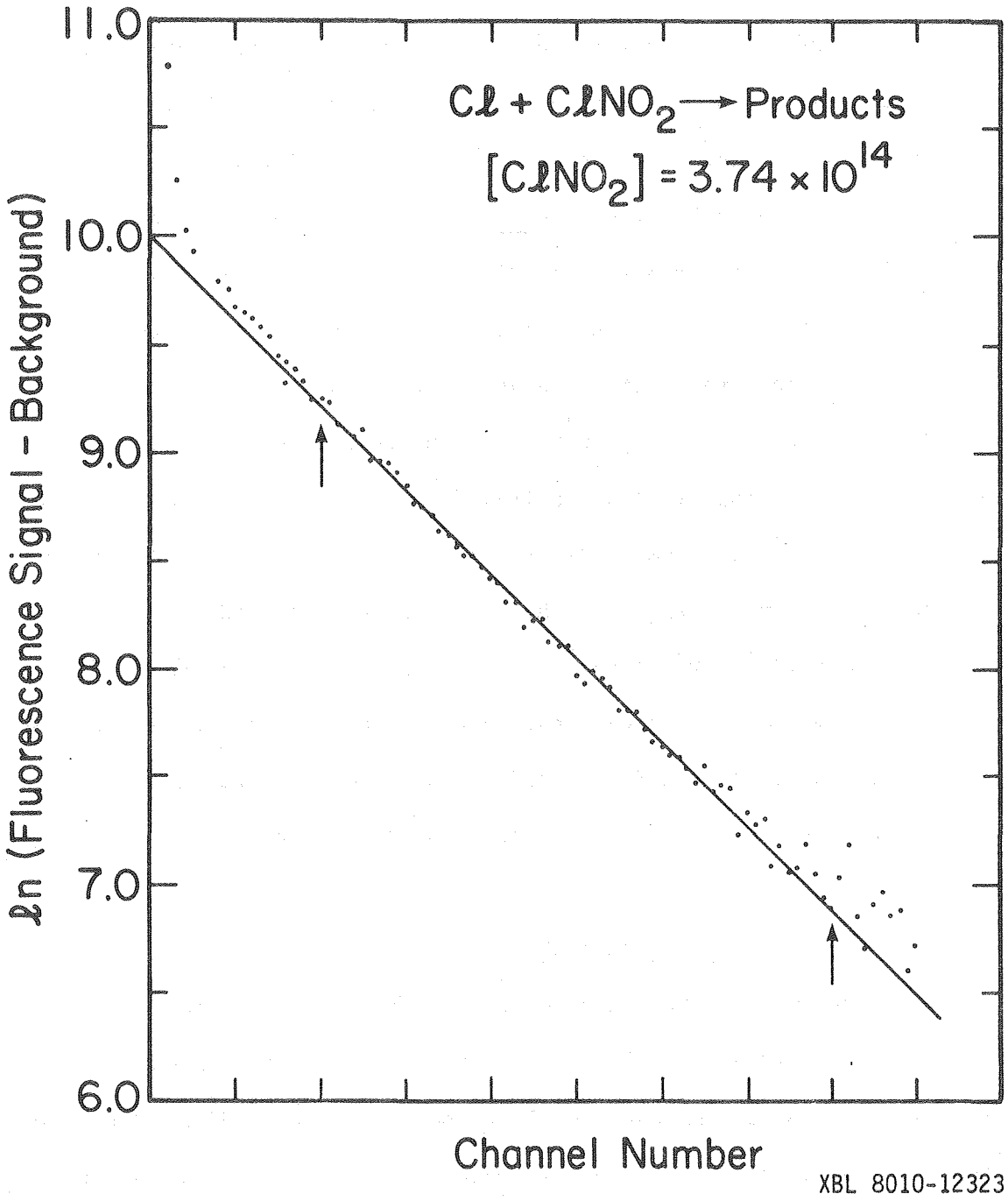

Fig. 19. ln(signal-background) vs time for the reaction of Cl + $ClNO_2$ with the limits of the computer fit denoted by arrows.

Table 15. Kinetic results for Cl + $ClNO_2$

$[ClNO_2]$ (molecules cm^{-3})	k' (s^{-1})	$\bar{E}$ (photons cm^{-2} $shot^{-1}$)	M
total presssure = 10 Torr			
5.37E13	519	9.13E15	Ar
1.36E14	1002	8.40E15	Ar
1.43E14	907	1.10E16	Ar
1.82E14	1147	1.34E16	N_2
2.23E14	1340	1.20E16	Ar
2.48E14	1455	1.30E16	N_2
3.62E14	2034	9.49E15	Ar
3.74E14	1954	8.59E15	Ar
4.61E14	2414	1.18E16	Ar
5.16E14	2920	5.80E15	Ar
5.68E14	3320	5.65E15	Ar
6.90E14	3874	4.62E15	Ar
7.95E14	4144	2.54E15	Ar
total pressure = 25 Torr			
7.97E13	555	6.39E15	Ar
1.74E14	1193	7.63E15	Ar
3.63E14	2072	6.92E15	Ar
7.27E14	3766	3.81E15	Ar

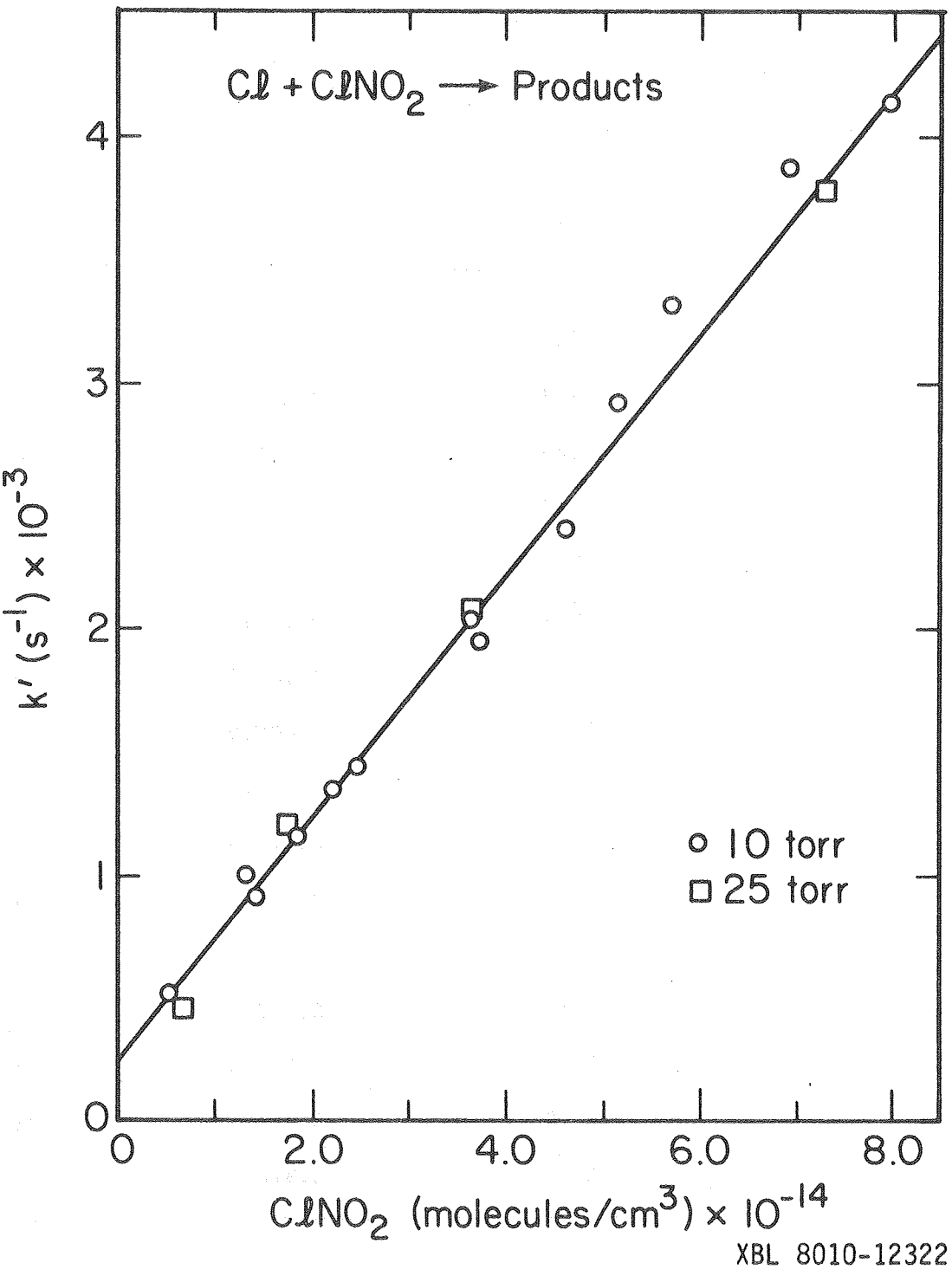

Fig. 20. Plot of k' vs $ClNO_2$ concentration for the reaction Cl + $ClNO_2$.

is always $> 10^3$ so no deviation from psuedo-first order kinetics is expected. After completion of this series of experiments, the total pressure in the ultraviolet absorption cell was found to differ from that in the photolysis cell. Therefore, only relative concentrations were obtained from the absorption measurements. These experiments still served to measure the contribution of third order reactions to the experimental rate constant and check for any enhanced reactivity of the $Cl(^2P_{1/2})$ state.

The rate constants measured in this series are listed in Table 16 and shown plotted in Fig. 21. The uncertainties on the points with added CCl_4 are much higher than for points measured in pure nitrogen. Carbon tetrachloride was chosen for its efficiency for quenching $Cl(^2P_{1/2})$ but it also has a very large absorption cross section in the region of the Cl resonance lamp. Sufficient quantities of CCl_4 to completely quench any possible $Cl(^2P_{1/2})$ also absorb a large fraction of the resonance radiation and reduce the experimental signal-to-noise correspondingly.

After correcting the flow path problems which led to the pressure drops discussed above and substituting the excimer for the Phase-R as photolysis source, quantitative experiments were performed at a total pressure of 10 Torr. Nitrosyl chloride was monitored for these runs at 196 nm which is the maximum of the absorption band observed by Ballash and Armstrong.[38] The ClNO cross section at the 350 nm photolysis wavelength is 1.4×10^{-19} cm^2 which leads to about 1% photolysis per shot.

Table 16. Initial data for the Cl + ClNO system

Relative ClNO	k' (s^{-1})	Total pressure (Torr)	CCl_4/ClNO
.52	814	10	---
.83	1057	10	---
1.59	1782	10	---
2.34	2450	10	---
2.62	2721	10	---
3.00	3361	10	---
3.43	2841	10	---
5.53	5374	10	---
5.58	6101	10	---
6.64	7670	10	---
.97	1077	10	40
1.67	2931	10	40
2.76	3542	10	40
1.46	1623	30	---
4.92	5155	30	---

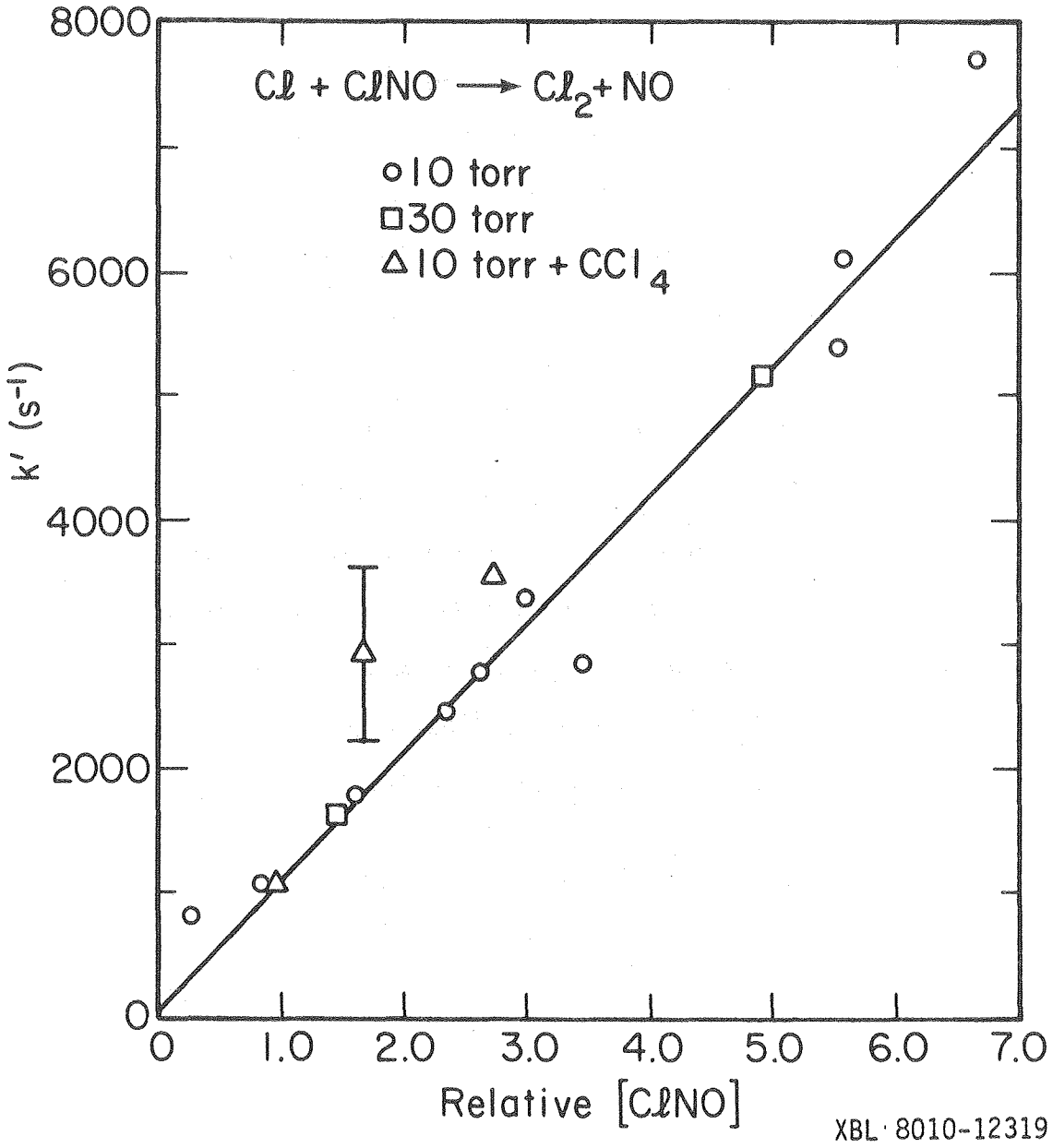

Fig. 21. Plot of k' vs relative ClNO showing the effect of total pressure and added CCl_4.

The first series of kinetic measurements on Cl + ClNO was run immediately after setting up the Cl atom system for the dual purpose of testing the system response and measuring the rate constant. Figure 22 shows the data colected in these early measurements which are also listed in Table 17. After completing all other Cl and O atom work planned, another series of experiments was done on the Cl + ClNO system. The results of these measurements are listed in Table 18 and plotted in Fig. 23. As can be seen, the rate constant calculated in the later experiments is 9% lower than that earlier and the intercept of the pseudo-first order rate constant vs ClNO concentration plot is significantly lower. The points listed in Table 17 were adjusted to the intercept of the later data and the entire data base is shown plotted in Fig. 24. The rate constant calculated from all the 10 Torr data is $1.65 \pm 0.12 \times 10^{-11}$ cm^3 $molecule^{-1}$ s^{-1} where the error limits quoted are twice the standard deviation of the mean.

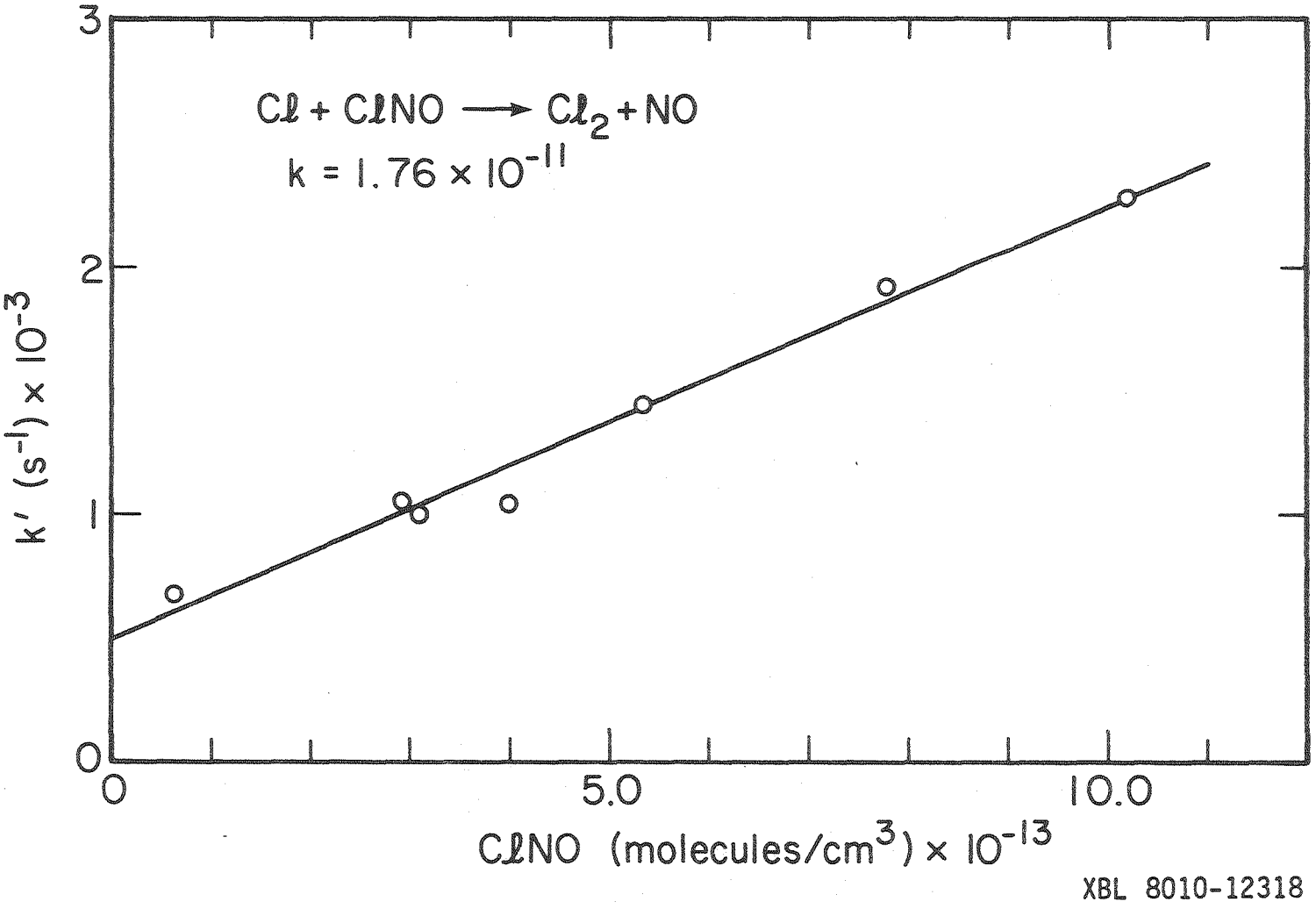

Fig. 22. Early data for the Cl + ClNO reaction.

Table 17. Kinetic results in the Cl + ClNO system.

ClNO (molecules cm^{-3})	$k'(s^{-1})$	Corrected k' $(s^{-1})^a$
6.46×10^{12}	674	546
2.92×10^{13}	1041	913
3.10×10^{13}	992	864
3.99×10^{13}	1034	906
5.34×10^{13}	1426	1298
7.80×10^{13}	1913	1785
1.02×10^{14}	2281	2153

[a]Intercept adjusted to match data of Table 17. See text.

From least squares fit: $k = 1.76 \times 10^{-11}$

Intercept = 485

Table 18. Kinetic results in the Cl + ClNO system.

ClNO (molecules cm^{-3})	k' (s^{-1})
5.79×10^{12}	483
1.39×10^{13}	532
2.41×10^{13}	724
2.42×10^{13}	675
3.41×10^{13}	886
4.01×10^{13}	1188
4.86×10^{13}	1068
6.35×10^{13}	1458
7.62×10^{13}	1531
8.02×10^{13}	1685
1.00×10^{14}	1990
1.16×10^{14}	2187

From least squares fit: $k = 1.62 \times 10^{-11}$

Intercept = 357

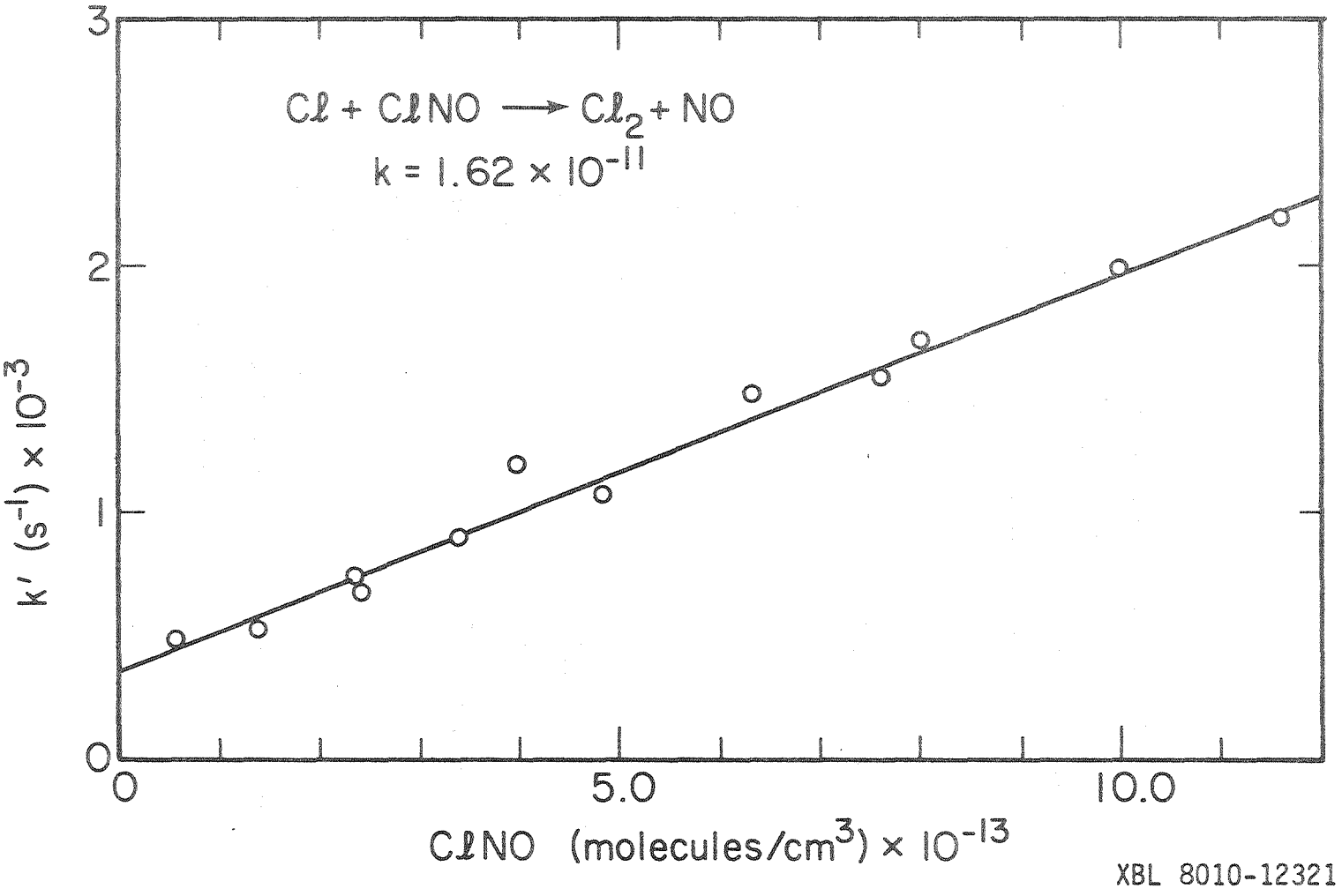

Fig. 23. Later data for the Cl + ClNO reaction.

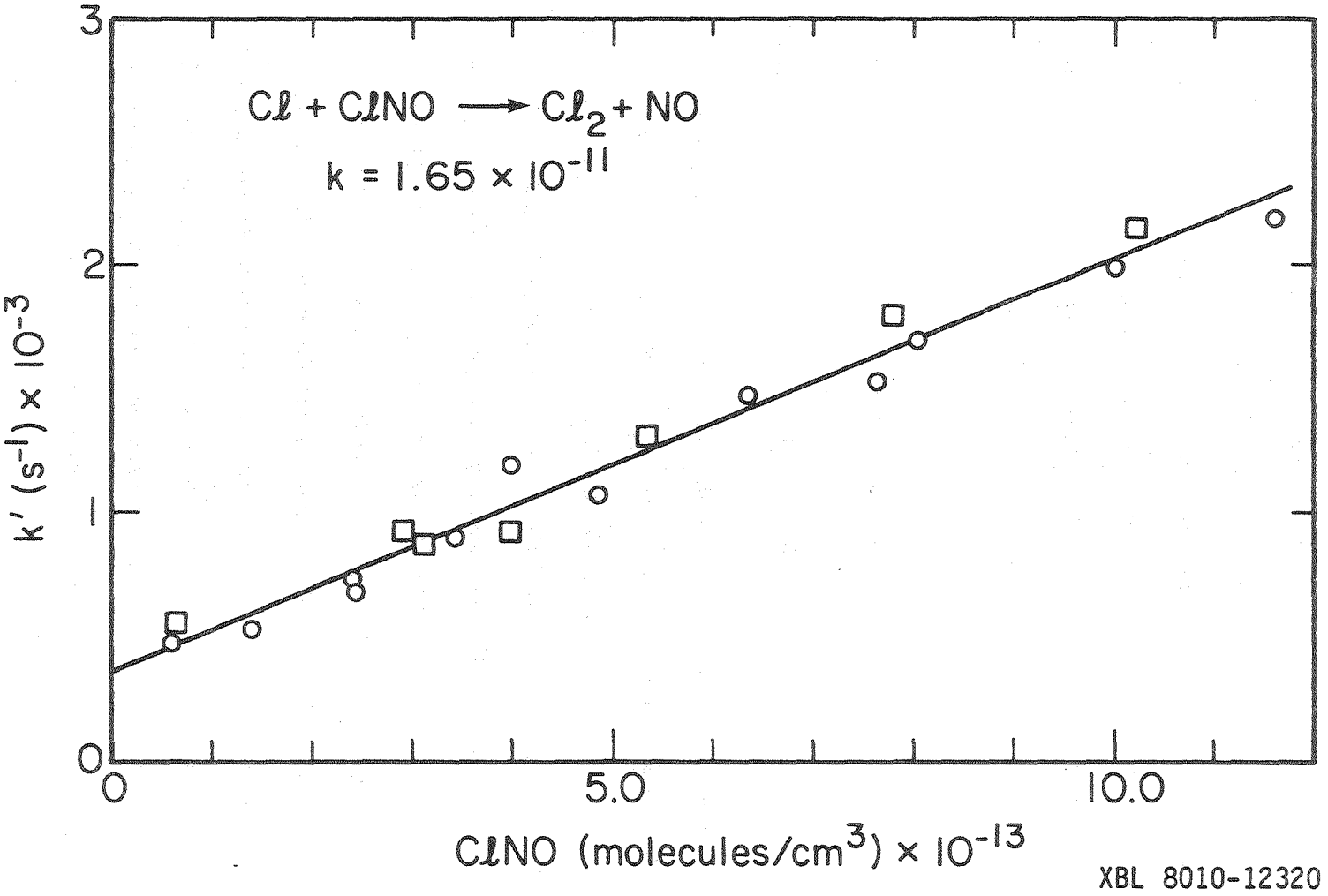

Fig. 24. All data for the reaction Cl + ClNO. Intercepts of the two data sets were adjusted to be equal.

B. Discussion

Both of the reactions being discussed in this section were studied as a function of pressure to insure that third order reactions were not contributing to the measured rate constant. Two possible impurities in these systems which arise both from the production and thermal decompostion of the precursors are NO and NO_2. The literature on the reaction of Cl with both of these molecules has been reviewed and rate constants recommended by a NASA panel.[74]

$$Cl + NO + M \longrightarrow ClNO + M \qquad (8)$$

$$Cl + NO_2 + M \longrightarrow ClNO_2 + M \qquad (9b)$$

At room temperature and in 10 Torr of N_2, the rate constants given are $k_8 = 2.9 \times 10^{-14}$ cm^3 $molecule^{-1}$ s^{-1} and $k_{9b} = 4.8 \times 10^{-13}$. NO is the impurity of most concern in the ClNO studies. The ratio of the measured rate constant and k_8 is at least 550 at room temperature therefore no interference from even a 100% NO impurity is expected. The same arguments can be made for an NO_2 impurity in the $ClNO_2$ used although with less force. The ratio of rate constants here is only 10 at 10 Torr and 4.4 at 25 Torr. A signficiant NO_2 impurity may have an effect on the measured rate constant. Reference to Fig. 20 however shows no apparent difference between the rate constant measured at total N_2 pressures of 10 or 25 Torr. In the light of this result and the low NO_2 (Chapter II), it is safe to conclude that reaction 9b makes a negligible contribution to the measured value of k_{10}.

1. Cl + ClNO

As mentioned above, the cross sections used for determination of the ClNO concentration were those measured by Ballash and Armstrong.[38] Figure 25 illustrates the differences in the cross sections reported by Ballash and Armstrong[38] from those by Illies and Takacs.[34] Relative cross sections measured as a part of this work confirm the shape of the curve reported by Ballash and Armstrong, therefore these cross sections were chosen. At 195 nm, the cross sections reported by the two groups only differ by 4%; a difference not resolved by these measurements.

The various literature reports of the rate constant for Cl + ClNO are listed in Table 19. As is immediately seen, the rate constants reported span a range of about a factor of ten and the value determined in this work is at the upper end of those reported. Burns and Dainton[28] also measured a small (1 kcal/mole) activation energy for this reaction. An attempt was made to determine if possible enhanced reactivity of meta stable (τ = 81s[56]) Cl $^2P_{1/2}$ was responsible for some of the rate constant measured. Production of Cl $^2P_{1/2}$ only takes an extra 2.51 kcal/mole (811 cm^{-1}) as compared to ground state Cl $^2P_{3/2}$. At the Phase-R photolysis wavelength of 500 nm, there is about 7000 cm^{-1} of excess energy available. Grimley and Houston[30] have shown that at photolysis wavelengths in excess of 480 nm, little if any vibrational excitation of the NO fragment is observed. No measurement of the fragment Cl $^2P_{1/2}/^2P_{3/2}$ ratio has been reported.

Donovan et al.[76] have measured the rate constant for collisional deactivation of Cl $^2P_{1/2}$ by various species. Of these, the most convenient for this study was CCl_4. The measured quenching rate constant

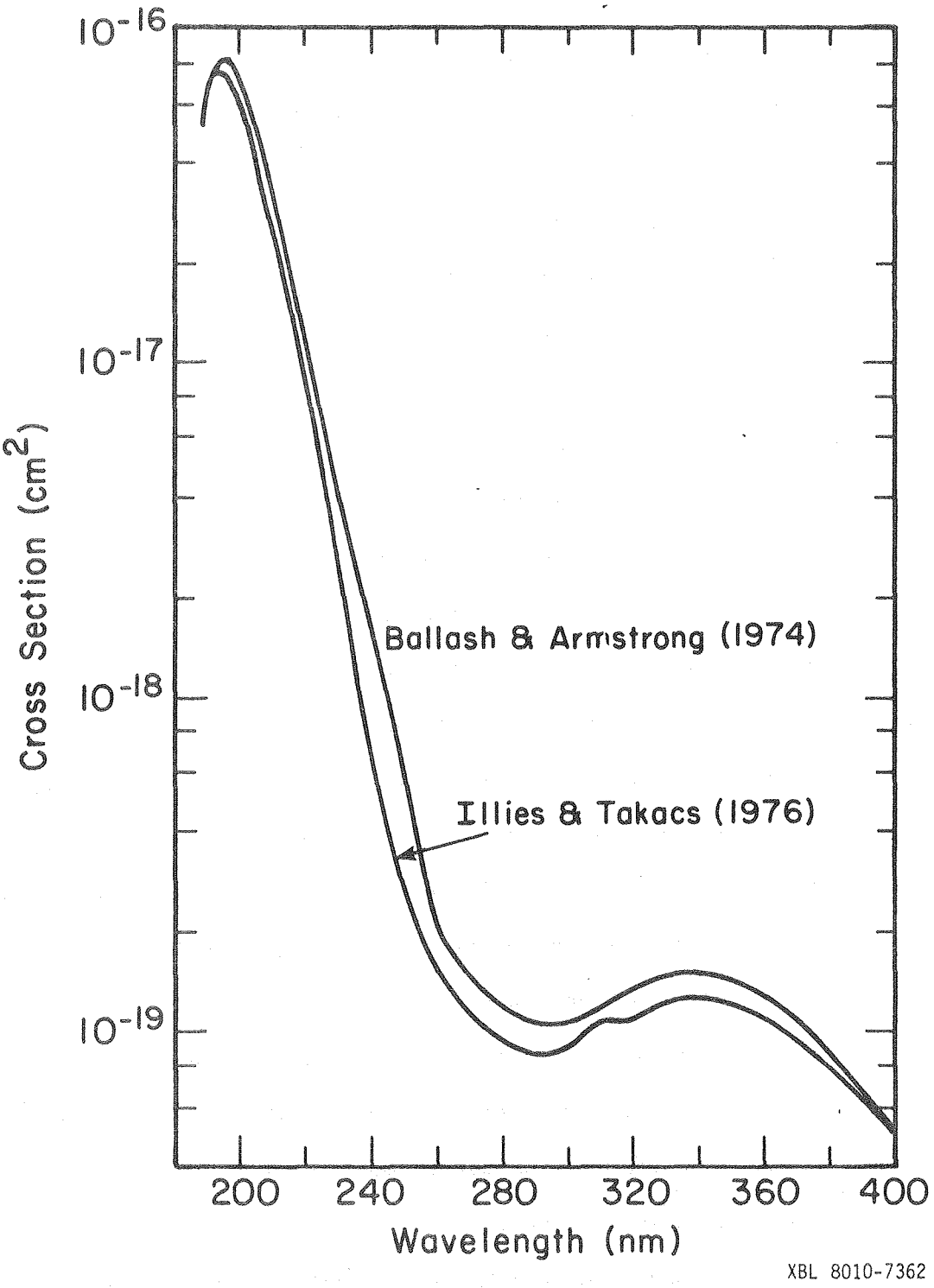

Fig. 25. The two measured ClNO absorption spectra. Ballash and Armstrong (ref. 38) and Illies and Takacs (ref. 34).

Table 19. Summary of measurements of $k_{Cl + ClNO}$

Method	k_7[a]	Reference
ClNO Retardation of Photochemical Phosgene Production	$1.91 \times 10^{-11} \exp(-530/T)$ $k_{298} = 3.2 \times 10^{-12}$	28
Discharge Flow/Resonance Absorption	$\geq 8.0 \times 10^{-12}$	71
Discharge Flow/Resonance Fluorescence	3.0×10^{-11}	29
Flash Photolysis/NO IR Emission	5.4×10^{-12}	30
Flash Photolysis/Resonance Fluorescence	1.62×10^{-11}	this work

was 5×10^{-11} cm^3 $molecule^{-1}$ s^{-1}. Addition of approximately 1×10^{15} molecules cm^{-3} of CCl_4 to the reaction mixture yields a half time for quenching metastable Cl of 20 μs or 1 channel time. The experimental signal-to-noise was also degraded, but the data obtained are of sufficient quality to eliminate the concern that the measured rate constant is larger due to a contribution from a more rapid reaction of excess Cl $^2P_{1/2}$ produced in the photolysis of ClNO.

In an attempt to understand the divergence illustrated in Table 19 several facets of the previous experiments need to be examined. Clyne and Cruse[29] have pointed out several factors in the experiments of Burns and Dainton[28] that might lead to an error in the interpretation of their data. These include: 1) cumulative errors in the equilibrium constant and the various rate constants used to derive their value for k_7, 2) possible systematic errors in the thermopile actinometry used in the calculation of k_7, or 3) absorption of ClNO on the walls of the vessel

used. Clyne, Cruse, and Watson[75] have measured ClNO adsorption on pyrex surfaces in the concentration range $5 \times 10^{13} < ClNO < 1 \times 10^{15}$. In a static system this adsorption leads to a value for the concentration of ClNO lower than that calculated based on initial pressure measurements. In this case, derived values of k_7 will underestimate the true value by the percentage of ClNO adsorbed. As pointed out by Clyne and Cruse,[29] this effect could also explain some of the activation energy measured. Adsorption becomes increasingly less important as the temperature is raised, leading to values closer to the true value at higher temperatures.

The lower limit in the Clyne, Cruse, and Watson study was derived from the observation that titration based on reaction (7) was complete in the minimum reaction time available in the flow tube used in their study. The present work is in agreement with the limit reported.

The possible systematic uncertainties in the Clyne and Cruse[29] measurements are those associated with all flow tube studies. Reaction times are calculated by a conversion of the flow rate of the gas samples and the reaction length. Careful calibration of flow rates is required to insure accurate values of reaction rate constants. This is especially true when the concentration of stable reactant is calculated from partial flow rates as was the ClNO in this study. Errors in this flow calibration directly translate into rate constant errors. Grimley and Houston[30] suggest that incomplete mixing of reactants and impurities in the ClNO used are also possibilities for error in this study. It has been demonstrated above that only an extremely large NO impurity could be responsible for the observed rate constant at 10 Torr total pressure. The flow tube experiments were run at a total pressure closer to 1 Torr so the

effect is further lessened. Incomplete mixing of reactants can only result in lengthened reaction times. This would make the true rate constant even larger than that measured by Clyne and Cruse[29] and only magnify the differences.

The work of Grimley and Houston[30] is susceptible to one of the same problems as that of Burns and Dainton.[28] Their flash photolysis studies were carried out in a static system with ClNO in the range of 6×10^{15} to 3×10^{16} molecules/cm^3. Adsorption of ClNO would have the same effect here as in the earlier work. In a parallel study reported in the same paper, Grimley and Houston[30] report the rate constant for reaction (28) as 5.16×10^{-12} cm^3 molecule^{-1} s^{-1}.

$$Br + BrNO \longrightarrow Br_2 + NO \qquad (28)$$

In 1978, Hippler, Luu, Teitlebaum, and Troe[77] published a study of the NO catalyzed recombination of Br atoms. They derive a value of $k_{28} = 3.65 \times 10^{-10}$ which is well above that reported by Grimley and Houston.[30]

The present experiments were designed to avoid some of the possible sources of systematic error discussed above. The kinetics were measured in a flowing system so ClNO adsorption on the walls of the photolysis cell can be ignored. No conversion of flow rates to reaction times is necessary so the calibration of flow meters is unimportant. The time base of the multichannel scaler is easily and accurately calibrated so the decay times measured are accurate to better than 1%. Interferences from ClNO impurities or excess Cl $^2P_{1/2}$ were discussed and discounted above. The major sources of error remaining include absorption cross

section uncertainties and the possible small pressure differential along the gas flow path.

The rate constant measured in this study is $k_7 = 1.65 \pm .32 \times 10^{-11}$ cm^3 $molecule^{-1}$ s^{-1}. The uncertainty quoted reflects twice the standard deviation of the data and an estimate of possible systematic errors in each component of the rate constant calculation.

2. $\underline{Cl + ClNO_2}$

The nitryl chloride absorption cross section reported by Illies and Takacs[34] at 210 nm was confirmed in this work. This will be discussed in more detail in the chapter on $ClNO_2$ photochemistry. The cross section was used to calculate $ClNO_2$ concentrations in this work.

There has been no report of a direct measurement of the rate constant for the reaction of Cl with $ClNO_2$. In his review of Cl chemistry, Watson[32] refers to unpublished, provisional data of Clyne and White that shows $k_{10} >> 3 \times 10^{-14}$. The value obtained in this work, $k_{10} = 5 \times 10^{-12}$, is in agreement with this limit and seems in line with the rate constants measured for analogous reactions.[32]

After consideration of the uncertainties of the components of the rate constant calculation and an estimate of possible systematic errors, the resulting rate constant and uncertainty is $5.05 \pm 0.75 \times 10^{-12}$ cm^3 $molecule^{-1}$ s^{-1}.

V. PHOTOCHEMISTRY OF $ClNO_2$ AND $ClONO_2$

The goal of this section of the work was the measurement of the photolysis quantum yields (ϕ) for each of the possible product channels. The quantum yield is defined as the ratio of the number of product atoms or molecules produced to the number of photons absorbed. A single photolysis experiment yields the ratio of fluorescence signal to precursor concentration. In order to obtain absolute quantum yields, several system calibrations are required.

The detection sensitivity of the product monitoring system can be calibrated by use of a reference compound for which the photolysis quantum yields and absorption cross sections are well known. For the atomic cases discussed in this chapter, the fluorescence quantum yield is controlled by carrier gas quenching of the upper state so no variation in detection sensitivity is expected between the reference and unknown systems. Use of this measured detection system sensitivity allows the calculation of the absolute number of product atoms produced in the photolysis.

The number of photons absorbed can be determined in two ways. A direct measurement of the light intensity before and after the photolysis cell is, in principle, the best method but the fraction of the total laser pulse absorbed in these experiments is much smaller than the precision possible in the laser energy measurements so this approach is not useful. The number of photons absorbed can also be calculated from the measured laser energy and the absorption cross section (σ) for the precursor molecule. This absorption cross section can be measured as a part of the quantum yield determination or taken from the literature.

Some care must be taken in the use of these results. The quantum yield calculated is based not only on the experimentally determined laser energy, detection sensitivity, and fluorescence signal, but the precursor absorption cross section as well. Quite often this cross section is the least certain quantity used in the determination of the quantum yield. The precursor cross sections used in this work are listed in the appropriate sections of the chapter. Any later corrections to these values can be factored in to the derived quantum yields.

Another important consideration is the purity of the chemicals used, both the reference compounds and the molecules of interest. For photolysis at 350 nm a trace NO_2 impurity will result in O atom production which interferes with the primary measurement; likewise a trace Cl_2 impurity results in Cl atom interference. In the ideal case, the quantum yield would be studied at a wavelength or wavelengths in the region of interest (the UV or near UV in this study) at which the primary reactant absorption cross section was a maximum or the cross sections of the likely impurities were at a minimum. Because of the problems with PMT sensitivity to laser excited cell fluorescence detailed in the introduction to the last chapter, this was not possible in the present work; in fact almost the opposite occurs. Meaningful results can be obtained with this handicap but only if extra care is taken to increase and measure reactant purities.

A. Experimental Results

1. Cl Atom Quantum Yields

The original expectation when these experiments were being planned was that each kinetic experiment would provide a simultaneous measure-

ment of the quantum yield. This proved not to be the case in practice for two reasons. The switch to 350 nm photolysis necessitated a greater degree of reactant purity for quantum yield measurements than for kinetic experiments and efficiency arguments led to a separation of the measurements. Periodic measurement of the atomic detection sensitivity throughout the course of the kinetic experiments showed that the sensitivity was decreasing constantly and the rate of decrease accelerating. Later experiments showed this to be due to a decrease in transmission of the MgF_2 resonance lamp window only; after replacing the window the intitial sensitivity was attained. For all the quantum yield measurements presented in this chapter, a fresh MgF_2 window was used. The detection sensitivity drifted less than 5% during the quantum yield experiments.

The most obvious choice as calibration compound for the Cl atom response was nitrosyl chloride. Its photochemistry has been long studied throughout the visible and ultraviolet region of the spectrum. This work is summarized by Okabe.[56] ClNO photolysis runs were performed throughout the course of the experiments as a check of the system response and it was these experiments that pointed out the decline in sensitivity noted above. The nitrosyl chloride in use at the time had a 5-10% Cl_2 impurity. This would not have been a problem if the photolysis wavelength was 249 nm but 350 nm is close to the peak of the Cl_2 cross section curve and the ratio $\sigma_{Cl_2}/\sigma_{ClNO}$ is 1.6. This situation is made even worse by the fact that the Cl quantum yield is 2 in Cl_2 photolysis. Because of this impurity and the simplicity of the Cl_2 photolysis system, the apparatus was calibrated using Cl_2 photolysis. Busch, Mahoney, Morse, and Wilson[78] have photolyzed Cl_2 with a doubled ruby laser at

347.1 nm and shown that photolysis at that wavelength leads to two ground state, $^2P_{3/2}$, atoms.

Two sets of quantum yield measurements were run, one before the change in resonance lamp window, the other after. The results agree to within 15% but the signal levels were very low in the first experiment so only the results obtained with the new window are presented here. The data collected are listed in Table 20.

Several atempts were made to observe Cl atom production from the photolysis of $ClONO_2$ without success. The limit of detection corresponds to a quantum yield of .1 in this system because of the relatively low absorption cross section of chlorine nitrate at the photolysis wavelength.

2. O Atom Quantum Yields

NO_2 photolysis was used as the calibration source for the O atom detection system. The sensitivity obtained by this calibration, 5.8×10^5 molecules cm^{-3}/Hz, was in agreement with those reported by Magnotta[54] and in line with the Cl atom sensitivity within the restrictions discussed in Chapter II. The data collected in this phase of the work is shown in Table 21. The detection limit for O atoms in this study was 1.2×10^9 atoms cm^{-3} under the experimental conditions used. With the laser energies available, this detection limit corresponds to a $ClONO_2$ quantum yield of 0.02 and a $ClNO_2$ quantum yield of 0.005.

Table 20. Cl atom quantum yield data for photolysis at 350 nm.

M	$[M]^a$	$I_{laser}{}^b$	Intercept[c]	$[Cl]_{calc}{}^{d,a}$	Sensitivity
Cl_2	1.28×10^{13}	1.12×10^{16}	3636	5.42×10^{10}	6.11×10^{5}
Cl_2	1.80×10^{13}	1.29×10^{16}	5628	8.78×10^{10}	6.40×10^{5}
Cl_2	1.17×10^{13}	1.33×10^{16}	3740	5.88×10^{10}	6.43×10^{5}
				Sensitivity =	6.31×10^{5}
				$Cl_{calc}{}^{a,e}$	ϕ^f
$ClNO_2$	2.48×10^{14}	1.30×10^{16}	3328	5.14×10^{10}	.893
$ClNO_2$	1.82×10^{14}	1.34×10^{16}	2721	4.19×10^{10}	.966

[a] molecules cm^{-3}

[b] photons cm^{-2} $shot^{-1}$

[c] cts/10 μs channel after 4096 laser shots

[d] calculated using $\sigma_{Cl_2} = 1.89 \times 10^{-20}$

[e] calculated from sensitivity measured using Cl_2

[f] calculated using $\sigma_{ClNO_2} = 1.78 \times 10^{-20}$, see text

Table 21. O atom quantum yield data for photolysis at 350 nm.

M	$[M]^a$	$I_{laser}{}^b$	Intercept[c]	$[O]_{calc}{}^{d,a}$	Sensitivity
NO_2	1.25×10^{13}	1.37×10^{16}	8,358	7.69×10^{10}	3.77×10^{5}
NO_2	2.04×10^{13}	1.47×10^{16}	15,301	1.34×10^{11}	3.59×10^{5}
NO_2	1.64×10^{13}	1.41×10^{16}	10,698	1.04×10^{11}	3.97×10^{5}
				Sensitivity =	3.78×10^{5}
				$[O]_{calc}{}^{a,e}$	ϕ^f
$ClNO_2$	4.23×10^{14}	1.34×10^{16}	427	4.20×10^{9}	.024
$ClNO_2$	6.97×10^{14}	1.36×10^{16}	601	5.87×10^{9}	.020
$ClONO_2$	2.13×10^{15}	1.34×10^{16}	639	6.24×10^{9}	.09
$ClONO_2$	1.54×10^{15}	1.32×10^{16}	525	5.13×10^{9}	.10

[a] molecules cm^{-3}

[b] photons cm^{-2} $shot^{-1}$

[c] cts/1.0 μs channel after 4096 laser shots

[d] calculated using $\sigma_{NO_2} = 4.48 \times 10^{-19}$ (reference 59)

[e] calculated from sensitivity measured using NO_2

[f] upper limit only, see text

B. Discussion

1. Cl Atom Quantum Yields

As mentioned above, an important condition for accurate calculation of the desired quantum yields is a knowledge of the absorption cross section. The $ClNO_2$ cross sections have been measured in this region by Illies and Takacs.[34] Their method for production and purification of $ClNO_2$ was discussed in Chapter II. During the course of purifying $ClNO_2$ for use in the kinetics experiments, a sample was obtained with significantly less color than all previous attempts. This sample and one other purified in this manner were used for all the photochemistry experiments described. The nitryl chloride absorption cross sections measured in the course of this work are shown along with those reported by Illies and Takacs[34] in Fig. 26. Also shown in this figure is the Cl_2 spectrum. Notice that at wavelengths below 300 nm, the cross sections determined in this work agree well with the earlier report but in the Cl_2 absorption region there is substantial disagreement. The difference between the two curves in this region is plotted with the Cl_2 spectrum for reference in Fig. 27. The two curves can be reconciled by assuming a Cl_2 impurity in the $ClNO_2$ sample used by Illies and Takacs[34] of 6%. The cross sections from the two measurements are listed in Table 22. The chlorine nitrate spectrum reported by Molina and Molina[39] was confirmed by Marinelli.[13]

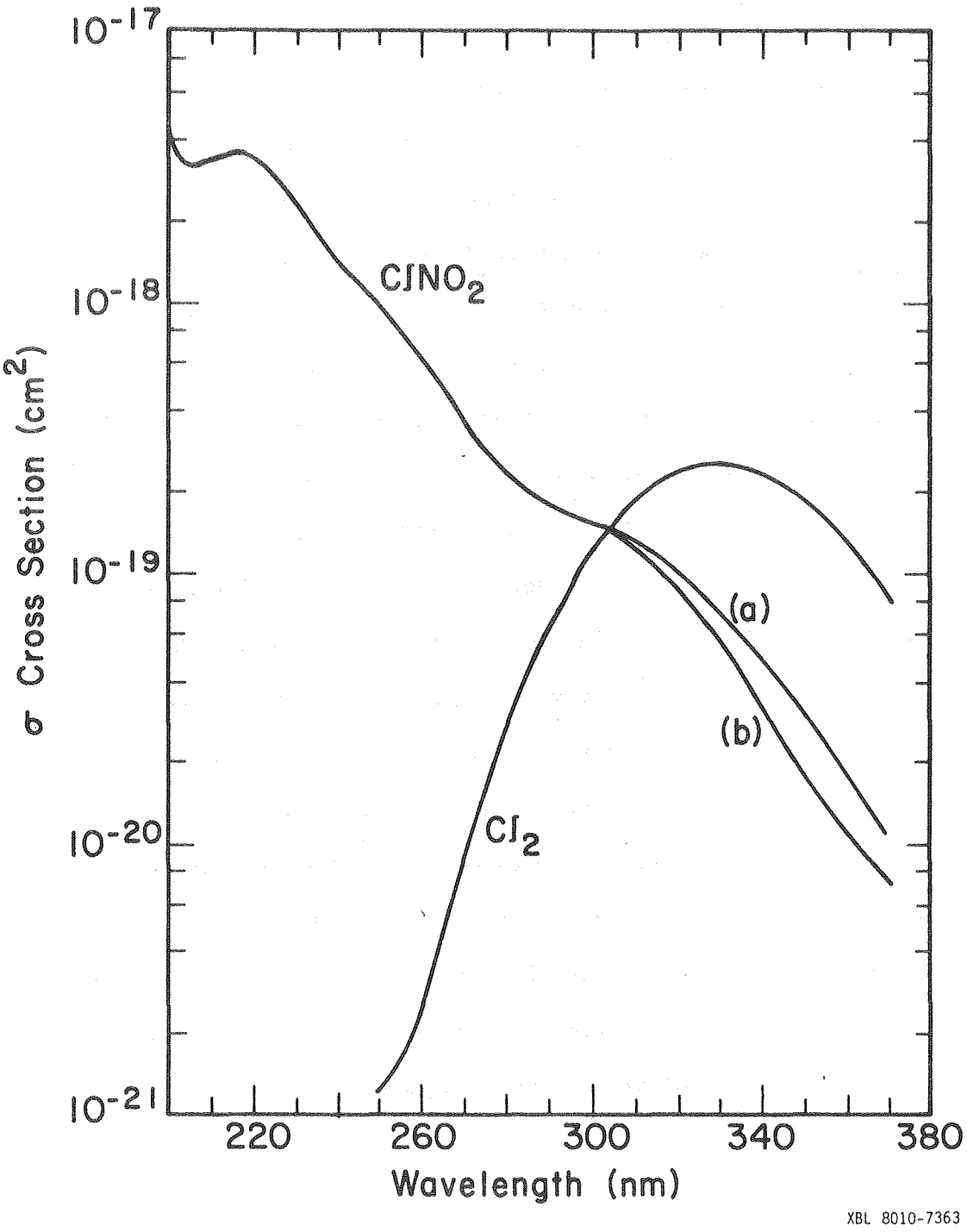

Fig. 26. Comparison of the measured $ClNO_2$ absorption cross sections with the Cl_2 spectrum for comparison. (a) Illies and Takacs (ref. 34). [2] (b) this work.

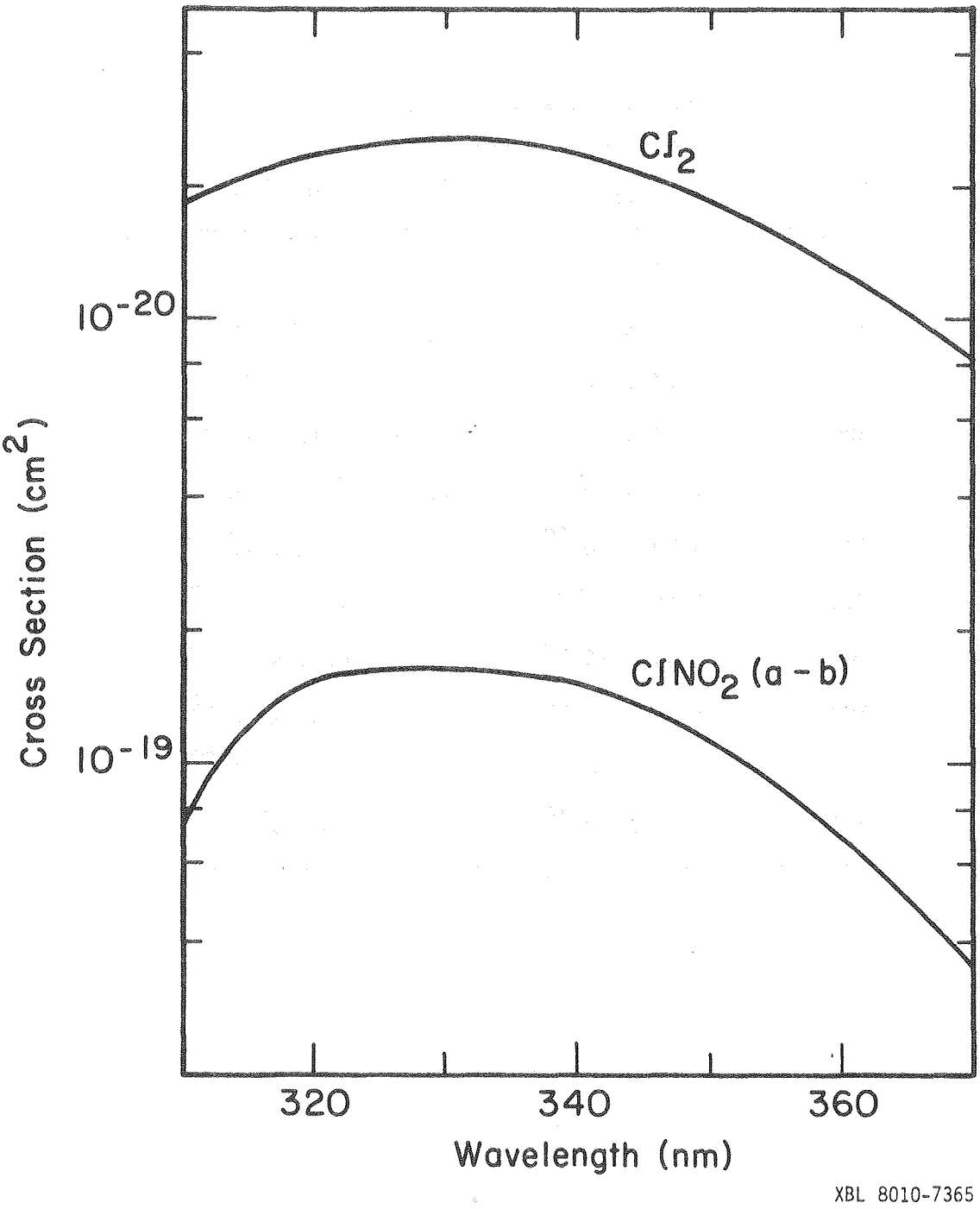

Fig. 27. The difference between the $ClNO_2$ absorption cross sections measured by Illies and Takacs (ref. 34) and in this work with the Cl_2 spectrum for reference.

Table 22. Nitryl chloride absorption cross sections.

λ(nm)	$\sigma_{\text{this work}}$ (cm^2)	$\sigma_{\text{Illies and Takacs}}$[34] ($cm^2$)
270	3.72×10^{-19}	3.73×10^{-19}
280	2.23×10^{-19}	2.31×10^{-19}
290	1.81×10^{-19}	1.80×10^{-19}
300	1.55×10^{-19}	1.54×10^{-19}
310	1.25×10^{-19}	1.32×10^{-19}
320	8.70×10^{-20}	1.02×10^{-19}
330	5.58×10^{-20}	7.11×10^{-20}
340	3.33×10^{-20}	4.81×10^{-20}
350	1.78×10^{-20}	3.06×10^{-20}
360	1.14×10^{-20}	1.82×10^{-20}
370	7.20×10^{-21}	1.07×10^{-20}

Use of the $ClNO_2$ cross section measured in this work results in a calculated Cl atom quantum yield of 0.93. This value is within the experimental uncertainty of the quantum yield of 1 that was expected based on the Cl-N bond strength and the continuous nature of the spectrum. Several experimental factors can explain a deviation to the low side of 1. The absorption cross section used for monitoring $ClNO_2$ concentration was taken from the paper by Illies and Takacs.[34] The value obtained in this work agrees with the earlier determination although if the $ClNO_2$ sample used by Illies and Takac[34] for short wavelength cross section measurements also contained a 6% Cl_2 impurity the true value of σ_{210} should be 6% higher. This alone would make the quantum yield 1. The $ClNO_2$ sample used for cross section determinations was a pale yellow color. This could indicate some residual Cl_2 and imply that the cross section at 350 nm is even lower. These two factors plus the normal uncertainty in flow rates, total pressures, etc. lead to a value for $\phi_{Cl} = 0.93 \pm 0.15$.

In view of the negative results obtained in both searches for products from $ClONO_2$ photolysis, other experiments were performed. As noted in the introduction, another possible channel would be the production of ClO and NO_2, the thermal products. This was investigated by means of the fast reaction of ClO with NO to yield Cl atoms.

$$ClO + NO \longrightarrow Cl + NO_2 \qquad (29)$$

The rate constant recommended for this reaction is 1.8×10^{-11}. Addition of 0.1 Torr NO to the $ClONO_2/N_2$ reaction mixture will result in conversion of 95% of any ClO into Cl within 2 channel times (20 μs). This

experiment was repeated with several ratios of $ClONO_2/NO$ without any success. In order to test the Cl detection system response in the presence of $ClONO_2$, samples of $ClONO_2$ doped with Cl_2 were then tried and still no Cl atom production was observed. The answer to this dilemma has been supplied by Marinelli.[13] Ray, Keyser, and Watson[79] have recently published a re-investigation of the kinetics of reaction (30).

$$Cl + Cl_2O \longrightarrow Cl_2 + ClO \qquad (30)$$

The rate constant measured was 9.8×10^{-11} cm^3 $molecules^{-1}$ s^{-1}, which is 150 times larger than previously thought. The absorption cross section of chlorine nitrate at 350 nm is small, therefore large concentrations, are necessary to allow sufficient Cl production ($1\text{-}3 \times 10^{15}$). At these concentrations, a small Cl_2O impurity is enough to remove all Cl produced by means of reaction (30) before it can be detected. No information about the chlorine nitrate photolysis products in the Cl or ClO channels can be gained in these experiments.

2. O Atom Quantum Yields

As in the Cl atom case, 350 nm is not the ideal wavelength for O atom quantum yield studies. Figure 28 shows the cross sections for both $ClNO_2$ and $ClONO_2$ along with that of a possible impurity, NO_2. It is evident from this figure that a sizeable NO_2 impurity, especially in the $ClONO_2$, would seriously interfer with the work.

The actual signal levels and quantum yields calculated from them were shown in Table 21. Both of these quantum yields should be regarded as an upper limit to the true value. The O atom signal in the nitryl chloride experiment can also be explained by a 0.15% NO_2 impurity. The

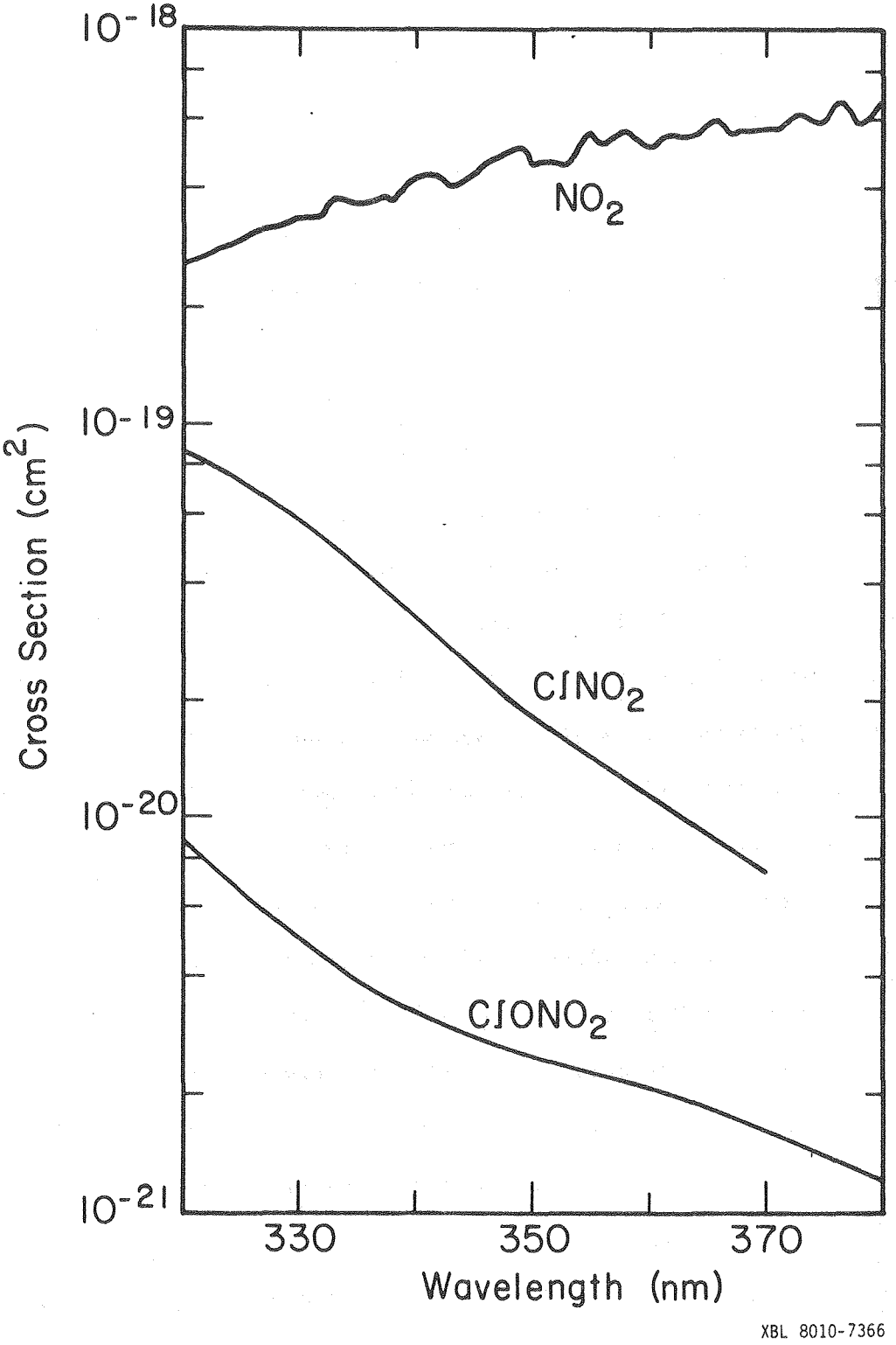

Fig. 28. The absorption spectra for NO_2 (ref 59), $ClNO_2$ (this work), and $ClONO_2$ (ref 39).

procedure for removing Cl_2 from the product $ClNO_2$ has the effect of concentrating any possible NO_2 impurity. The product was re-distilled after this, but 0.15% NO_2 is not impossible. Combining this with the fact that the Cl quantum yield was shown to be 1 in the companion measurement, the O atom quantum yield is reported as < 2.5%.

The chlorine nitrate study is an even better example of this problem. The observed signal levels in this case can also be explained by a 0.05% NO_2 impurity. The O atom quantum yield from $ClONO_2$ photolysis is therefore 10%. This matches the upper limit reported by Chang et al.[37] from their direct measurement of the photolysis products by Very Low Pressure Photolysis. It is in sharp contrast to the work of Smith, Chou, and Rowland[36] who find that $\phi_O = 1$ based on the analysis of final products of photolysis in a static system. Because of this agreement on the O atom quantum yield by the two direct measurements, it is likely that the major photo dissociation channel leads to Cl and NO_3 as was found in the work by Chang et al.[37] Rowland's group[36] tested for the production of Cl atoms by addition of excess ethane. The reaction of Cl and C_2H_6 leads to HCl which Smith et al.[36] then expect to undergo a rapid heterogeneous reaction with $ClONO_2$ to form Cl_2 and HNO_3. The absence of HNO_3 in the final product mixture leads them to rule out Cl production. Possibly, the heterogeneous reaction was not as rapid as expected in this case.

The O atom decay rate in these runs is a measure of the reaction of O with $ClONO_2$. The value obtained in this work for k_{31},

$$O + ClONO_2 \longrightarrow \text{products} \qquad (31)$$

is 1.7×10^{-11} cm^3 $molecule^{-1}$ s^{-1} which agrees well with the recommended[19] value of 1.9×10^{-11}.

VI. CONCLUSION

Several conclusions can be drawn from the result of this work both for stratospheric chemistry and for the feasibility of future laboratory studies. The rate constant measured for the reaction of HO with H_2O_2 confirms the values recently obtained at room temperature by Keyser[20] and Kaufman's group.[21] Although this is the first flash photolysis study to obtain this value, several possible problems with the earlier flash photolysis work and the measures taken to avoid them in this work were discussed earlier. Keyser[20] has calculated the magnitude of various atmospheric removal processes for H_2O_2 using the rate constant measured in his work and confirmed here. The loss rate due to reaction with HO increases by factors ranging from 2.5 at 20 km to 4.5 at 50 km and is essentially equal to the photolysis loss rate at 40 km. The steady state concentration of H_2O_2 in the atmosphere is therefore considerably reduced. The ratio [HOO]/[HO] is also increased when the present value of this rate constant is considered.

This value for k_3 necessitates a major reinterpretation of some laboratory investigations of HOO radical reactions. Burrows, Harris, and Thrush[14,80] have determined the rate constant for the reaction of O + HOO by ratio to both HO + H_2O_2 and O + HO with apparent agreement. These results will have to be reinterpreted based on the new value for k_3. They also measured the ratio of k_3 to the rate constant for the reaction of HO + HOO and HOO + NO. Both of the values they derived will be doubled when the new value for the rate constant for HO + H_2O_2 is considered. This places both measured rate constants substantially above the accepted values.[19]

The agreement observed with the recent flow tube determinations of k_3 also serves as a calibration of the experimental system used in this work. The H_2O_2 concentration was measured using absorption cross sections from the literature and the rate constant obtained agrees well. This tends to rule out any problem associated with concentration mismatches between the UV absorption cell and the photolysis cell.

The rate constant measured for the reaction of HO with HNO_3 agrees much more closely with the earlier work than the recent determination of Wine et al.[12] The competition between this reaction and the photolysis of HNO_3 to HO + NO_2 helps to determine the HO_x balance in the atmosphere and the rate of the reaction affects the $[HNO_3]/[NO_2]$ ratio.[81] Extensive model calculations were performed by Wine et al.[12] using the rate constant expression derived from this work as input for the LLL one dimensional transport-kinetic model of the troposhere and stratosphere. As expected, the ratio $[HNO_3]/[NO_2]$ is lower than calculated previously and more in agreement with the measurements of Evans et al.[82] and Harries.[83] Fontanella[84] and Lowenstein[85] have measured higher values of this ratio in the atmosphere, however, more in agreement with calculations based on the temperature independent value for the rate constant of the HO + HNO_3 reaction.

This brings up an important fact. The major atmospheric effect of the Wine et al.[12] measurement results from the larger rate constant measured for the low temperatures that occur in the lower stratosphere where the nitric acid concentration is largest. The result of this work at room temperature cannot by itself disprove the low temperature values of Wine et al.[12] but the agreement of this work with the earlier

measurements by Smith and Zellner[10] and Margitan, Kaufman, and Anderson,[11] which showed no temperature dependence, casts some doubts on the work of Wine et al.[12] More work is needed on this system and a temperature dependent kinetics study is planned in this laboratory.[13]

The rate constant for collisional quenching of $HO(A^2\Sigma^+)$ by HNO_3 measured in this work will allow more accurate prediction of expected signal levels in future experiments and aid in their interpretation by model calculations.

The reaction of Cl + ClNO has been used as a titration reaction for Cl atom concentration determinations, especially in discharge flow experiments. The rate constant measured in this work is within the limit of Clyne, Cruse, and Watson[75] although it is 3.3 times larger than the recent measurement of Grimley and Houston.[30] No reevaluation of the previous titration work is required if the value measured in this work is correct.

This work is the only reference to $ClNO_2$ reactions except the early, high temperature unimolecular decomposition studies.[33] The photolysis quantum yield of Cl was shown to be close to 1 as expected from the continuous nature of the spectrum and the Cl-N bond strength. The rate constant measured for the reaction of Cl with $ClNO_2$ seems to agree well with other Cl reactions of this sort. The reaction of O plus $ClNO_2$ appears to be very slow although quantitative work still needs to be done.

The O atom quantum yield measured for $ClONO_2$ photolysis agrees with the limit measured by the SRI group.[37] Assuming that the rest of their work is correct, the primary photolysis channel in chlorine

nitrate yields Cl + NO_3. Recent results of Magnotta[54] show that 89% of the atmospheric NO_3 photolysis leads to O + NO_2. Thus, only a small net change in odd oxygen results from $ClONO_2$ photolysis.

ACKNOWLEDGEMENTS

I would like to take this opportunity to thank the many individuals who were of great help in the course of this work. This study was carried out under the direction of Professor Harold Johnston whose patience allowed me to develop a research plan along the lines of my own choosing. His wealth of knowledge and oft repeated reminder that "this is an educational institution" saw me through many dark periods.

The assistance and encouragement of my coworkers was greatly appreciated. John Girman introduced me to Physical Chemistry research and along with Peter Connell taught me many of the techniques needed to make a lab work. Jim Podolske and David Littlejohn were constantly available with advice on electronics and experiments in general. Frank Magnotta developed the general photolysis reactor and taught me about light detection. Bill Marinelli supplied a needed burst of enthusiasm and much appreciated experimental assistance especially in the difficult syntheses.

Gratitude is also due the personnel of the Department of Chemistry and Lawrence Berkeley Laboratory for excellent support, especially Andy, Howard, Chuck and Fred from the Chemistry machine shop who spent many hours patiently helping me.

Thanks are due to the US Department of Energy which supported this work through the Materials and Molecular Research Division of the Lawrence Berkeley Laboratory under Contract No. W-7405-ENG-48.

Thanks also for the loan of the laser to Dr. Andy Kung and the San Francisco Laser Center which is supported by the National Science

Foundation under Grant No. CHE79-16250 awarded to the University of California at Berkeley in collaboration with Stanford University.

APPENDIX A

The data analysis scheme can be illustrated by the HNO_3 system. The time evolution of HO after the laser flash is described by:

$$\frac{d[HO]}{dt} = - k_2[HO][HNO_3] - k_d[HO] \quad . \tag{A1}$$

Making the usual pseudo-first order assumption and integrating yields

$$[HO]_t = [HO]_o \exp(-(k' + k_d)t) \tag{A2}$$

$$k' = k_2[HNO3] \quad . \tag{A3}$$

The resonance fluorescence signal is proportional to the HO concentration so:

$$(Signal)_t = (Signal)_o \exp(-(k' + k_d)t) \quad . \tag{A4}$$

By taking the natural log of both sides of A4, the result is:

$$\ln(Signal)_t = \ln(Signal)_o -(k' + k_d)t) \quad . \tag{A5}$$

Plotting $\ln(Signal)_t$ vs t results in a straight line with intercept $\ln(Signal)_o$ and slope $-(k' + k_d)$. This can be fit using the methods of least squares to yield these constants. Normally each point for the fit would be weighted by the square of its uncertainty which, since the data is in the form of counts collected per unit time, would be $1/(Signal)_t$. After linearizing the function to be fit however, the use of these weighting factors overemphasizes the uncertainties for large values of signal and underemphasizes it for small signals.

If an operation f is performed on the data so that we fit f(y) instead of y, the uncertainties must be compensated.[43]

$$\sigma_i' = df(y_i)/dy_i \cdot \sigma_i \tag{A6}$$

In the present case this means

$$\sigma_i' = d\ln y/dy \cdot \sigma_i = \sigma_i/y \quad , \tag{A7}$$

and the weighting factor becomes

$$\sigma_i = \frac{1}{(\sigma_i')^2} = (\text{Signal})_t^2 \frac{1}{(\sigma_i)^2} = (\text{Signal})_t \quad . \tag{A8}$$

The fit otherwise proceeds according to the standard form.[43]

APPENDX B

Troe[64] has described a method for representing the fall-off behavior of a recombination reaction in terms of simple equations which can be fit to the available data. He has found that under atmospheric conditions, the broadening of the fall-off curve compared to the Lindemann-Hinshelwood Model is not very pronounced and therefore several simplifications can be made to the equations he derived by fitting full RRKM calculations. The rate constant is of the form

$$\log k \simeq \log \left(\frac{k_o}{1 + k_o/k_\infty} \right) + \log F^{wc} \quad , \tag{B1}$$

where the first term on the right hand side is the Lindemann-Hinshelwood expression and the second term is a broadening factor to take into account the effects of weak collisions (where the collision efficiency $\beta_c < 1$). By several simplifications discussed by Troe,[64] the broadening term can be represented by

$$\log F^{wc} = \log F_{cent} \, (1 + [\log(k_o/k_\infty)]^2 \; ^{-1} \tag{B2}$$

where F_{cent} is determined from a fit to the data (often in the range .7 to .9). Making use of the expression $k_o/k_\infty = [M]/[M]_c$, where the "center of the reduced fall-off curve" $[M]_c$ indicates the third body concentration for which the extrapolated k_o would be equal to k_∞, Eq. (B1) can be recast as

$$\log k = \log \left(\frac{k_o}{1 + [M]/[M]_c} \right) + \log F_{cent} \, (1 + [\log([M]/[M]_c)]^2)^{-1} \quad . \tag{B3}$$

The data in the rate constant evaluation of the CODATA panel[19] are represented in this format.

REFERENCES

1. H. S. Johnston, Science 173, 517 (1971)
2. (a) M. J. Molina and F. S. Rowland, Nature 249, 810 (1974)
   (b) F. S. Rowland and M. J. Molina, Rev. Geophys. Space Phys. 13, 1 (1975)
3. H. S. Johnston, L. Foering, and R. J. Thompson, J. Phys. Chem. 57, 390 (1953)
4. T. S. Godfrey, E. D. Hughes, and C. Ingold, J. Chem. Soc., 1063 (1965)
5. K. Glanzer and J. Troe, Ber. Bunsenges. Phys. Chem. 78, 71 (1974)
6. R. F. Hampson, J. Phys. Chem. Ref. Data 2, 267 (1973)
7. D. Husain and R. G. W. Norrish, Proc. Royal Soc. A 273, 165 (1963)
8. C. Morley and I. W. M. Smith, J. Chem. Soc. Faraday Trans. II 68, 1016 (1972)
9. R. Zellner and I. W. M. Smith, Chem. Phys. Lett. 26, 72 (1974)
10. I. W. M. Smith and R. Zellner, Int. J. Chem. Kinet. Symposium 1, 341 (1975)
11. J. J. Margitan, F. Kaufman, and J. G. Anderson, Int. J. Chem. Kinet. Symposium 1, 281 (1975)
12. P. H. Wine, A. R. Ravishankara, N. M. Kreutter, R. C. Shah, J. M. Nicovich, and R. L. Thompson, to be published
13. W. J. Marinelli, private communication
14. J. P. Burrows, G. W. Haris, and B. A. Thrush, Nature 267, 233 (1977)
15. W. Hack, A. W. Preuss, and H. G. Wagner, Ber. Bunsenges. Phys. Chem. 82, 1167 (1978)
16. N. R. Greiner, J. Phys. Chem. 72, 406 (1968)

17. W. Hack, K. Hoyerman, H. G. Wagner, Int. J. Chem. Kinet. Symposium 1, 329 (1975)

18. G. W. Harris and J. N. Pitts Jr., J. Chem. Phys. 70, 2581 (1979)

19. D. L. Baulch, R. A. Cox, R. F. Hampson Jr., J. A. Kerr, J. Troe, and R. T. Watson, J. Phys. Chem. Ref. Data 9, 295 (1980)

20. L. F. Keyser, J. Phys. Chem. 84, 1659 (1980)

21. U. C. Sridharan, B. Reimann, and F. Kaufman, J. Chem. Phys. 73, 1286 (1980)

22. G. B. Kistiakowsky, J. Am. Chem. Soc. 52, 102 (1930)

23. J. G. Calvert and J. N. Pitts Jr., Photochemistry (John Wiley and Sons, Inc., New York, 1967) and references therein

24. H. Hippler and J. Troe, Int. J. Chem. Kinet. 8, 501 (1976)

25. E. A. Ogryzlo, Can. J. Chem. 39, 2556 (1961)

26. E. Hutton and M. Wright, Trans. Farad. Soc. 61, 78 (1965)

27. M. A. A. Clyne and D. H. Stedman, Trans. Farad. Soc. 64, 1816 (1968)

28. W. G. Burns and F. S. Dainton, Trans. Farad. Soc. 48, 52 (1952)

29. M. A. A. Clyne and H. W. Cruse, J. Chem. Soc. Farad. Trans. II 68, 1281 (1972)

30. A. J. Grimley and P. L. Houston, J. Chem. Phys. 72, 1471 (1980)

31. H. Niki, P. D. Maker, C. M. Savage, L. P. Breitenbach, Chem. Phys. Lett. 59, 78 (1978)

32. R. T. Watson, J. Phys. Chem. Ref. Data 6, 871 (1977)

33. (a) H. F. Cordes and H. S. Johnston, J. Am. Chem. Soc. 76, 4264 (1954)

(b) M. Volpe and H. S. Johnston, J. Am. Chem. Soc. 78, 3903 (1956)

34. A. J. Illies and G. A. Takacs, J. Photochem. 6, 35 (1976/77)

35. (a) F. S. Rowland, J. E. Spencer, and M. J. Molina, J. Phys. Chem. 80, 2711 (1976)

(b) F. S. Rowland, J. E. Spencer, and M. J. Molina, J. Phys. Chem. 80, 2713 (1976)

36. W. S. Smith, C. C. Chou, and F. S. Rowland, Geophys. Res. Lett. 4, 517 (1977)

37. J. S. Chang, J. R. Barker, J. E. Davenport, and D. M. Golden, Chem. Phys. Lett. 60, 385 (1979)

38. N. M. Ballash and D. A. Armstrong, Spectrochim. Acta 30A, 941 (1974)

39. L. T. Molina and M. J. Molina, J. Photochem. 11, 139 (1979)

40. L. T. Molina and M. J. Molina, U.S. Dept. of Transportation Report #FAA-EE-80-07, 1980

41. C. L. Lin, N. K. Rohatgi, and W. B. DeMore, Geophys. Res. Lett. 5, 113 (1978)

42. K. Schofield, J. Quant. Spectrosc. Radiat. Trans. 17, 13 (1977)

43. P. R. Bevington, Data Reduction and Error Analysis for the Physical Sciences (McGraw-Hill, New York, 1969) Chapter 9

44. H. S. Johnston, S. G. Chang, and G. Whitten, J. Phys. Chem. 78, 1 (1974)

45. H. S. Johnston, private communication

46. R. A. Cox, J. Photochem. 3, 291 (1974/75)

47. J. A. Myer and J. A. R. Samson, J. Chem. Phys. 52, 266 (1970)

48. L. T. Molina, S. D. Schinke, M. J. Molina, Geophys. Res. Lett. 4, 580 (1977)

49. M. Volpe, Ph.D. dissertation, Stanford University, 1956

50. M. Schmeisser, Inorg. Syn. 9, 127 (1967)

51. G. H. Cady, Inorg. Syn. 5, 156 (1957)

52. G. Schott and N. Davidson, J. Amer. Chem. Soc. 80, 1841 (1958)

53. P. S. Connell, Ph.D. thesis, University of California, Berkeley, and Lawrence Berkeley Laboratory Report LBL-9034 (1979)

54. F. Magnotta, Ph.D. thesis, University of California, Berkeley, and Lawrence Berkeley Laboratory Report LBL-9981 (1979)

55. R. T. Watson, private communication

56. H. Okabe, Photochemistry of Small Molecules (Wiley-Interscience, New York, 1978)

57. D. J. Seery and D. Britton, J. Phys. Chem. 68, 2263 (1964)

58. Y. V. Rao and P. Venkateswarlu, J. Mol. Spectr. 9, 173 (1962)

59. R. A. Graham, Ph.D. thesis, University of California, Berkeley, and Lawrence Berkeley Laboratory Report, LBL-4147 (1975)

60. P. H. Wine, N. M. Kreutter, and A. R. Ravishankara, J. Phys. Chem. 83, 3191 (1979)

61. K. Schofield, J. Phys. Chem. Ref. Data 8, 743 (1979)

62. H. Okabe, J. Chem. Phys. 72, 6642 (1980)

63. F. Biaume, J. Photochem. 2, 139 (1973/74)

64. J. Troe, J. Phys. Chem. 83, 114 (1979)

65. K. Glanzer and J. Troe, Ber. Bunsenges. Phys. Chem. 78, 71 (1974)

66. J. G. Anderson, J. J. Margitan, and F. Kaufman, J. Chem. Phys. 60, 3310 (1974)

67. G. W. Harris and R. P. Wayne, J. Chem. Soc. Faraday Trans. II, 71, 610 (1975)

68. C. Anastasi and I. W. M. Smith, J. Chem. Soc. Faraday Trans. II 72, 1459 (1970)

69. P. H. Wine, N. M. Kreutter, and A. R. Ravishankara, J. Phys. Chem. 83, 3191 (1979)

70. C. J. Howard and K. M. Evenson, Geophys. Res. Lett. 4, 437 (1977)

71. L. J. Stief and V. J. DeCarlo, J. Chem. Phys. 50, 1234 (1969)

72. P. P. Bemand and M. A. A. Clyne, J. Chem. Soc. Faraday Trans. II 68, 1758 (1972)

73. P. P. Bemand and M. A. A. Clyne, J. Chem. Soc. Faraday Trans. II 71, 1132 (1975)

74. Chemical Kinetic and Photochemical Data for Use in Stratospheric Modeling, Evaluation #2, (NASA - Jet Propulsion Laboratory, Pasadena, CA, April 1979)

75. M. A. A. Clyne, H. W. Cruse, and R. T. Watson, J. Chem. Soc. Faraday Trans. II 68, 183 (1972)

76. R. J. Donovan, D. Hussain, A. M. Bass, W. Braun, and D. D. Davis, J. Chem. Phys. 50, 4115 (1969)

77. H. Hippler, S. H. Luu, H. Teitlebaum, and J. Troe, Int. J. Chem. Kinet. 10, 155 (1978)

78. G. E. Busch, R. T. Mahoney, R. I. Morse, and K. R. Wilson, J. Chem. Phys. 51, 449 (1969)

79. G. W. Ray, L. F. Keyser, and R. T. Watson, J. Phys. Chem. 84, 1674 (1980)

80. J. P. Burrows, D. I. Cliff, G. W. Harris, B. A. Thrush, and J. P. T. Wilkinson, Proc. Royal Soc. London Ser. A 368, 463 (1979)

81. H. S. Johnston and J. Podolske, Rev. Geophys. and Space Phys. 16, 491 (1978).

82. W. F. J. Evans, J. H. Kerr, D. I. Wardle, J. C. McConnel, B. A. Ridley, and H. I. Schiff, Atmosphere 10, 180 (1976)

83. J. E. Harries, Nature 274, 239 (1978)

84. J. G. Fontanella, A. Girard, L. Graimont, and N. Louishard, Applied Optics 14, 825 (1975)

85. M. Lowenstein, W. L. Starr, and D. G. Murcray, Geophys. Res. Lett. 5, 531 (1978)